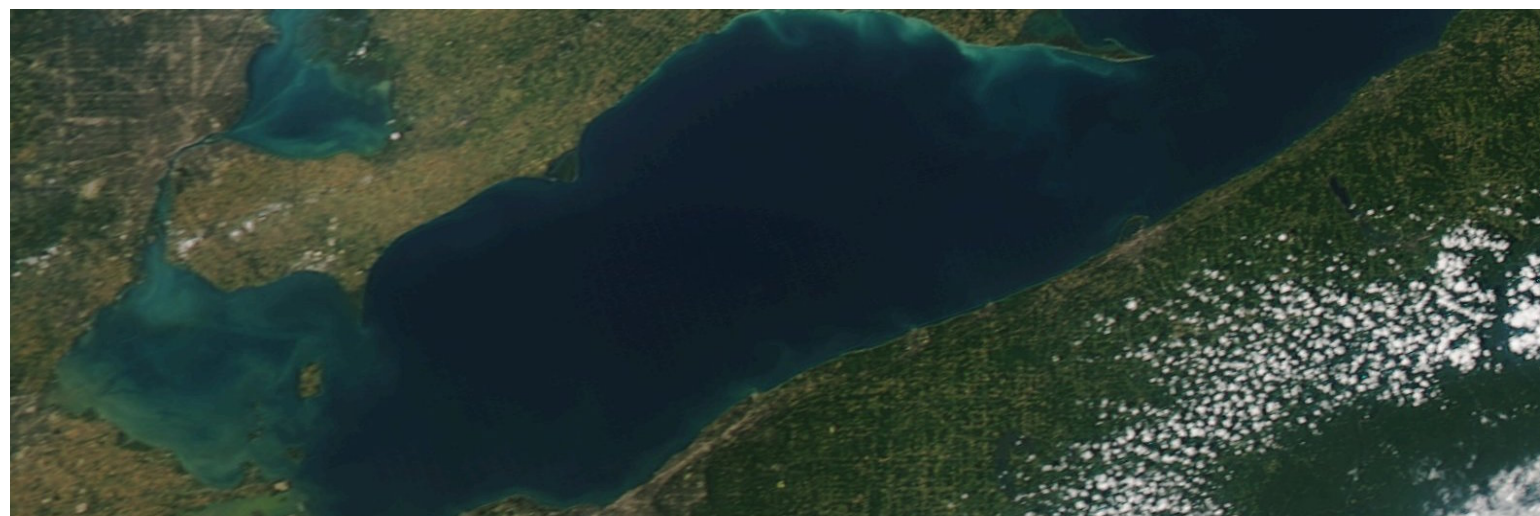
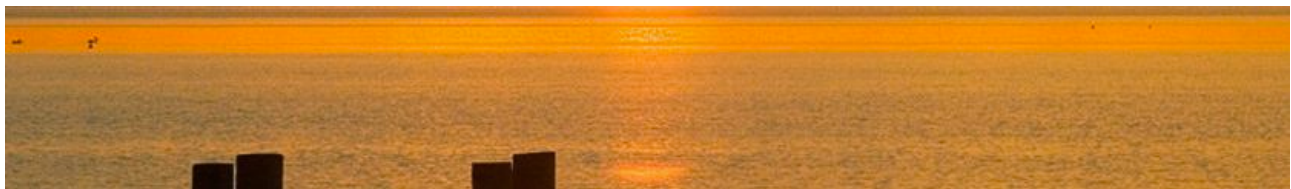


Mar 2019

A finite volume hydrodynamic-ecological model of Lake Erie

Development and testing of the TUFLOW-FV – AED2 coupled modelling platform





CONTRIBUTORS

Matthew R Hipsey ^a

Daniel A. Botelho ^b

Brendan D. Busch ^a

Lars G. Rudstam ^c

Daniel Paraska ^a

^a Aquatic Ecodynamics, UWA School of Agriculture & Environment, The University of Western Australia, Crawley WA 6009, Australia.

^b Catchment and Receiving Environments, BMT Global, Brisbane, QLD 6009, Australia.

^c Cornell University, Ithica, NY, United States.

ACKNOWLEDGEMENTS

The authors acknowledge funding support for model development from Environment Canada (EC contract number 3000627426). Casper Boon supported AED2 model development.

REVISION AND DISTRIBUTION HISTORY

Issue	Issued to	Qty	Date	Reviewed	Approved
<i>V1</i>	<i>Luis Leon</i>	<i>e</i>			
<i>V2</i>	<i>Luis Leon</i>	<i>e</i>	<i>16 March 2018</i>		
<i>V3</i>	<i>Luis Leon</i>	<i>e</i>	<i>30 March 2019</i>		

RELEASE STATUS:

Confidential: YES

DRAFT – UNDER REVIEW

DOCUMENT DETAILS

Citing this report:

Hipsey, M.R., Botelho D.A., Busch, B.D., Rudstam, L.G. and Paraska, D. 2019. **A finite volume hydrodynamic-ecological model of Lake Erie: Development and testing of the TUFLOW-FV – AED2 coupled modelling platform.** AED Report #R44 prepared for Environment Canada, The University of Western Australia, Perth, Australia. 65pp.

Copyright © 2019. The University of Western Australia (UWA), BMT Global Pty Ltd. (BMT), and Environment Canada (EC) .

Contents

EXECUTIVE SUMMARY.....	5
1 INTRODUCTION AND SCOPE	7
2 MODEL OVERVIEW AND SETUP	9
2.1 OVERVIEW	9
2.2 HYDRODYNAMICS.....	9
2.3 BIOGEOCHEMISTRY	11
3 TUFLOW-FV ICE MODEL DEVELOPMENT	13
3.1 MODEL FORMULATION	13
3.2 SNOW PROPERTIES	15
3.3 WHITE-ICE FORMATION.....	15
3.4 HEAT FLUX FROM RAINFALL	15
3.5 ACCRETION AND ABLATION OF ICE	16
3.6 WATER TEMPERATURE PREDICTION	16
3.7 ADJUSTABLE MODEL PARAMETERS	16
3.8 LAKE ERIE ICE MODEL TESTING & RESULTS.....	16
4 AED2 MUSSELS MODEL IMPLEMENTATION.....	31
4.1 MODEL FORMULATION	31
4.2 INGESTION	33
4.3 RESPIRATION.....	34
4.4 EXCRETION	35
4.5 EGESTION.....	35
4.6 MORTALITY	35
4.7 SETUP FOR LAKE ERIE	36
5 CLADOPHORA MODEL IMPLEMENTATION.....	41
5.1 PHOTOSYNTHESIS AND NUTRIENT UPTAKE.....	41
5.2 RESPIRATION.....	41
5.3 SLOUGHING.....	41
6 SEDIMENT BIOGEOCHEMISTRY	43
6.1 PRIMARY REDOX REACTIONS.....	44
6.2 SECONDARY REDOX REACTIONS	44
6.3 EQUILIBRIUM GEOCHEMISTRY.....	45
6.4 SETUP.....	45
6.5 RESULTS.....	47
7 INTEGRATED SIMULATIONS	49
8 MODEL ACCESS AND VERSION CONTROL.....	57
9 CONCLUDING REMARKS	57
10 REFERENCES.....	59
APPENDIX A: MODEL PARAMETERS	61
APPENDIX B: OBSERVATION DATA FORMAT FOR VALIDATION PLOTTING	64

Executive Summary

The report summarises work undertaken as part of Environment Canada (EC) contract 3000627426, to support the setup, application and development of the TUFLOW-FV hydrodynamic model and AED2 ecological model on Lake Erie.

The hydrodynamic model TUFLOW-FV:

- was configured to have a variable mesh ranging from <200m to ~2800m, thereby capturing high spatial resolution in the littoral regions and around complex coastlines, and coarser resolution in the interior,
- the vertical resolution adopted hybrid co-ordinates to resolve surface water level variation accurately as well as thermal stratification and internal wave dynamics,
- was able to accommodate spatially variable meteorological forcing,
- was extended to allow ice cover over winter.

The ecological model AED2:

- was configured to capture light (PAR & UV) and turbidity, including feedback of biological particles on thermal extinction,
- included oxygen, nutrients, organic matter and relevant cycling processes equivalent to prior studies that have been undertaken,
- simulated five phytoplankton groups,
- was extended to include a new multi-group bivalve model for simulating mussels, with ability for spatial heterogeneity in mussel density,
- had the previously developed Cladophora Growth Model (CGM) implemented and coupled with the other modules,
- includes a sediment biogeochemistry model able to resolve sediment vertical profiles in discrete zones.

The coupled model was run for 2013 with acceptable run-times, and was able to simulate vertical stratification well and seasonal gradients in water quality properties, including horizontal variation. In addition, the AED2 was also configured to run with the 1D General Lake Model (GLM) to allow for quick development, checking and calibration of the complex biogeochemical model configuration. Example outputs from the modelling activity showing the new model features are presented.

This phase of model setup and development has further extended the model platform to be useful tool to support management scenario assessment and exploration of a range of contemporary science questions about the lake, though further efforts at validation are now required. Next steps therefore require the model parameters to be optimally calibrated, bearing in mind recent advances in model parameter testing and data availability, for a range of different conditions.

The model files and supporting scripts are made available via the GitHub version control repository.

1 Introduction and Scope

Water quality issues have occurred within Lake Erie for several decades and continue to challenge policy makers and managers within the region. These issues have motivated numerous modelling studies, that have included the recent Annex 4 Ensemble Modeling Report in 2015. Arguably, one of the most comprehensive depiction of water quality was previously done using the ELCOM-CAEDYM model platform and this was able to capture the physical and biogeochemical dynamics of the water column, and also capture benthic biotic communities such as Cladophora and Mussels.

A pilot study using a new platform was undertaken in 2016 to demonstrate the potential of the TUFLOW-FV hydrodynamic model and AED2 ecological model as an option for use by Environment Canada for assessing water quality and the impact of nutrient loads on Lake Erie. The initial pilot phase of model setup identified the model had several features and advantages making it attractive for operational use, therefore, the potential of the platform as a state-of-the-art tool to support management scenarios and scientific understanding of the lake has been identified.

Under EC contract 3000627426, this project was created to support training on the best use of the model to ensure current workflows used within EC are able to replicate adequate results with the model platform. Model developments to integrate various features were also required to be undertaken. The final model delivery is comprehensive in its ability to now simulate 3D hydrodynamics, waves, ice cover, water quality, benthic ecology, and sediment chemistry.

This project reported on herein involved a) model setup, b) model development and c) handover and basic remote support. Specifically the project scope was to:

- Provide Lake Erie model setup advice and guidance
- Support Lake Erie hydrodynamic model (TUFLOW-FV) installation and validation advice
- Provide the AED2 model library and updates associated with developments
- Setup and maintain model input files to simulate light, oxygen, nutrients and phytoplankton
- Provide Lake Erie ecological model calibration support
- Develop plotting and post-processing analysis scripts (including MATLAB scripts)
- Setup benthic maps for mussel distribution and configuration of mussel model to support benthic filtration of water column variables and nutrient recycling.
- Implement an ice model within TUFLOW-FV to allow for over-winter simulation
- Implement sediment biogeochemical model with vertical resolution, able to account for horizontal variation in sediment geochemical properties.
- In addition to the contracted scope, the Cladophora Growth Model (CGM) was also implemented into AED2.

The aim of this report is to summarise developments to the Lake Erie finite volume hydrodynamic-biogeochemical model and document its setup for future reference. Note that, based on the scope above, the report doesn't cover details of model validation, which is being undertaken by EC. The specific focus areas covered in the report include:

- General model setup summary
- Summarise the newly developed ice model within TUFLOW-FV and demonstrate its predictions
- Summarise the newly developed mussels and Cladophora models, and sediment biogeochemistry model within AED2
- Demonstrate the integrated model operation over the year 2013, and the range of post-processing outputs now available.

2 Model Overview and Setup

2.1 Overview

The model software is a full-featured platform able to simulate 3D hydrodynamics, biogeochemistry and aquatic ecology. Optionally, users may also link the hydrodynamic predictions to the open-source wave model SWAN, and the open-source turbulence model GOTM. The organisation of the models and associated input and output files are shown in Figure 1. The lake hydrodynamic setup is primarily managed through the `erie.fvc` file, and the lake water quality setup is managed through the `aed2.nml` file. A brief summary of TUFLOW-FV and AED2 platforms is described next.

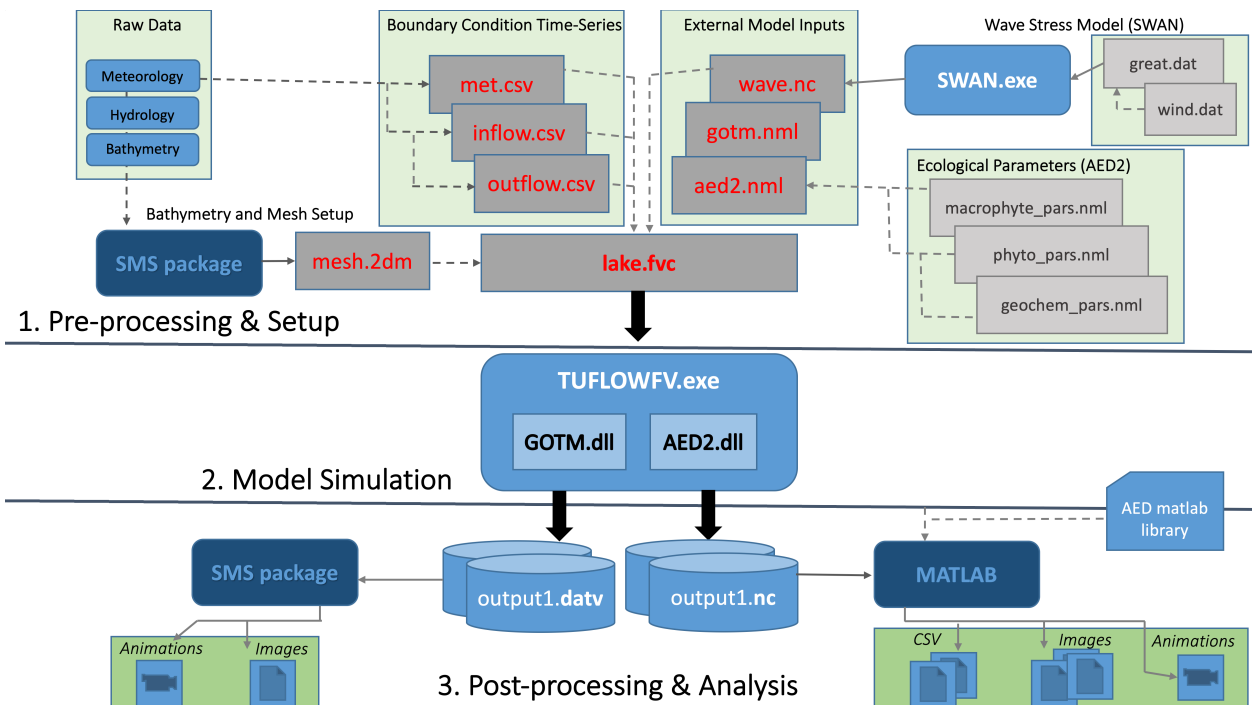


Figure 1. Organisation of data, files and models for a coupled TUFLOW-FV – AED2 simulation.

2.2 Hydrodynamics

TUFLOW-FV is a 3D flexible-mesh (finite volume) hydrodynamic model to simulate the water level, velocity and temperature within the lake (<http://tuflow.com>, BMTWBM, 2014). The model accounts for variations in water level, the horizontal salinity distribution and vertical density stratification in response to inflows, salt-wedge dynamics and surface thermodynamics. The mesh (in plan view), consists of triangular and quadrilateral elements of different size that are suited to simulating the morphometry within the lake littoral zone, islands and embayments. The vertical mesh discretization uses a hybrid scheme usually set with a variable thickness z-coordinate scheme for the permanently inundated region, and sigma coordinates within the region of water level variation. The finite volume numerical scheme solves the conservative integral form of the non-linear shallow water equations in addition to the advection and transport of scalar constituents such as temperature, as well as the state variables from the coupled biogeochemical model. Surface momentum exchange and heat dynamics are solved internally within TUFLOW-FV, where appropriate meteorological boundary conditions are supplied. In the current application, turbulent mixing of momentum and scalars has been calculated using the Smagorinsky scheme in a horizontal plane and through coupling with the General Ocean Turbulence Model (GOTM) for vertical mixing (Umlauf and Burchard, 2003).

In order to predict resuspension in shallow regions, it is necessary to account for the contribution of surface waves to the shear stress at the lake-bed. The wave climate (e.g., significant wave height, wave period and wave length) can be highly variable within the lake due to changes in fetch, water depth and wind-speed. To simulate wave properties (and

subsequent impacts such as resuspension) it is possible to use the SWAN model, however, that was not utilised in these simulations.

For the application to Lake Erie, the model mesh was designed to have high resolution in the littoral zones and embayments (Figure 2). The model mesh was designed using principles of mesh generation and aiming to capture a resolution that compromises resolution with computation run-times. The cell length scales vary from ~200 – 2800m, with an average cell length of ~1000m. This compares with prior studies using FVCOM (Niu, 2015), POM (Schwab et al., 2009) and ELCOM (Leon et al., 2011; Valipour et al., 2015), which have adopted resolutions ranging from ~600m to 2000m.

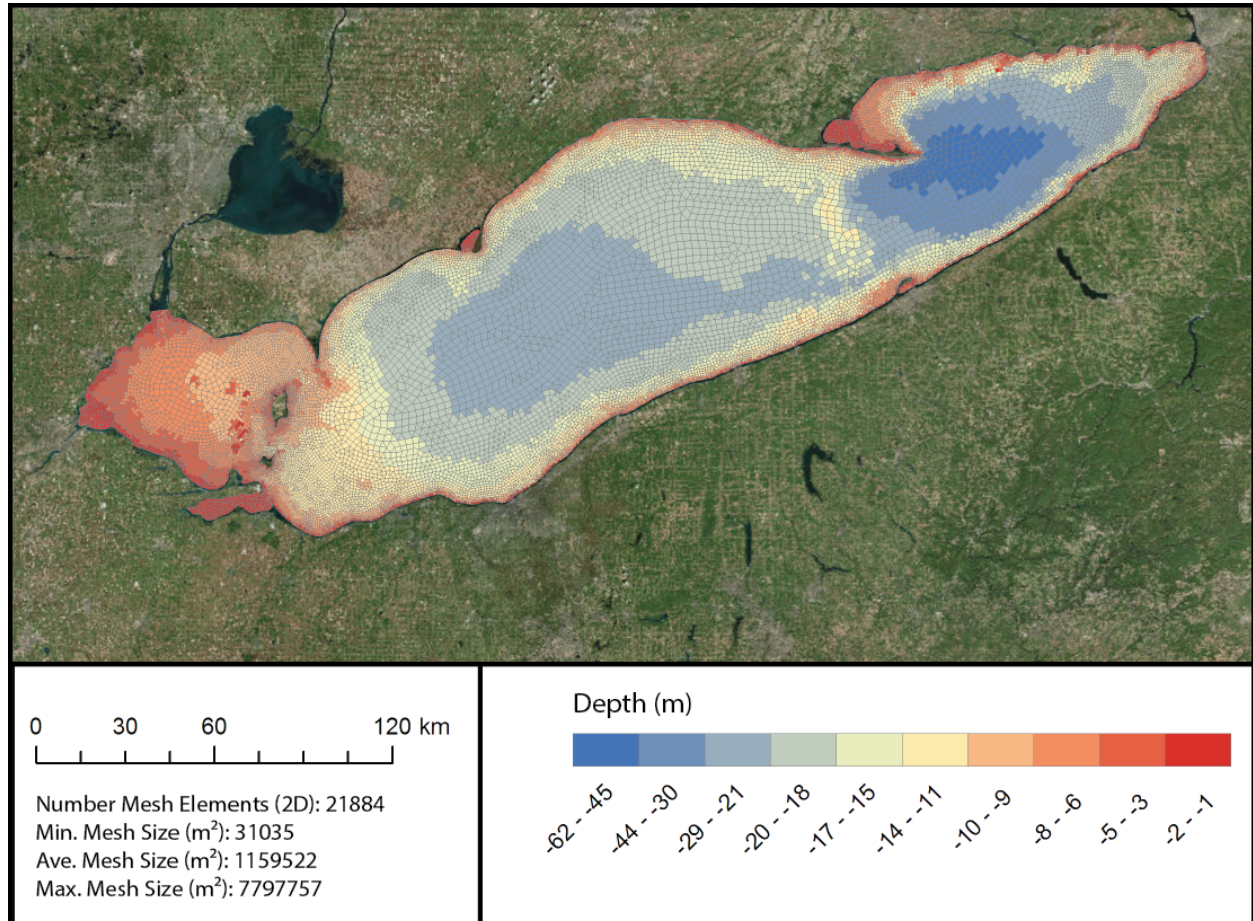


Figure 2. Finite Volume mesh used for the Lake Erie hydrodynamic-water quality simulations.

Boundary conditions were configured as for the previous ELCOM-CAEDYM simulations (Leon et al., 2011) with 3 meteorological forcing regions, and 6 river inputs (Table 1). Data for boundary conditions for the inflows and meteorological conditions were setup spanning the period matching previous ELCOM simulations, based on data provided by EC.

Table 1. Summary of the boundary condition data used for the simulations and testing.

Boundary Condition	Description
<i>Meteorological forcing</i>	West basin Central basin East basin
<i>Rivers</i>	Niagara (ID Nia) Detroit (ID Det) Maumee River (ID Mau) Cuyahoga River (ID Cuy) Grand River (ID Gra_ON) Sandusky (ID SND)

2.3 Biogeochemistry

The AED2 model framework was used to simulate biogeochemistry and water quality variables. It has been developed in response to the need to develop improved standards and flexibility in model integration as part of an active development community (Trolle et al., 2012; Hipsey et al., 2019). It has been designed to facilitate integration of different biogeochemical/ecological model approaches (both process-based and empirical), model currencies and to enable coupling with a diverse array of physical (hydrodynamic) driver models. The mathematical approach implemented in the AED modules has a similar basis to other aquatic ecological models, including the model CAEDYM used previously for Lake Erie.

The AED2 Model has ability to simulate a range of physical, chemical and biological processes, that can be generally classified as:

- Feedback of chemical or biological attributes to physical properties of water (light extinction, drag, density)
- Water column kinetic (time-varying) chemical / biological transformations (e.g., denitrification or algal growth)
- Water column equilibrium (instantaneous) chemical transformations (e.g., PO₄ adsorption)
- Biogeochemical transformations in the sediment or biological changes in the benthos
- Vertical sedimentation or migration
- Fluxes across the air-water interface
- Fluxes across the sediment-water interface
- Fluxes across the terrestrial-water interface (riparian interactions)
- Ecohydrological dynamics and biogeochemical transformations in the exposed (dry) cells
- Feedbacks of soil and vegetation dynamics onto lake hydrodynamics and water balance

The model is organised as a series of "modules" that can be connected or "linked" through specific variable dependencies. The AED modules are highly flexible and support simulation of various water quality aspects, but in this study the modules are configured to simulate the C, N, P and DO, including the inorganic nutrients, organic matter, and phytoplankton. For this configuration, four dissolved inorganic nutrients (FRP, NO₃, NH₄, PIP), three dissolved (DOC, DON, DOP) and three particulate (POC, PON, POP) detrital organic matter groups, and dissolved oxygen (DO) were modelled plus 5 phytoplankton groups. The simulated state variables, which are mixed, transported and subject to boundary forcing by the hydrodynamic model, are listed in Table 2, along with other derived properties useful for comparison with field data (e.g., TN, TP).

For detailed overview of these variables and how they are computed the reader is referred to the AED2 online manual. A summary of parameters used in the oxygen nutrient and phytoplankton modules is included in Appendix A.

Table 2: Simulated water column and benthic variables as part of TUFLOW-FV – AED2 Lake Erie simulations. Note sediment biogeochemical variables are listed separately in Table 10.

Variable	Units *	Common Name	Process Description
Physical variables			
<i>hs, he, hi</i>	m	Thickness of ice and snow layers	Ice simulated by TUFLOW-FV, subject to surface heating/melting and cooling, heat conduction, and ablation.
V	m s ⁻¹	Velocity	Velocity simulated by TUFLOW-FV, impacting density. Subject to inflow and wind boundary conditions, plus simulation of density gradients.
T	°C	Temperature	Temperature modelled by TUFLOW-FV, subject to surface heating and cooling processes
S	psu	Salinity	Salinity simulated by TUFLOW-FV, impacting density. Subject to tributary, drain and groundwater inputs, and evapo-concentration
EC	uS cm ⁻¹	Electrical conductivity	Derived from salinity variable
I _{PAR}	mE m ⁻² s ⁻¹	Shortwave light intensity	The PAR fraction of incident light, I ₀ , is attenuated as a function of depth
I _{UV}	mE m ⁻² s ⁻¹	UV light intensity	The UV fraction of incident light, I ₀ , is attenuated as a function of depth
η_{PAR}	m ⁻¹	PAR extinction coefficient	Bandwidth specific extinction coefficient computed based on organic matter and suspended material
η_{UV}	m ⁻¹	UV extinction coefficient	
Core biogeochemical variables			
DO	mmol O ₂ m ⁻³	Dissolved oxygen	Impacted by photosynthesis, organic decomposition, nitrification, surface exchange, and sediment oxygen demand
RSi	mmol Si m ⁻³	Reactive Silica	Algal uptake and subsequent sedimentation, sediment flux
FRP	mmol P m ⁻³	Filterable reactive phosphorus	Algal uptake, organic mineralization, sediment flux; adsorption/desorption to/from particles
FRP-ADS	mmol P m ⁻³	Particulate inorganic phosphorus	Adsorption/desorption of/to free FRP
NH ₄ ⁺	mmol N m ⁻³	Ammonium	Algal uptake, nitrification, organic mineralization, sediment flux
NO ₃ ⁻	mmol N m ⁻³	Nitrate	Algal uptake, nitrification, denitrification, sediment flux
N ₂ O [.]	mmol N m ⁻³	Nitrous oxide	Nitrifications, denitrification and atmospheric exchange
DOC	mmol C m ⁻³	Dissolved organic carbon	
DON	mmol N m ⁻³	Dissolved organic nitrogen	
DOP	mmol P m ⁻³	Dissolved organic phosphorus	
POC	mmol C m ⁻³	Particulate organic carbon	
PON	mmol N m ⁻³	Particulate organic nitrogen	
POP	mmol P m ⁻³	Particulate organic phosphorus	
TP	mmol P m ⁻³	Total Phosphorus	Sum of all P state variables
TN	mmol N m ⁻³	Total Nitrogen	Sum of all N state variables
TKN	mmol N m ⁻³	Total Kjedahl Nitrogen	Sum of relevant N state variables
CDOM	mmol C m ⁻³	Chromophoric Dissolved Organic Matter	Related from DOC-R and DOC concentrations
Plankton groups			
BGA	mmol C m ⁻³	Cyanobacteria	
CRYPT	mmol C m ⁻³	Cryptophytes	
DIATOM	mmol C m ⁻³	Diatoms	
DINO	mmol C m ⁻³	Dinoflagellate group	
GRN	mmol C m ⁻³	Chlorophytes	
TCHLA	ug Chla L ⁻¹	Total Chlorophyll-a	Sum of the algal groups, converted to pigment concentration
Benthic groups			
BIV	mmol C m ⁻²	Bivalve (mussel) biomass	Filtration, excretion, respiration and mortality; refer to Section 4
CGM	mmol C m ⁻²	Attached macroalgal (cladophora) biomass	Photosynthesis, respiration and sloughing, refer to Section 5
SLG	mmol C m ⁻³	Free-floating macroalgal (cladophora) biomass	Photosynthesis, respiration and drifting, refer to Section 5
Suspended sediment and related properties			
SS _s	g SS m ⁻³	Suspended solids groups	Settling, resuspension
Turbidity	NTU	Turbidity	Computed based on SS, TCHLA and POM

3 TUFLOW-FV Ice Model Development

The ice cover module in TUFLOW FV was developed based on the one-dimensional (vertical) model of Rogers et al. (1995) and Oveisy et al. (2012). The model consists of an ice cover development that may consist of three layers: blue ice, white ice (also known as snow-ice) and snow. White ice and snow layers only occur if snowfall is taken into consideration. The model assumes the ice-cap is immobile, therefore it does not predict ice transport in the surface layer. It also assumes the heat budget is in equilibrium over the time step.

The ice cover representation schematic is shown in Figure 3 below:

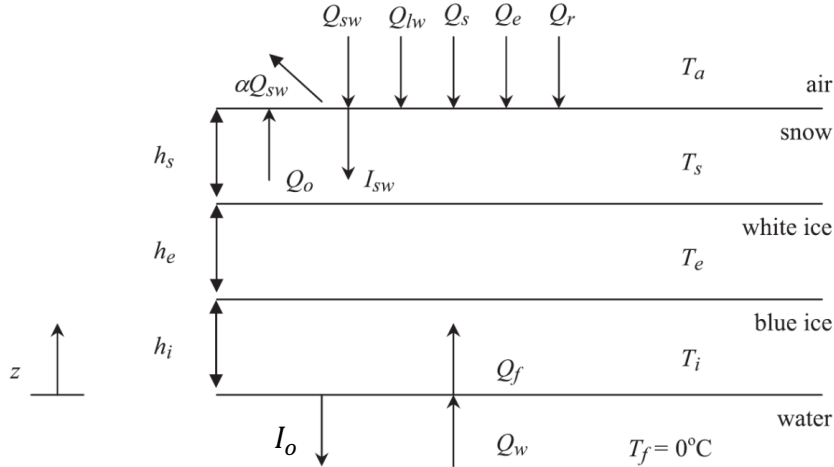


Figure 3. Schematic of heat fluxes and vertical layers considered in the ice-cover model

3.1 Model Formulation

The heat conduction equation through the ice is given by the following (Oveisy et al., 2012):

$$\kappa_h \frac{\partial^2 T}{\partial z^2} = \frac{1}{\rho_n c_n} \frac{\partial Q}{\partial z}$$

Defining the thermal conductivity as

$$K = \kappa_h \rho_n c_n$$

and a Beer's law equation for the radiation penetrating through the ice

$$I = I_{sw} e^{-\lambda(h-z)}$$

the schematic in Figure 3 leads to:

$$K_s \frac{\partial^2 T_s}{\partial z^2} = A_1 \lambda_{s1} I_{sw} e^{[-\lambda_{s1}(h_i+h_e+h_s-z)]} + A_2 \lambda_{s2} I_{sw} e^{[-\lambda_{s2}(h_i+h_e+h_s-z)]} + Q_{si} = 0, \\ \text{for } h_i + h_e + h_s \geq z \geq h_i + h_e;$$

$$K_e \frac{\partial^2 T_e}{\partial z^2} = A_1 \lambda_{e1} I_{sw} e^{[-\lambda_{s1}h_s - \lambda_{e1}(h_e+h_i-z)]} + A_2 \lambda_{e2} I_{sw} e^{[-\lambda_{s2}h_s - \lambda_{e2}(h_e+h_i-z)]} = 0, \\ \text{for } h_e + h_i \geq z \geq h_i; \text{ and}$$

$$K_i \frac{\partial^2 T_i}{\partial z^2} = A_1 \lambda_{i1} I_{sw} e^{[-\lambda_{s1}h_s - \lambda_{e1}h_e - \lambda_{i1}(h_i-z)]} + A_2 \lambda_{i2} I_{sw} e^{[-\lambda_{s2}h_s - \lambda_{e2}h_e - \lambda_{i2}(h_i-z)]} = 0, \\ \text{for } h_i \geq z \geq 0;$$

where the incoming solar radiation I_{sw} is given by

$$I_{sw} = (1 - \alpha Q_{sw})$$

α is the snow or ice cover albedo and Q_{sw} is the incident solar radiation. In the approximation, the solar radiation has been split into two components $A_1=0.7$ and $A_2=0.3$, representing the visible and near infrared bands of the light

spectrum, respectively. The subscripts s , e and i refer to the snow, white ice and blue ice, respectively, therefore λ being assigned for the equivalent light spectra and ice layer. Q_{si} is the heat flux per volume released from white-ice formation. In this case, the white ice forms as a result of flooding of snow. The albedo is calculated according to Vavrus et al. (1996):

$$\text{Ice: } \begin{cases} \alpha_i = 0.6 \rightarrow T_a \leq -5^\circ C \\ \alpha_i = 0.44 - 0.032T_a \rightarrow -5^\circ C \leq T_a \leq 0^\circ C \\ \alpha_i = 0.44 \rightarrow T_a \geq 0^\circ C \\ \alpha_i = 0.08 - 0.44(h_i + h_e)^{0.28} \rightarrow h_i + h_e \leq 0.5m \end{cases}$$

$$\text{Snow: } \begin{cases} \alpha_{s_o} = 0.7 \rightarrow T_a \leq -5^\circ C \\ \alpha_{s_o} = 0.50 - 0.04T_a \rightarrow -5^\circ C \leq T_a \leq 0^\circ C \\ \alpha_{s_o} = 0.50 \rightarrow T_a \geq 0^\circ C \\ \alpha_s = \alpha_{s_o} - \left(\frac{0.1-h_i}{0.1}\right)(\alpha_{s_o} - \alpha_i) \rightarrow \begin{matrix} h_i + h_e \leq 0.5m \\ h_s \leq 0.1m \end{matrix} \end{cases}$$

Applying the following boundary conditions

$$\begin{aligned} T_i &= T_f = 0 & z = 0 \\ \left. \begin{aligned} T_i &= T_e \\ K_i \frac{\partial T_i}{\partial z} &= K_e \frac{\partial T_e}{\partial z} \end{aligned} \right\} && z = h_i \\ \left. \begin{aligned} T_e &= T_s \\ K_e \frac{\partial T_e}{\partial z} &= K_s \frac{\partial T_s}{\partial z} \end{aligned} \right\} && z = h_i + h_e \\ T_s &= T_a & z = h_i + h_e + h_s \end{aligned}$$

to the equation above leads to

$$\begin{aligned} &\left(\frac{h_s}{K_s} + \frac{h_e}{K_e} + \frac{h_i}{K_i} \right) (Q_o - I_{sw}) = T_f - T_a \\ &- A_1 I_{sw} \left[\frac{1 - e^{-\lambda_{s1} h_s}}{K_s \lambda_{s1}} + \frac{e^{-\lambda_{s1} h_s}}{K_e \lambda_{e1}} (1 - e^{-\lambda_{e1} h_e}) + \frac{e^{(-\lambda_{s1} h_s - \lambda_{e1} h_e)}}{K_i \lambda_{i1}} (1 - e^{-\lambda_{i1} h_i}) \right] \\ &- A_2 I_{sw} \left[\frac{1 - e^{-\lambda_{s2} h_s}}{K_s \lambda_{s2}} + \frac{e^{-\lambda_{s2} h_s}}{K_e \lambda_{e2}} (1 - e^{-\lambda_{e2} h_e}) + \frac{e^{(-\lambda_{s2} h_s - \lambda_{e2} h_e)}}{K_i \lambda_{i2}} (1 - e^{-\lambda_{i2} h_i}) \right] \\ &+ Q_{si} h_s \left(\frac{h_s}{K_s} + \frac{h_e}{K_e} + \frac{h_i}{K_i} \right) - \frac{Q_{si} h_s^2}{2K_s} \end{aligned}$$

This equation is solved so the resulting outgoing heat flux Q_o and external meteorological forcing are in balance by adjusting T_a , the temperature at the snow (or ice) interface. The resulting T_a will then control surface melting, thus:

$$Q_o(T_a) + H(T_a) = \begin{cases} 0, & T_a < T_m \\ -\rho L \frac{dh}{dt}, & T_a = T_m \end{cases}$$

where the density ρ and melted thickness h depend on the property of the surface medium (i.e. snow, white ice or blue ice). $H(T_a)$ is the net incoming meteorological flux:

$$H(T_a) = Q_{lw}(T_a) + Q_s(T_a) + Q_e(T_a) + Q_r(T_a)$$

where Q_{lw} is the long wave radiation, Q_s is the sensible heat flux, Q_e is the latent heat flux and Q_r is the heat flux associated with rainfall. These terms are calculated similarly to TVA (1972).

The heat flux from ice to water Q_f is given as follows:

$$Q_f = Q_o - A_1 I_{sw} \{ 1 - e^{[-(\lambda_{s1} h_s + \lambda_{e1} h_e + \lambda_{i1} h_i)]} \} - A_2 I_{sw} \{ 1 - e^{[-(\lambda_{s2} h_s + \lambda_{e2} h_e + \lambda_{i2} h_i)]} \}$$

The heat flux from water to ice Q_w is given by the contribution of molecular and turbulent fluxes:

$$Q_w = Q_m + Q_t$$

where

$$Q_m = -K_w \frac{dT_w}{dz} \Big|_{z=0}$$

and

$$Q_t = C_s \rho_w C_p U_w (T_w - T_f)$$

where K_w is the water heat conductivity, C_s is sensible heat transfer coefficient, ρ_w is the water density and U_w is the water flow speed under the ice.

Ice production or melting at the water-ice interface is given by:

$$Q_f - Q_w = \rho_i L \frac{dh_i}{dt}$$

where t is time and ρ_i is the ice density.

3.2 Snow Properties

Snow conductivity is calculated as per the relation given in Ashton (1986).

$$K_s = 0.021 + 0.042\rho_s + 2.2 \times 10^{-9}\rho_s^3$$

The snow density is calculated based on fresh snow and rainfall. The following is adopted in TUFLOW FV, similarly to the relations in GLM (Hipsey et al. 2019b). Any fresh snow is given a minimum density, which can be specified by the user. The default value is $\rho_{s\min} = 50 \text{ kg/m}^3$. The snow density is also bounded by a maximum value that can also be specified by the user, with a default value $\rho_{s\max} = 300 \text{ kg/m}^3$. Compaction factor is given by:

$$C_F(T_a) = \begin{cases} 0.166 + 0.834(1 - e^{-P}), & T_a \leq 0 \\ 0.088 + 0.912(1 - e^{-P}), & T_a > 0 \end{cases}$$

where P is the daily rainfall rate. The existing snow pack density is the calculated as:

$$\rho_{s_e} = \rho_s + C_F(\rho_{s\max} - \rho_s)$$

3.3 White-Ice Formation

White ice is formed when the ice cap is not strong enough to support the weight of the snow. In this circumstance, the model assumes water floods the snow pack, thus forming white ice. This formulation is similar to Rogers et al. (1995) and Ovesi et al. (2012). The maximum height the ice cap can support is given by:

$$h_{s\max} = \frac{h_i(\rho_w - \rho_i) + h_e(\rho_w - \rho_e)}{\rho_s}$$

The conversion between snow and white ice layer thickness is then given by

$$\Delta h_e = h_s - h_{s\max}, h_s \geq h_{s\max}$$

The heat released in this process (note this is a heat flux per volume and not per area) is given by

$$Q_{si} = \frac{(T_w c_a + L_f) \rho_w \frac{\Delta h_e}{h_s} \left(1 - \frac{\rho_s}{\rho_w}\right)}{\Delta t}$$

3.4 Heat Flux from Rainfall

Heat flux is released from rainfall to the snow/ice cap due to sensible heat transfer or rain freezing, as follows:

$$Q_r = (T_a - T_o)P, T_a = 0^\circ C$$

$$Q_r = L_f \rho_o P, T_a < 0^\circ C$$

3.5 Accretion and Ablation of Ice

Accretion and ablation of ice (Δh_i) is calculated based on the balance between Q_f and Q_w as

$$\Delta h_i = \left(\frac{Q_f - Q_w}{\rho_i L_f} \right) dt$$

3.6 Water Temperature Prediction

Water temperature prediction is calculated by the distribution of the solar radiation heat conducted through the ice and snow cap. This distribution follows the same algorithms implemented in the heat module of TUFLOW-FV.

3.7 Adjustable Model Parameters

The following model parameters (Table 3) can be adjusted by the user, via the driver files (e.g., `erie.fvc`):

Table 3: Summary of ice model parameters and example/default values.

Parameter	Default Value
Maximum snow density: $\rho_{s_{max}}$	300 kg/m ³
Minimum snow density: $\rho_{s_{min}}$	80 kg/m ³
Heat conductivity of blue ice: K_i	2.3 W/m ² /°C
Heat conductivity of white ice: K_e	2.0 W/m ² /°C
Heat conductivity of water: K_w	0.57 W/m ² /°C
Density of blue ice: ρ_i	917 kg/m ³
Density of white ice: ρ_e	890 kg/m ³
Latent heat of fusion: L_f	334000 J/kg
Freezing or melting temperature: T_f or T_m	0.0 °C
Visible fraction of the light spectrum: A_1	0.7
Near-infrared fraction of the light spectrum: A_2	0.3
Light attenuation coefficients through blue ice: $\lambda_{i1}, \lambda_{i2}$	1.50, 20.0 m ⁻¹
Light attenuation coefficients through white ice: $\lambda_{e1}, \lambda_{e2}$	3.75, 20.0 m ⁻¹
Light attenuation coefficients through snow: $\lambda_{s1}, \lambda_{s2}$	6.00, 20.0 m ⁻¹

Initial conditions can also be supplied for h_i , h_e , h_s and ρ_s . These conditions can be both uniform or spatially distributed over the extent of the model. Additionally, the model can be restarted with ice conditions from a prior simulation.

The same parameters can be output in the form of NetCDF files. Specification of both initial conditions and output parameters are made via driver files in similar formats to the existing TUFLOW-FV specifications.

3.8 Lake Erie Ice Model Testing & Results

The Lake Erie model set-up operating for the period over 2013 and the 2013-2014 winter was adopted to test the ice model. The model has been populated with new meteorological boundary conditions for the lake freezing period (December to April). A simulation between October 2013 and May 2014 was undertaken with the default parameters in Table 1. Note that snowfall was not included as a boundary condition. As a result, only blue ice was simulated. It is expected further testing of the model will be undertaken by Environment Canada with improved data. Additionally, for this test, no manipulation of river input files was undertaken, such that their flow and temperature were kept constant for most of the simulation period.

Continuous temperature profiles were extracted from the central basin of Lake Erie (Figure a) are shown in 4b. These profiles indicate the model was able to conduct temperature simulations through the winter period. It is noted that initial water temperatures were not based on any observations and as such it is likely that the model was initialised too cold, as per the ensuing temperature increase.

Water temperatures did not drop below 0.0 °C, As indicated by the black colour map adopted for temperatures below 0 °C. Over the ice-covered period (December to May), water levels can be seen to reduce and subsequently increase. This drop is associated with freezing and melting of the ice cover. By mid May, lake temperatures started rising and stratification developed from June through September.

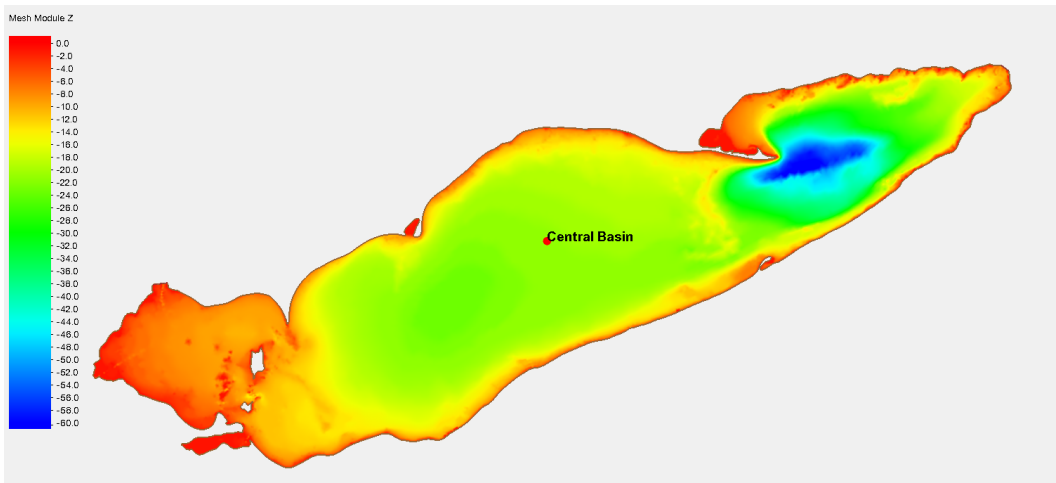


Figure 4a. Central Basin location at which temperature profiles were extracted

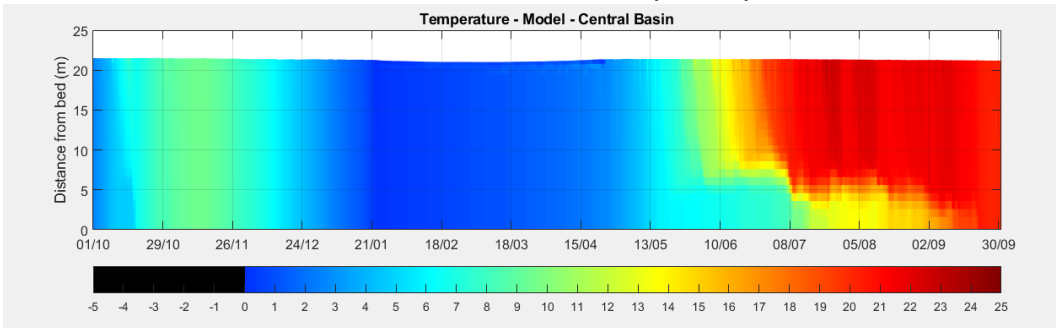


Figure 4b. Temperature evolution in Lake Erie Central Basin

In addition to temperatures results, blue-ice thicknesses are shown from the simulation start to the time at which no ice cover remained in the lake (Figure a – 5z). This example shows that the model was capable of producing and disintegrating the ice cover as a result of the meteorological forcing. Timing of freezing and melting as well as the general patterns of ice cover evolution were similar to the ones shown in the Great Lakes Environmental Research Laboratory Digital Ice Charts (https://www.glerl.noaa.gov/data/pgs/glice/glice_2014.html).

It is noted that lack of ice cover near the Detroit River mouth was a direct result of assigned temperatures at the inflow boundary conditions which require updating. Also, the persistent ice cover in north-eastern end of the lake is somewhat agreeable with the Digital Ice Charts (not shown). For a completely uncalibrated model, results are very encouraging.

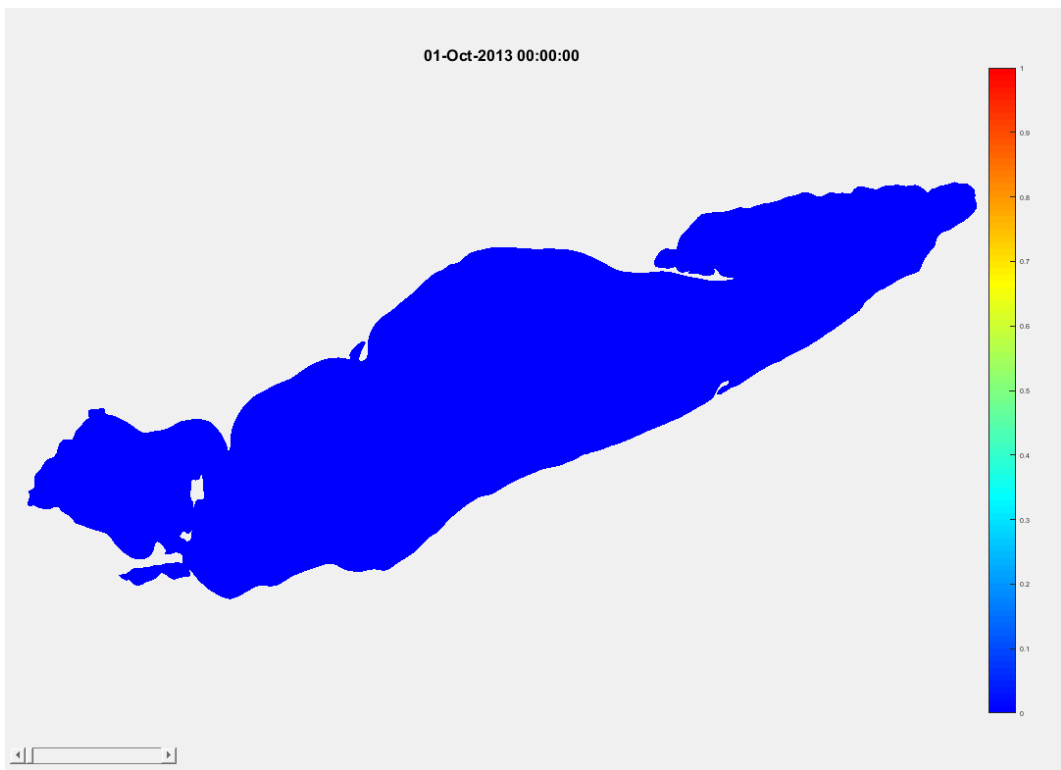


Figure 5a. Lake Erie, simulated Blue Ice thickness on 01/10/2013

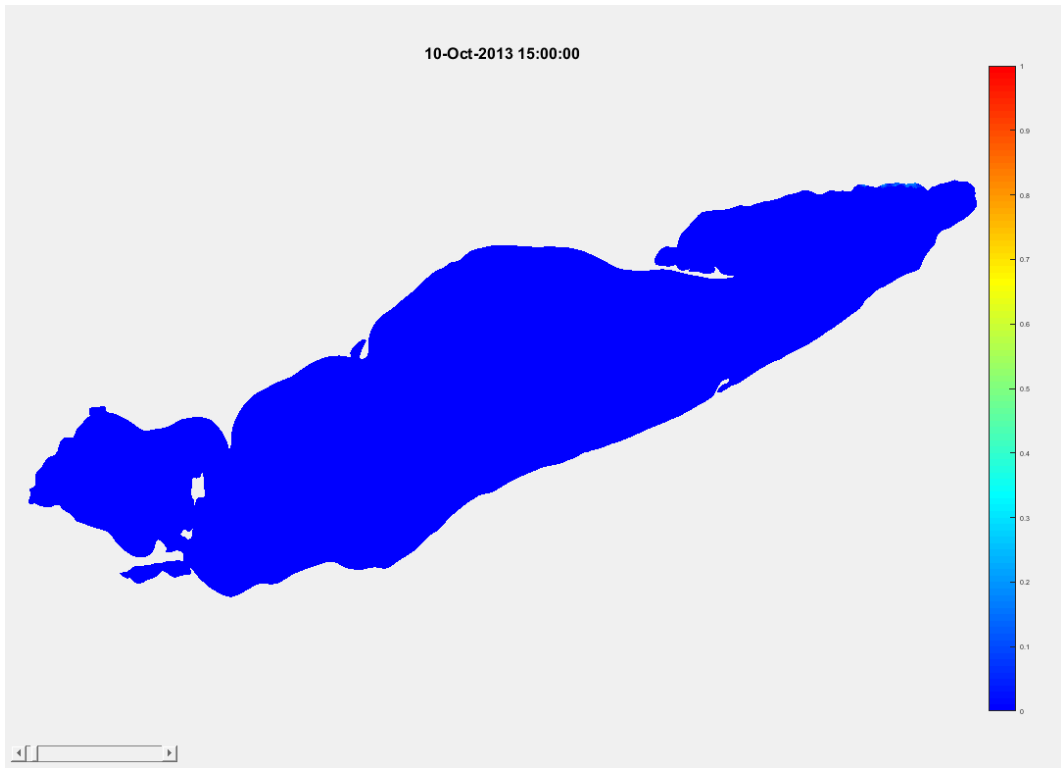


Figure 5b. Lake Erie, simulated Blue Ice thickness on 10/10/2013

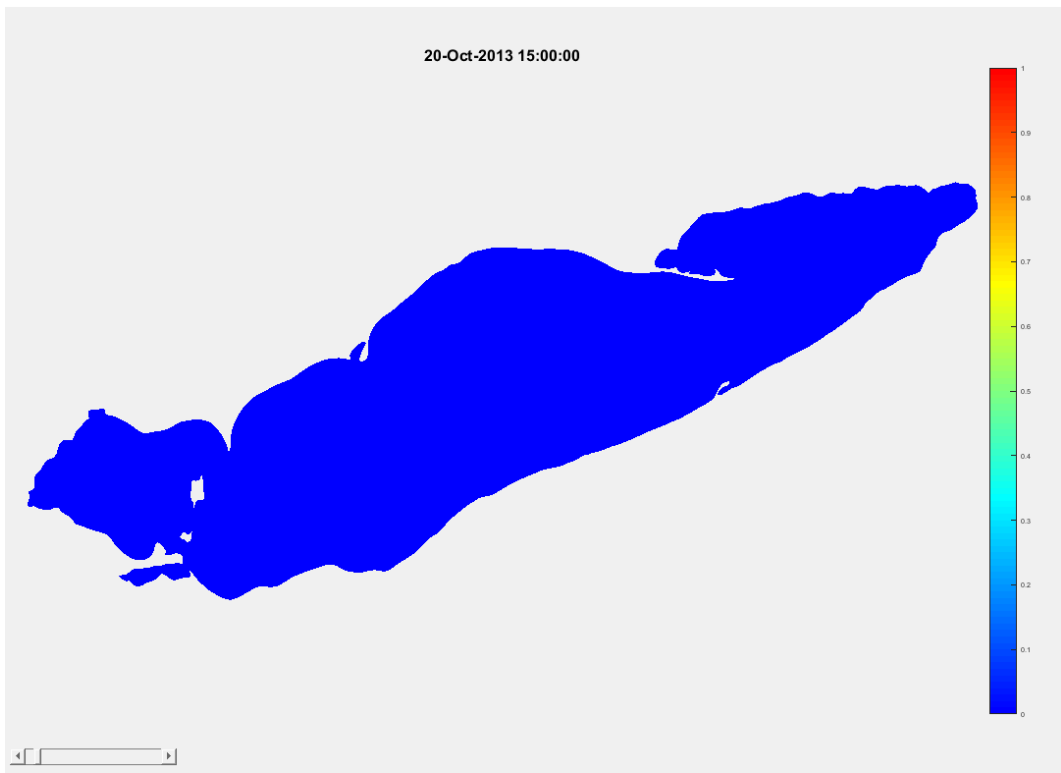


Figure 5c. Lake Erie, simulated Blue Ice thickness on 20/10/2013

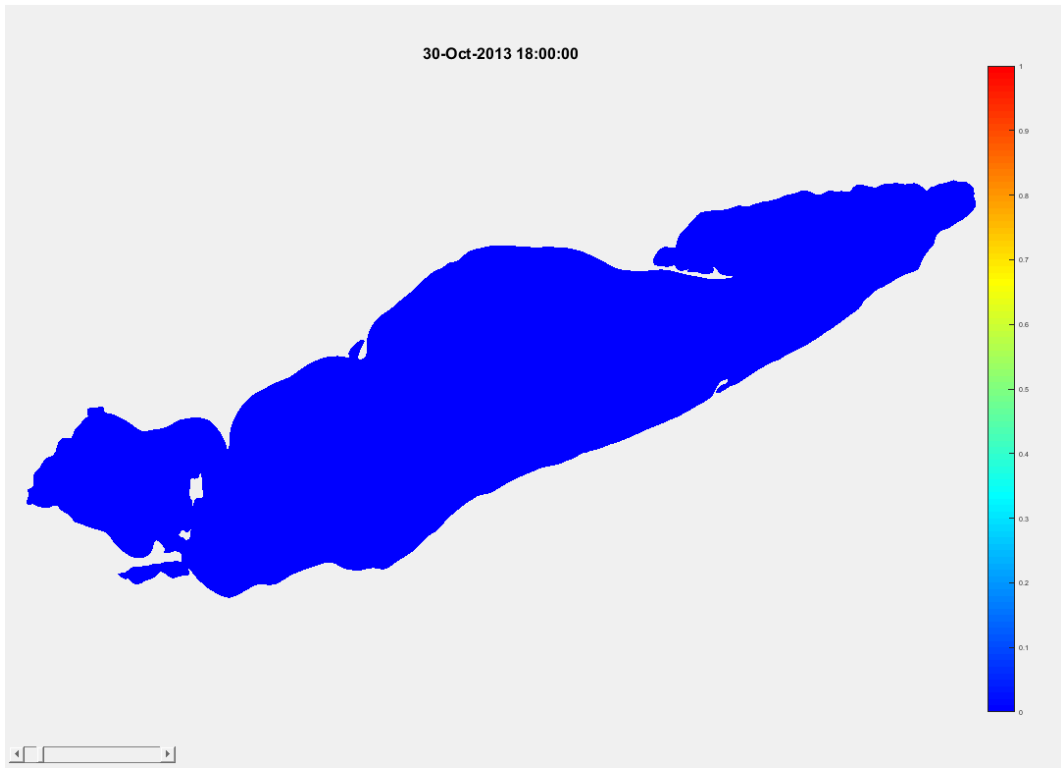


Figure 5d. Lake Erie, simulated Blue Ice thickness on 30/10/2013

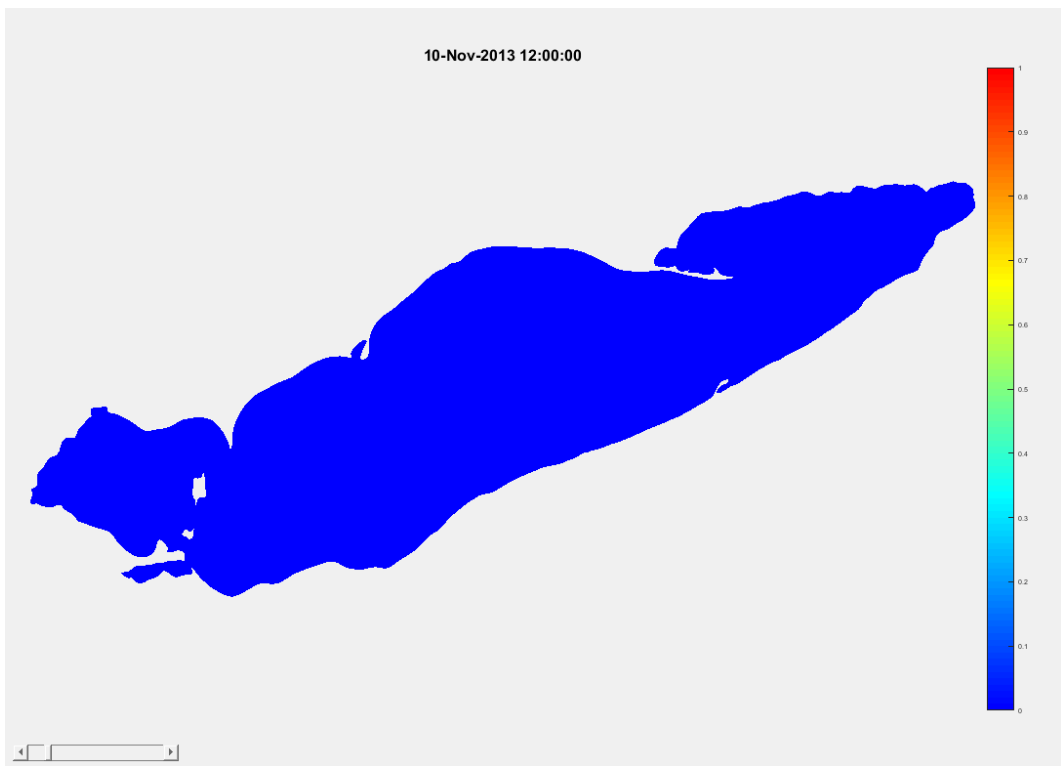


Figure 5e. Lake Erie, simulated Blue Ice thickness on 10/11/2013

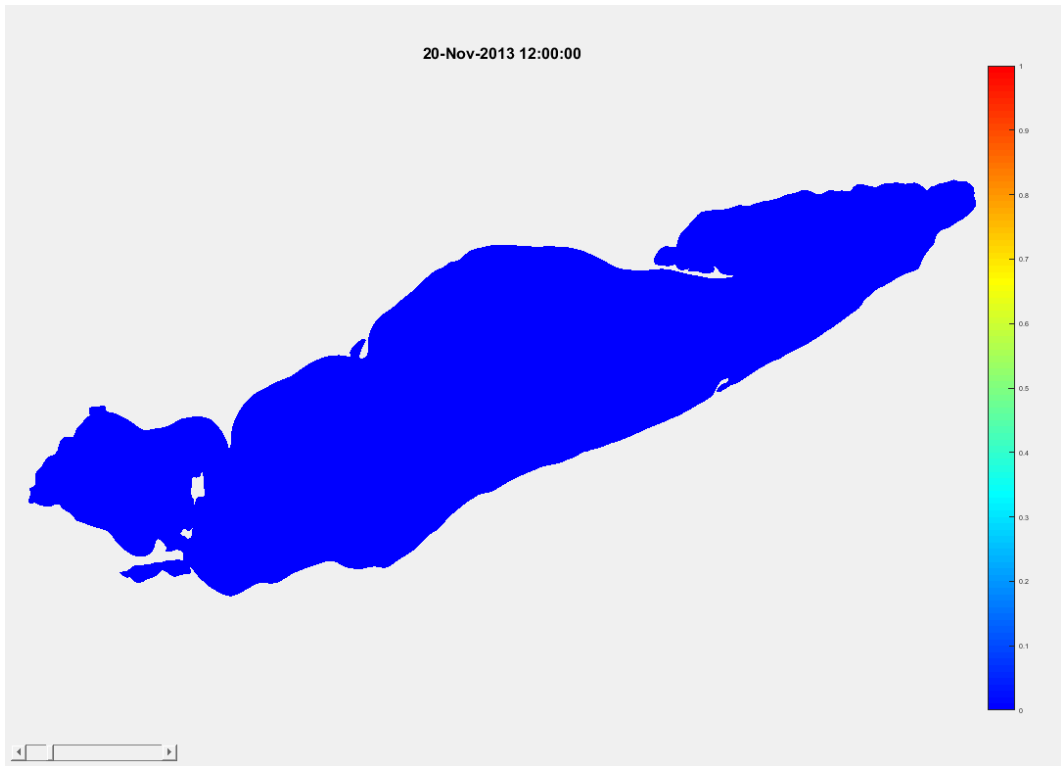


Figure 5f. Lake Erie, simulated Blue Ice thickness on 20/11/2013

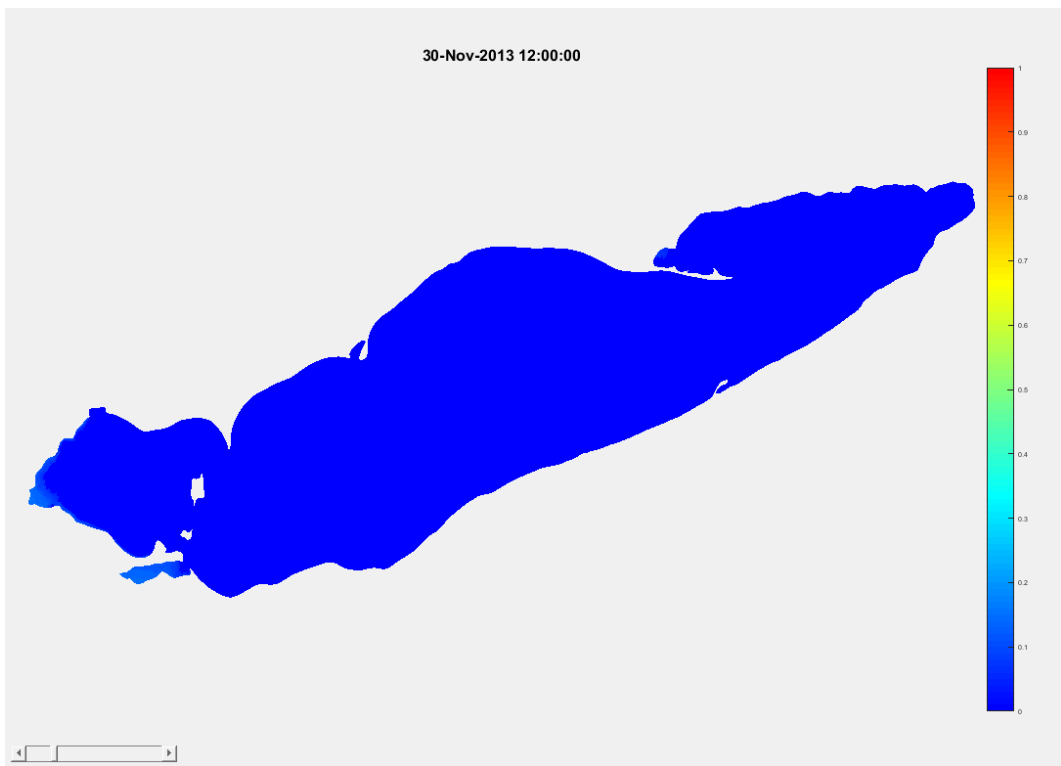


Figure 5g. Lake Erie, simulated Blue Ice thickness on 30/11/2013

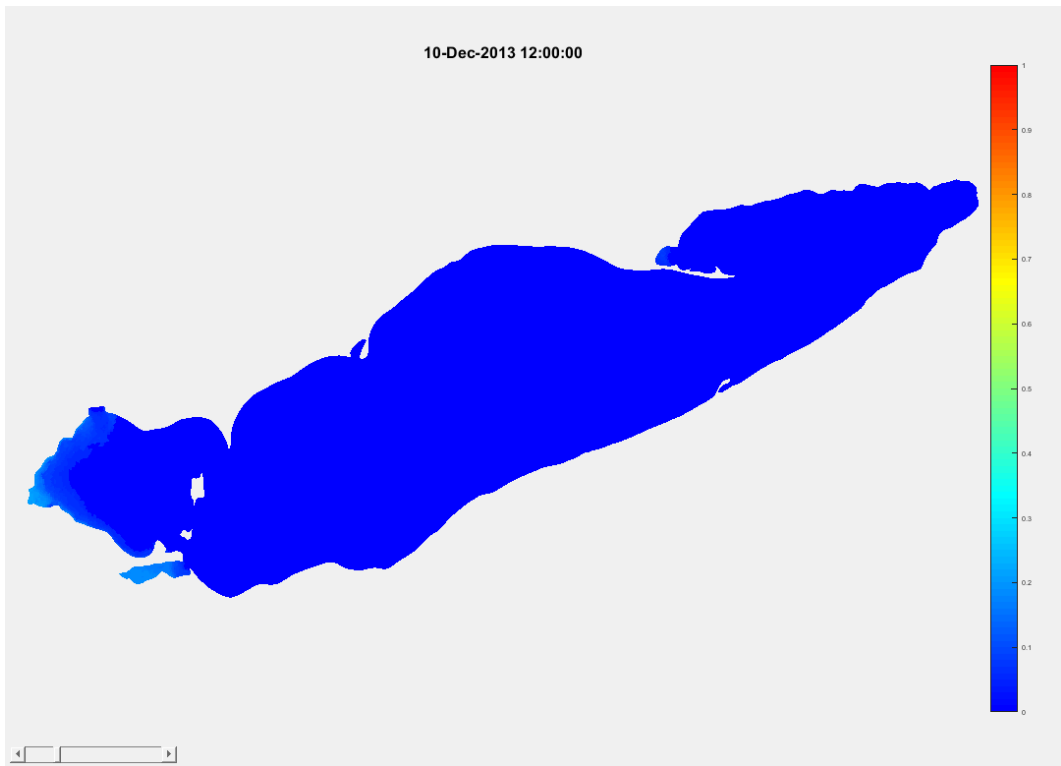


Figure 5h. Lake Erie, simulated Blue Ice thickness on 10/12/2013

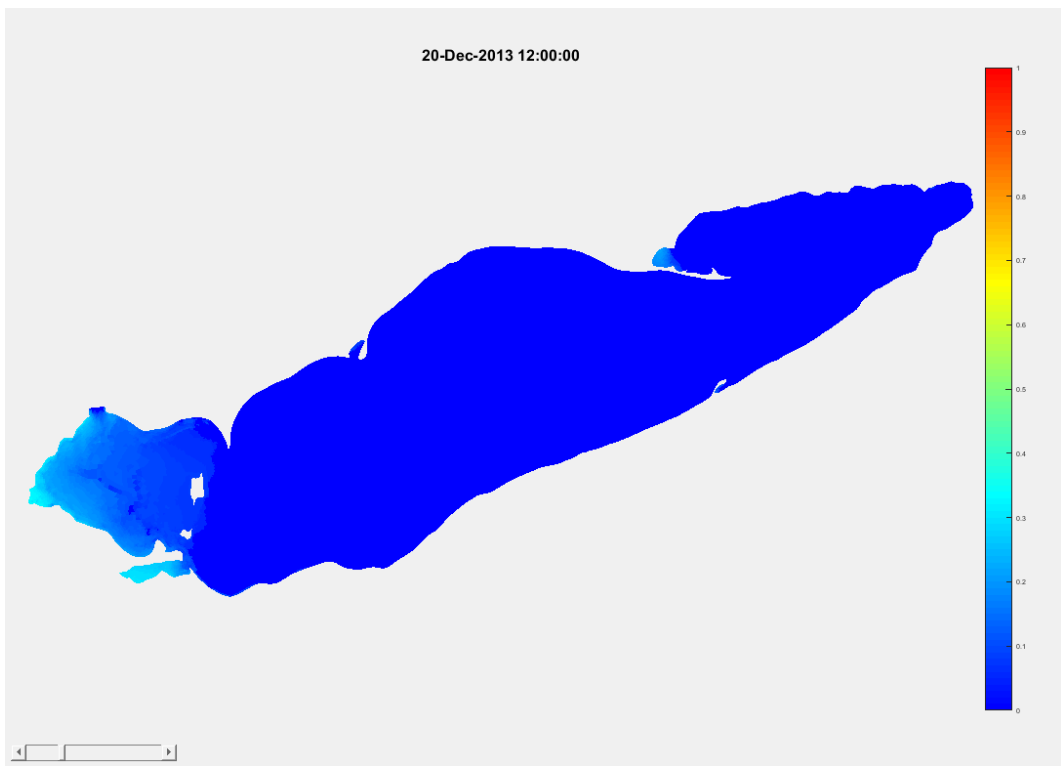


Figure 5i. Lake Erie, simulated Blue Ice thickness on 20/12/2013

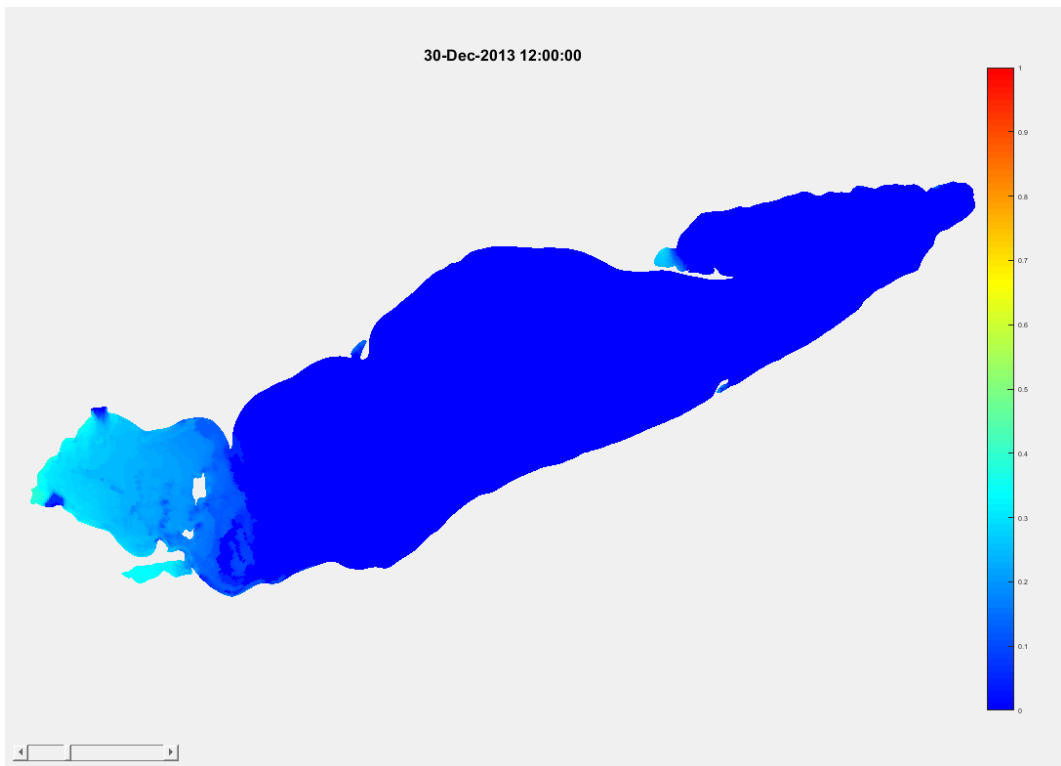


Figure 5j. Lake Erie, simulated Blue Ice thickness on 30/12/2013

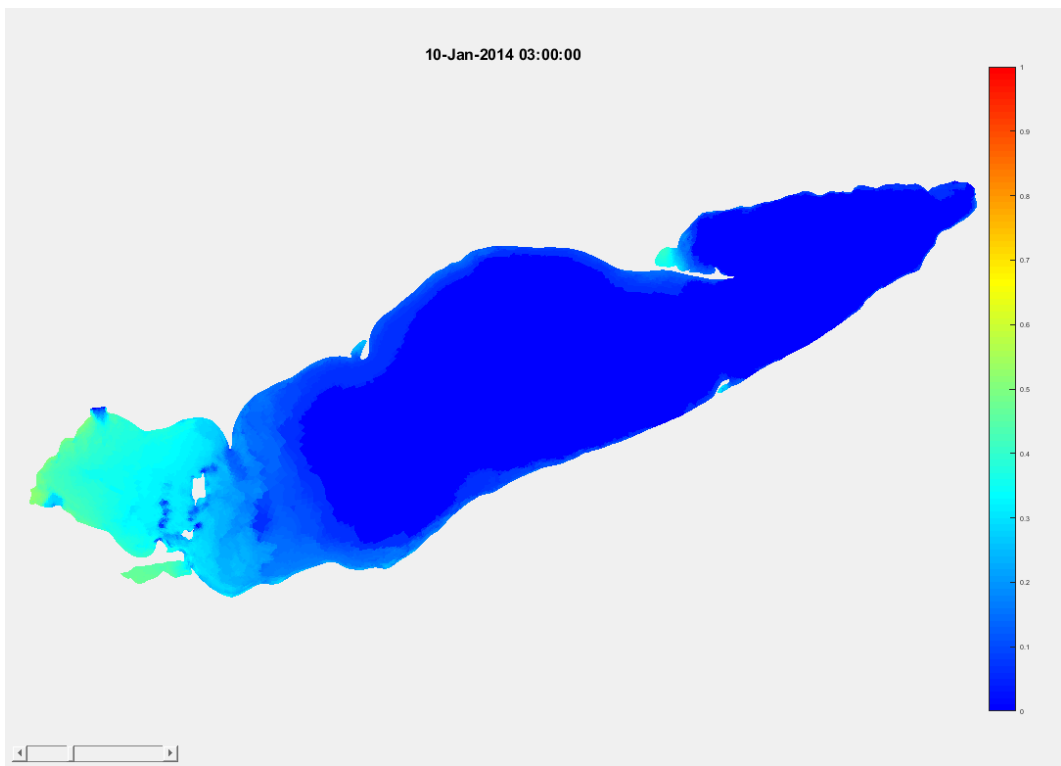


Figure 5k. Lake Erie, simulated Blue Ice thickness on 10/01/2014

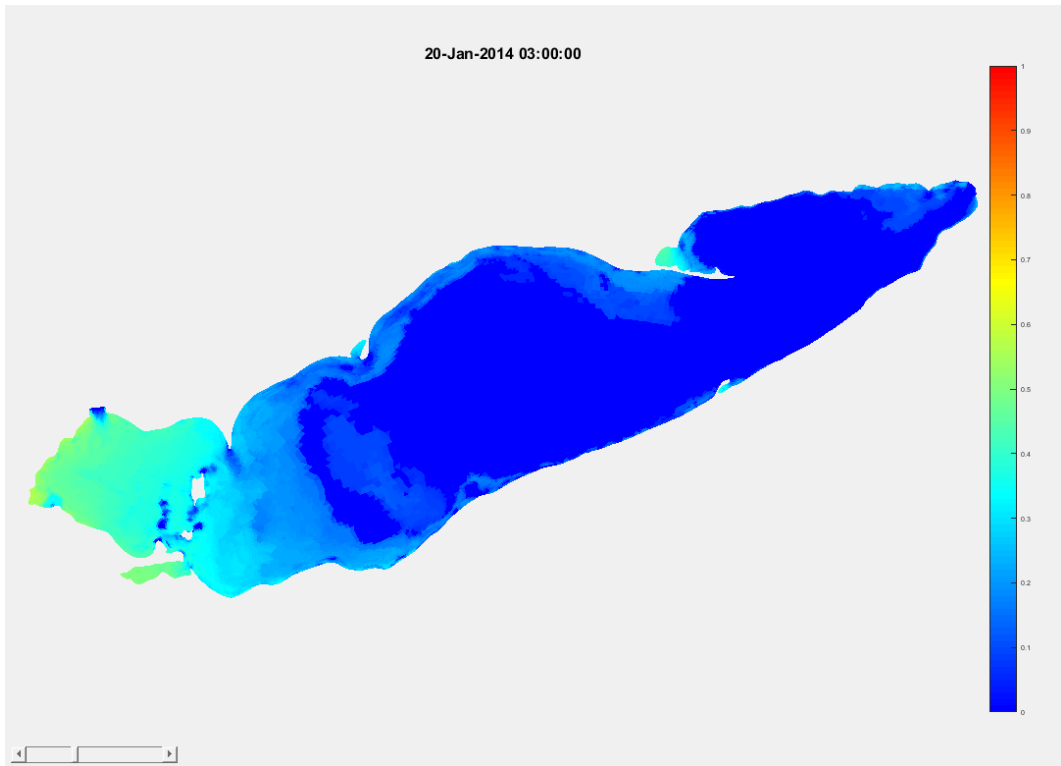


Figure 5l. Lake Erie, simulated Blue Ice thickness on 20/01/2014

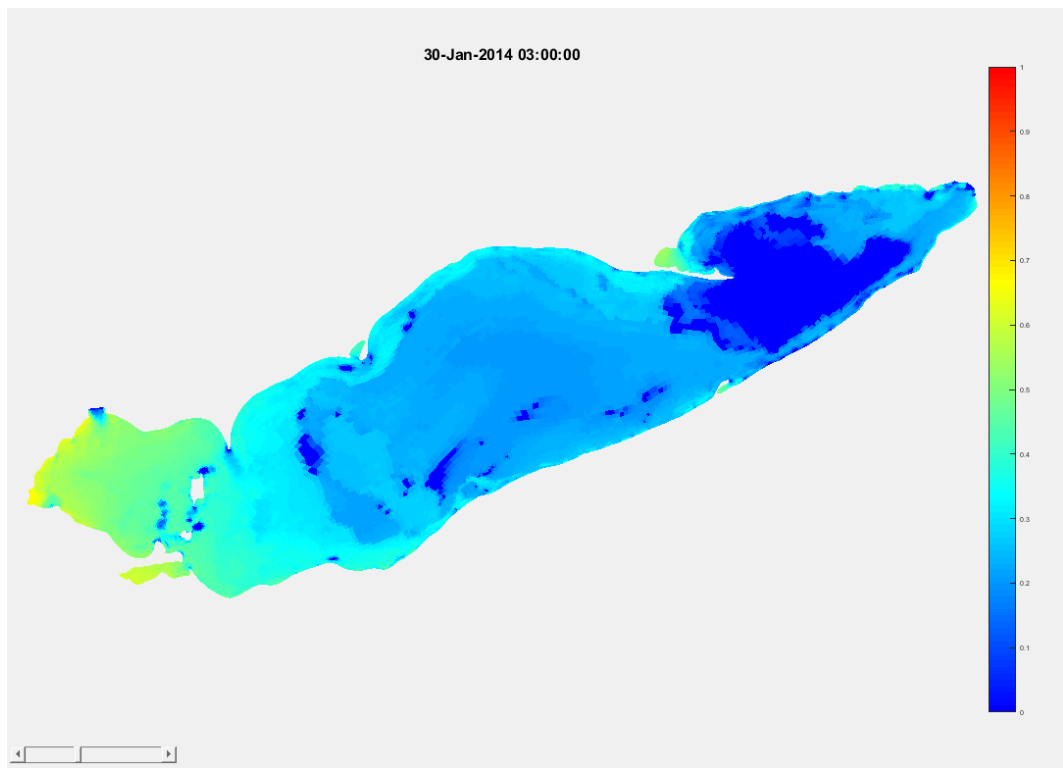


Figure 5m. Lake Erie, simulated Blue Ice thickness on 30/01/2014

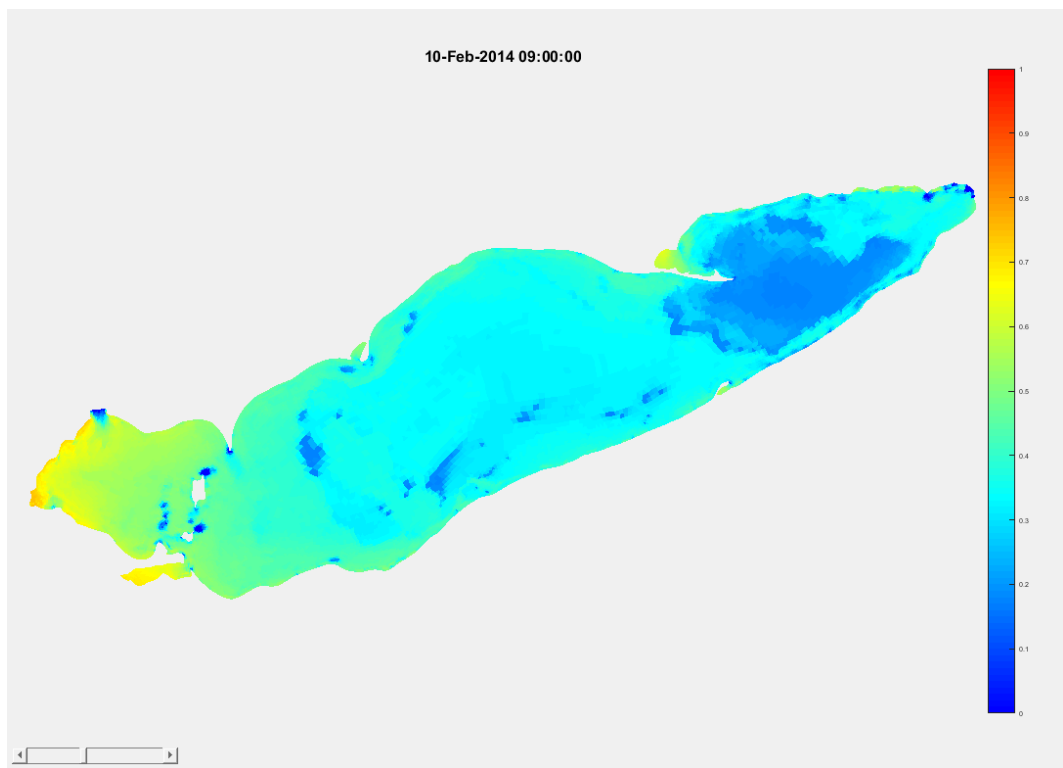


Figure 5n. Lake Erie, simulated Blue Ice thickness on 10/02/2014

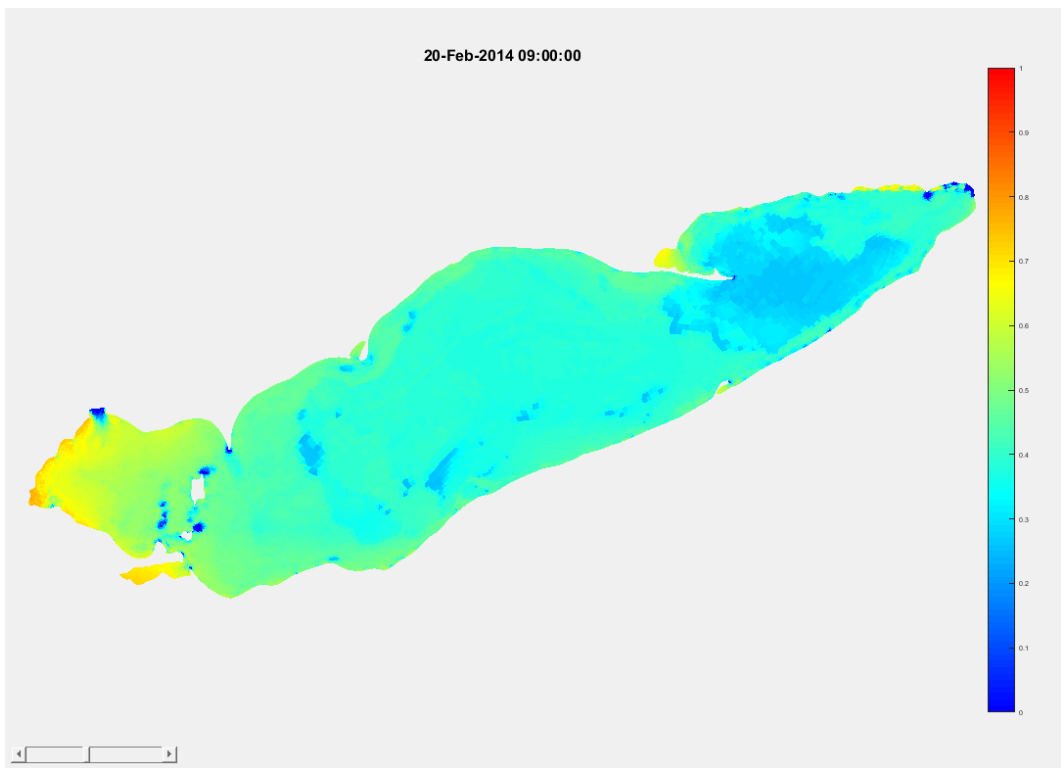


Figure 5o. Lake Erie, simulated Blue Ice thickness on 20/02/2014

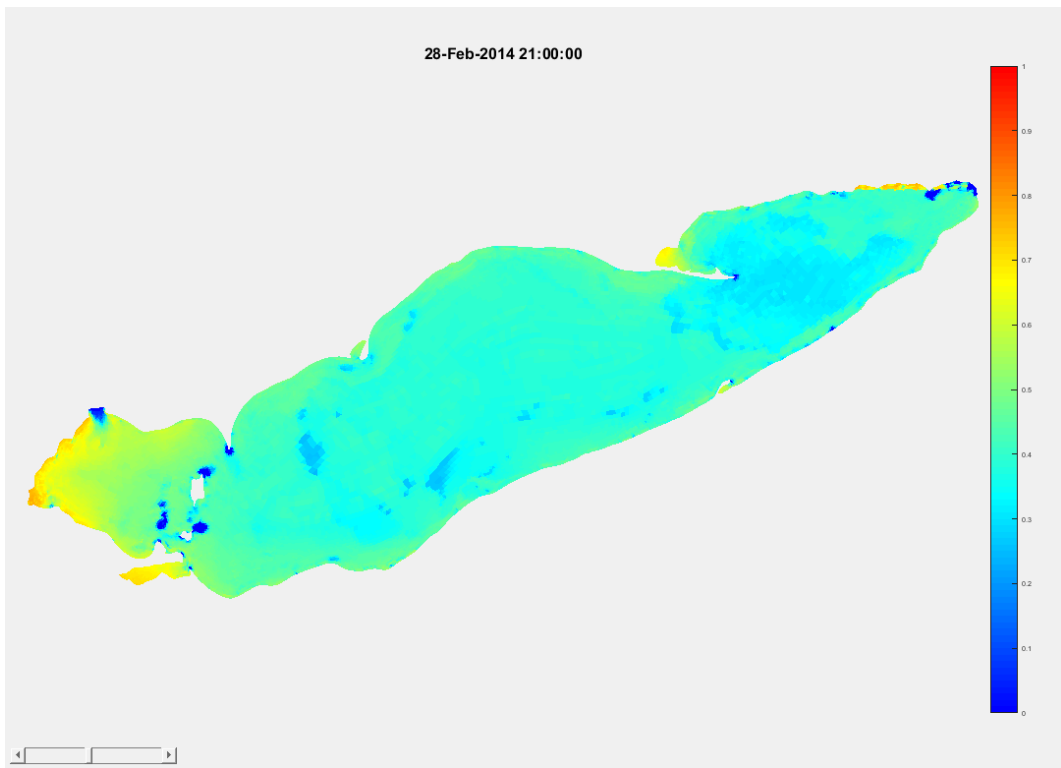


Figure 5p. Lake Erie, simulated Blue Ice thickness on 28/02/2014

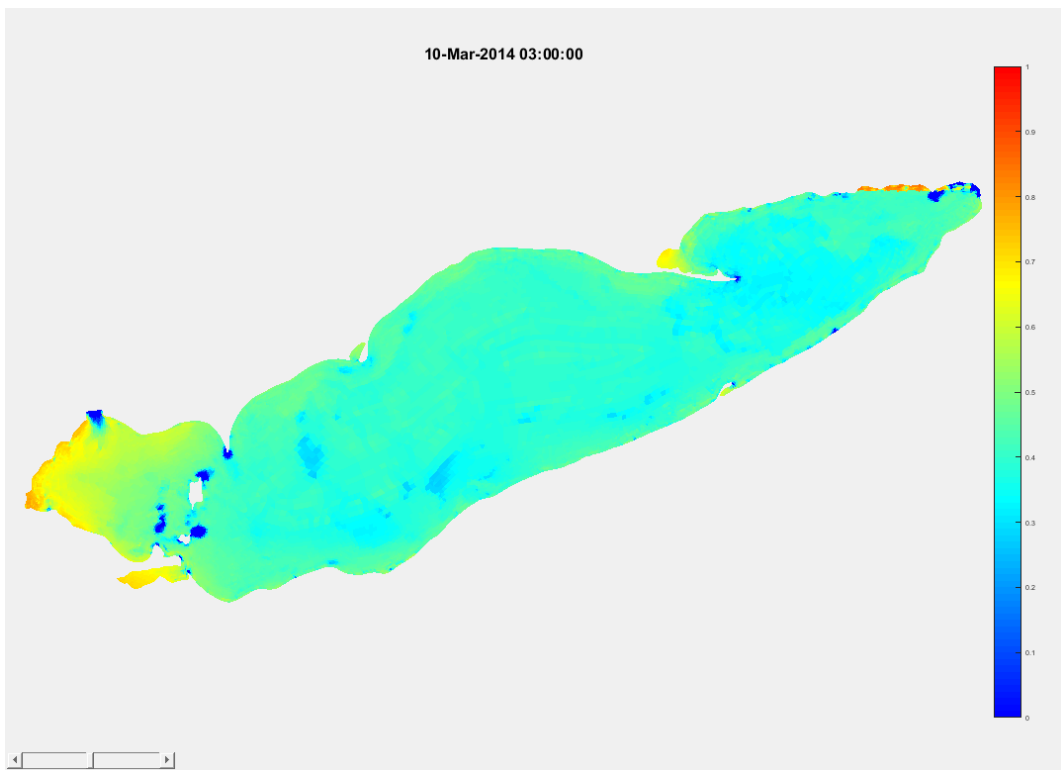


Figure 5q. Lake Erie, simulated Blue Ice thickness on 10/03/2014

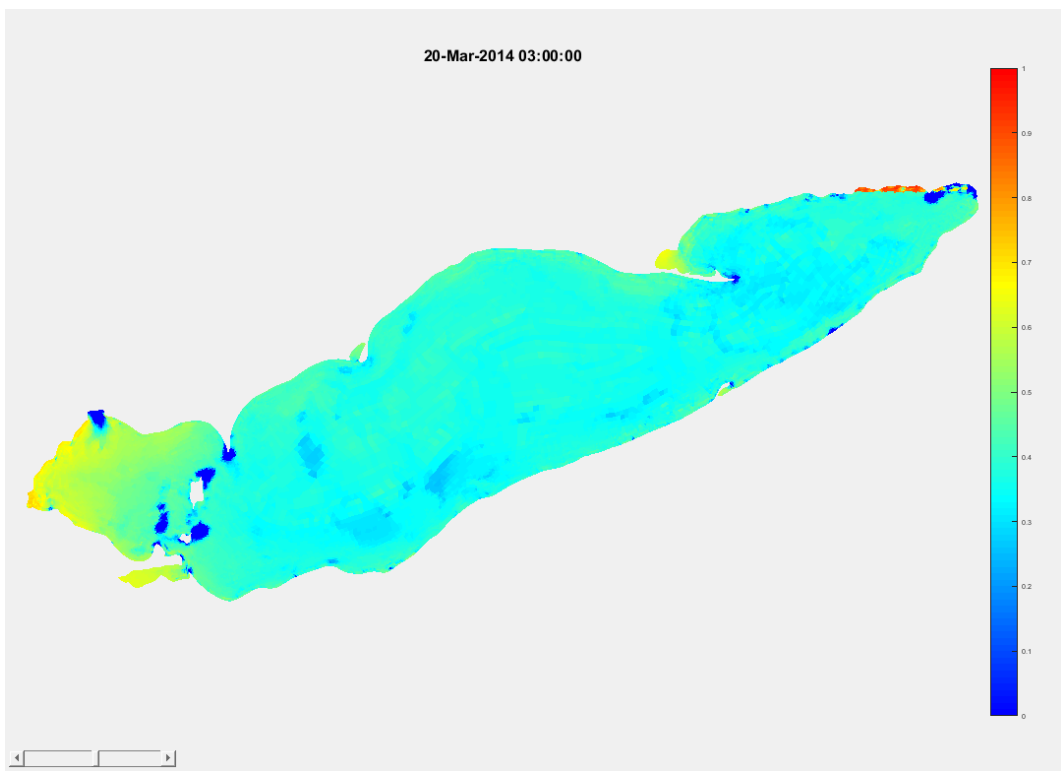


Figure 5r. Lake Erie, simulated Blue Ice thickness on 20/03/2014

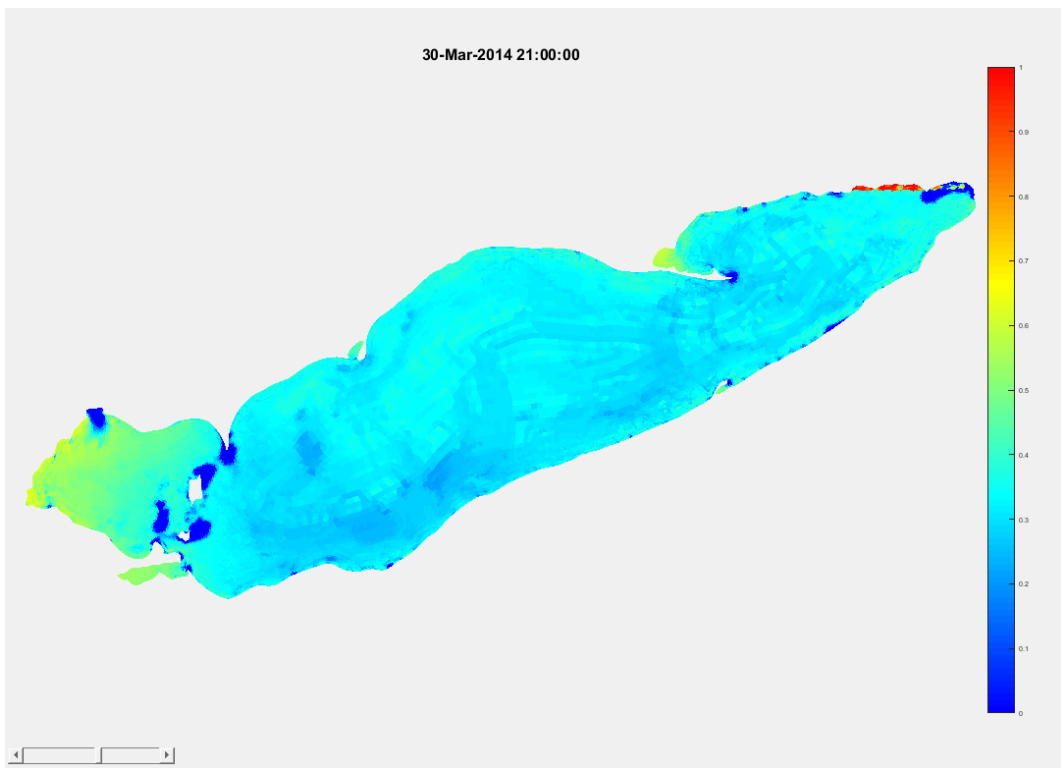


Figure 5s. Lake Erie, simulated Blue Ice thickness on 30/03/2014

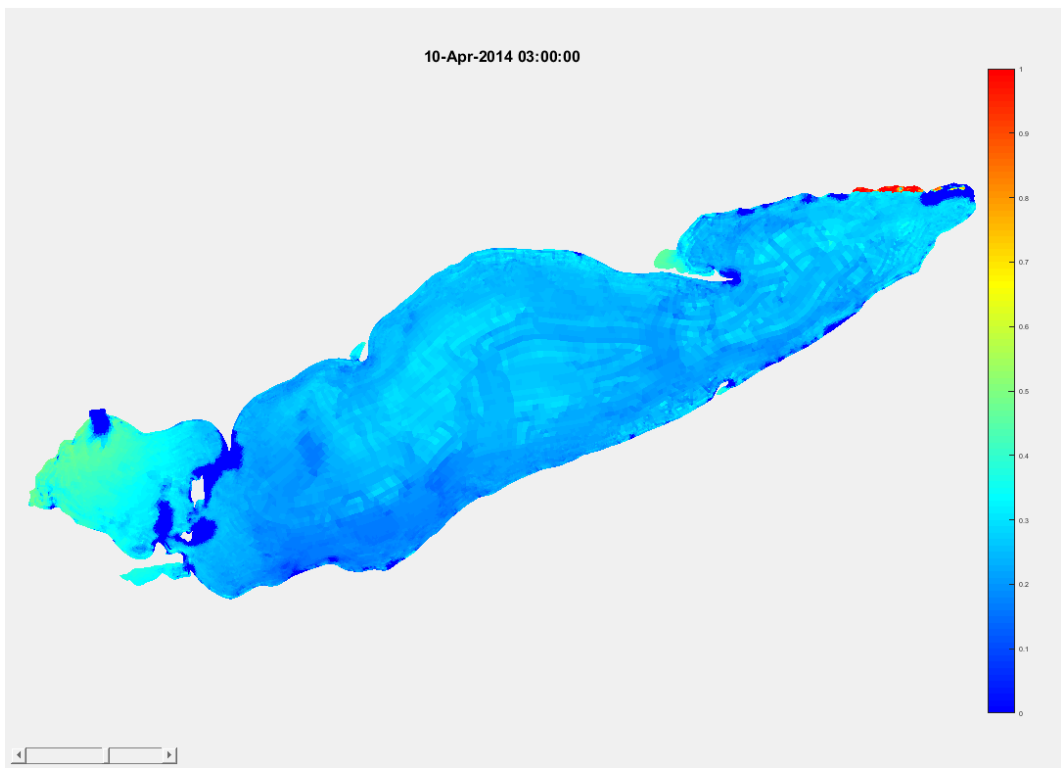


Figure 5t. Lake Erie, simulated Blue Ice thickness on 10/04/2014

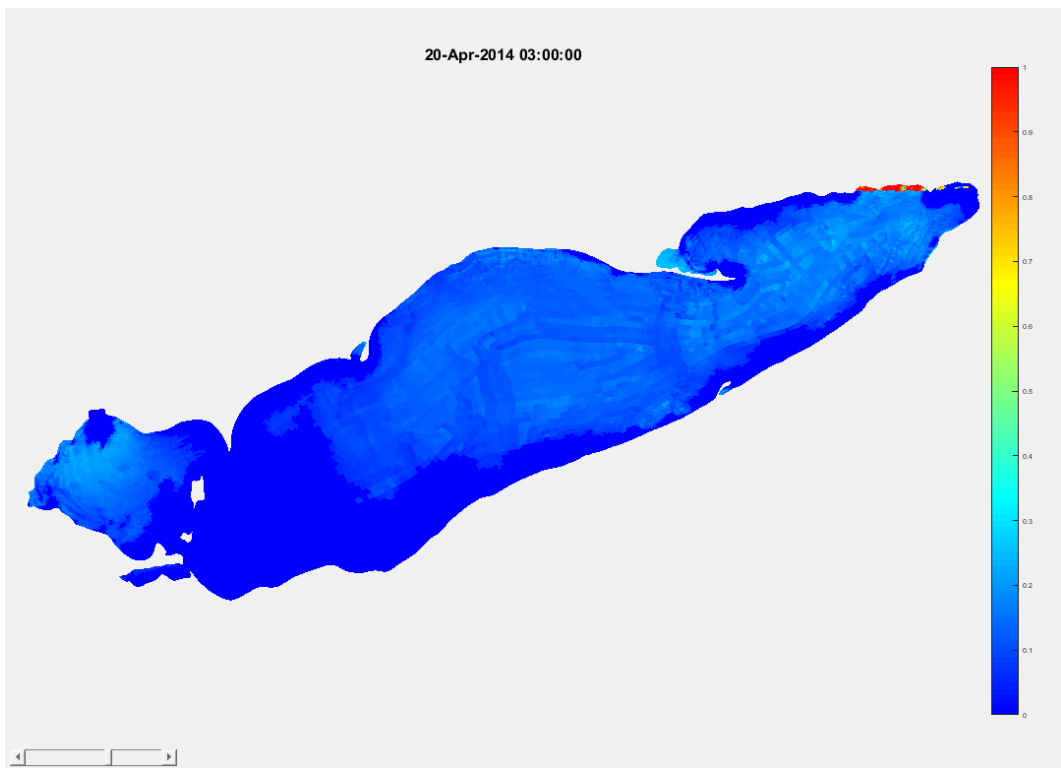


Figure 5u. Lake Erie, simulated Blue Ice thickness on 20/04/2014

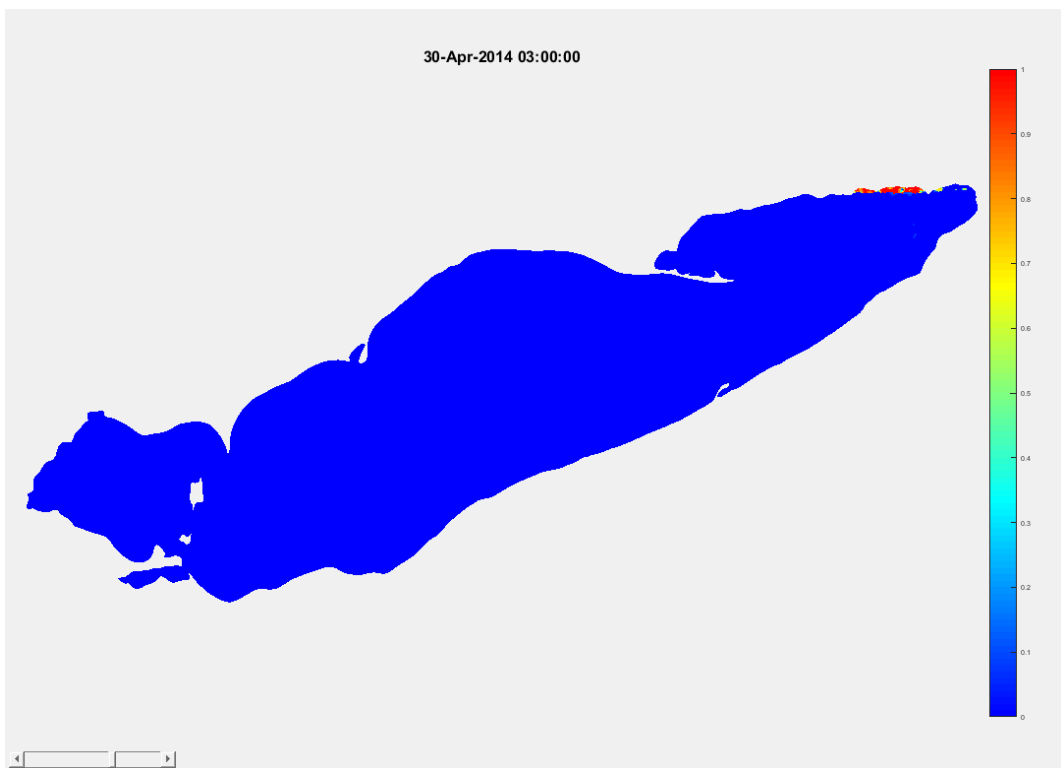


Figure 5v. Lake Erie, simulated Blue Ice thickness on 30/04/2014

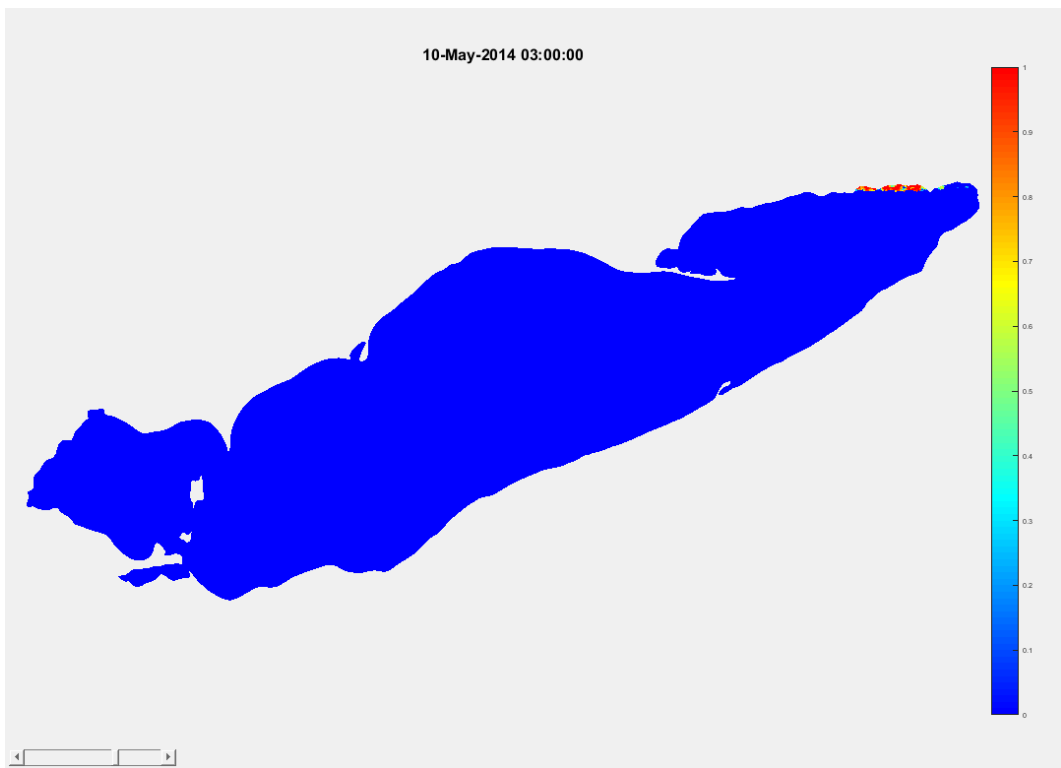


Figure 5w. Lake Erie, simulated Blue Ice thickness on 10/05/2014

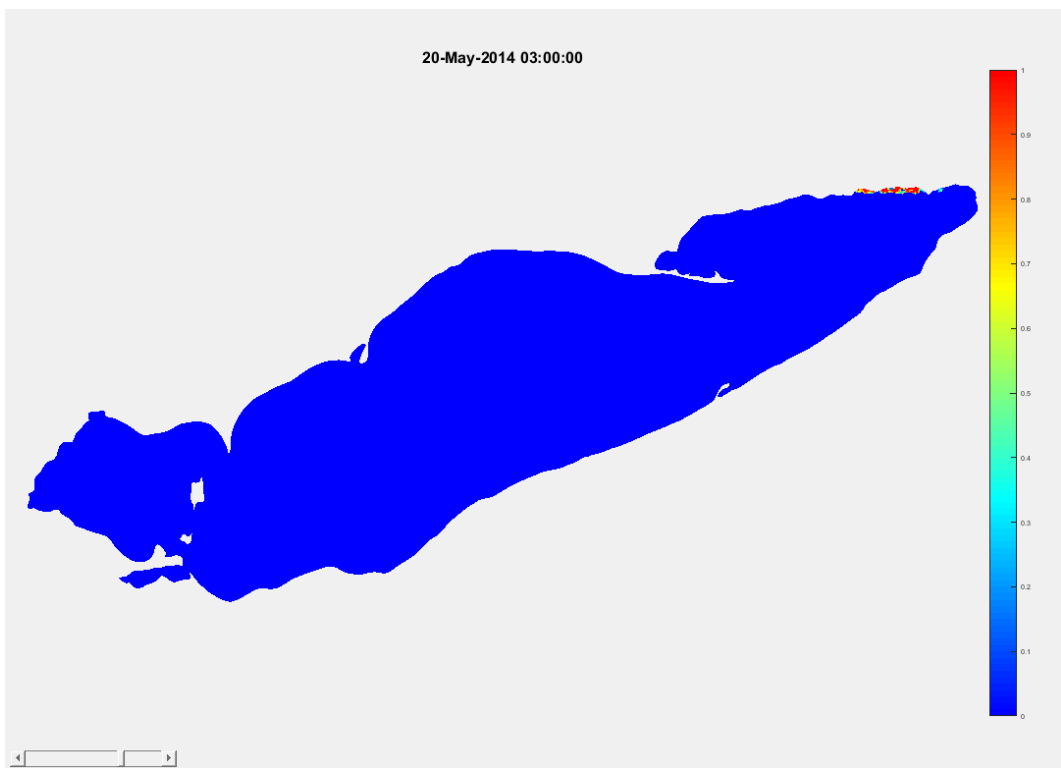


Figure 5x. Lake Erie, simulated Blue Ice thickness on 20/05/2014



Figure 5y. Lake Erie, simulated Blue Ice thickness on 30/05/2014

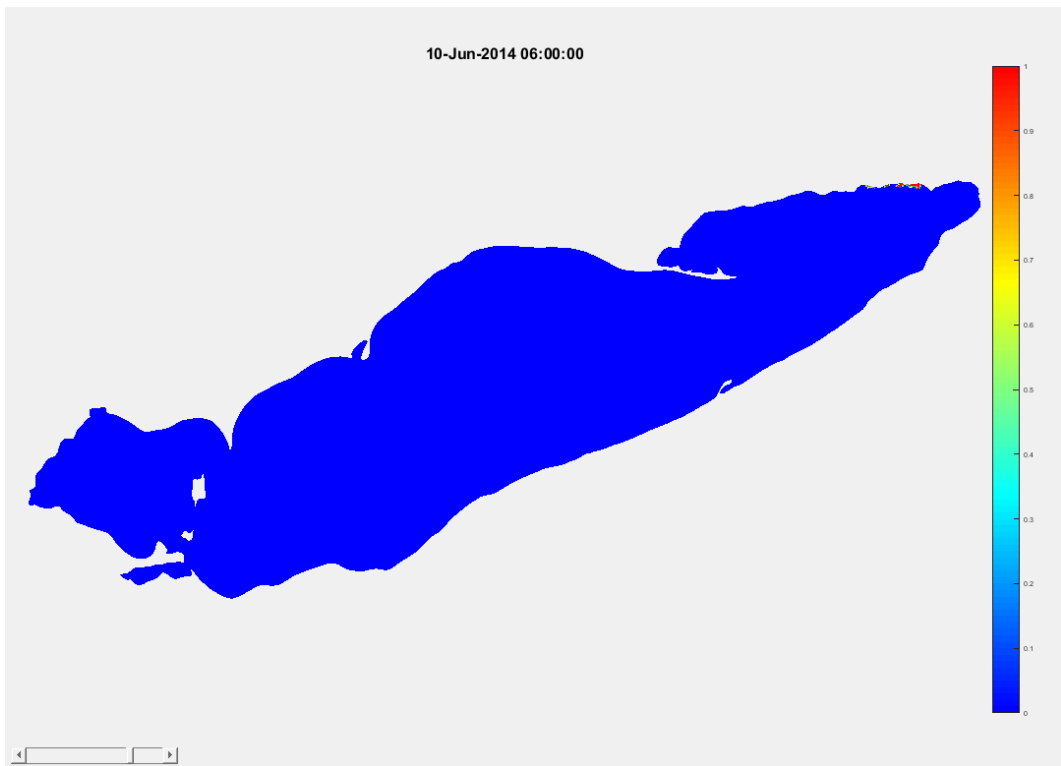


Figure 5z. Lake Erie, simulated Blue Ice thickness on 10/06/2014

4 AED2 Mussels Model Implementation

4.1 Model Formulation

In addition to the base water quality model setup capturing water column nutrient cycling and algal competition, a mussel module to simulate growth, production, and population dynamics has been incorporated into the AED2. One to several size classes of mussels are simulated based on physiological parameters assembled by Schneider et al. (1992) and modified by Bierman et al. (2005) to estimate effect of mussels on Saginaw Bay, Michigan, USA; a formulation also used by Gudimov et al. (2015) to estimate mussel effects in Lake Simcoe, Ontario, Canada. Additionally, some model structure was taken from the Spillman et al. (2008) model of *Tapes* clams in the Barbamarco Lagoon, Italy, as modified by Bocaniov et al. (2013) for mussels in Lake Erie.

The physiology of mussels are set to be size dependent, and can vary between species (e.g., Zebra vs Quagga)(Hetherington, 2016). Three size classes of mussels can be incorporated in the model, roughly corresponding to age-0, age-1 and age>1 mussels. Physiological parameters are calculated for the weight assigned to each age class, using equations in Table 4. Individual mussel mass is given in mmol C or in the case of calculations of N and P budgets, in mmol N and mmol P. The stoichiometric ratios (C:N:P) are fixed. Group mussel biomass is calculated at each time step by calculating ingestion and subtracting pseudofeces production, standard dynamic action, respiration, excretion, egestion and mortality (expressed in mmol C/mmol C/day, mmol N/mmol N/day; mmol P/mmol P/day). Several of these processes are also functions of temperature, algal+POC concentrations, salinity, suspended solids and mussel density. The effect of salinity, suspended solids and mussel density is incorporated as a multiplier of filtration rate with the multipliers having values between -0 – (no filtering) and 1 (no effect). Mussel nitrogen and phosphorus concentrations are fixed ratios of mussel carbon concentrations. Since the various input and output fluxes have variable C:N:P ratios, the excretion of nutrients is dynamically adjusted each time-step to maintain this ratio at each time step. Reproduction and larval dynamics are not simulated. There is no transfer of biomass between age groups.

Table 4. Mussel mass balance equations and process parameterisations.

State Variable Mass Balance Equation
$dB_i/dt = [I - (R + Ex + Eg + M)] * B$ <p>where B is biomass, i is the size class, gains are ingestion (I) (C,N,P), and losses are respiration (R) (C), excretion (Ex) (C,N,P), egestion (Eg) (C,N,P), and mortality (M) (C,N,P).</p>
Process Parameterisations
<p>Ingestion</p> $I = I_{max} * F(T) * FR * [A]$ <p>where I is ingestion (mmol/mmol/d), FR is filtration rate (m³/mmol/d), $[A]$ is algal + POC concentration (mmol/m³).</p> $FR = FR_{max} * g(A) * f(D) * f(SS) * f(S)$ <p>FR is filtration rate (see below, m³/mmol/d), $[A]$ is algal + POC concentration (mmol/m³), $f(D)$ is a function of density (D, mmol/m²) with values between 0 and 1 that account for decrease filtering rates at high densities, $f(SS)$ is a function of suspended solids (SS, mg/L) with values between 0 and 1 that decrease filtering rates at high suspended solid concentrations and $f(S)$ is a function of salinity (S, ppt) with values between 0 and 1 that decrease filtering rates at high salinities.</p> $FR_{max} = a W^b.$ <p>This is the maximum filtration rate at optimal temperature for a given individual mussel weight (mmol C).</p> <p>Respiration</p> $R = R_{20} * f(T)_{RSpillman}$ <p>where R is respiration (mmol/mmol/d), R_{20} is respiration rate coefficient at 20°C (mmol/mmol/d), T is temperature (°C) (Spillman et al. 2008).</p> $R = R_{30} * f(T)_{RSchneider} + SDA * (I-Eg)$ <p>where R is respiration (mmol/mmol/d), R_{30} is respiration rate coefficient at 30°C (mmol/mmol/d), T is temperature (°C), SDA is specific dynamic action (-), I is ingestion (mmol/mmol/d), and Eg is egestion (mmol/mmol/d) (Schneider 1992; Bierman et al. 2005; Gudimov et al. 2015).</p> <p>Excretion</p> $Ex = K_{EXCR} * (I-Eg)$ <p>where Ex is excretion (mmol/mmol/d), K_{EXCR} is excretion fraction of ingestion (-), I is ingestion (mmol/mmol/d), and Eg is egestion (mmol/mmol/d).</p> <p>Egestion</p> $Eg = \alpha_{EG} EXP (\gamma_{EG} * MIN ([A] / K_A, 1)) * I$ <p>where Eg is egestion (mmol/mmol/d), α_{EG} is minimum proportion egested as feces (-), γ_{EG} is coefficient for food availability dependence (-), $[A]$ is algal concentration (mmol/m³), K_A is optimum algal and particulate organic carbon (POC) concentration (mmol/m³), and I is ingestion (mmol/mmol/d).</p> <p>Mortality</p> $M = K_{MORT} * f(DO) + PR$ <p>where M is mortality (mmol/mmol/d), K_{MORT} is mortality rate coefficient (mmol/mmol/d), DO is dissolved oxygen (mmol/m³), and PR is mortality rate from predation (mmol/mmol/d).</p>

4.2 Ingestion

Ingestion is modelled as a function of filtration rate, food availability, pseudofeces production, density, suspended solids, and salinity (Equation 2) (Schneider 1992; Bierman et al. 2005; Spillman et al. 2008; Gudimov et al. 2015). Filtration rate is based on maximum ingestion, temperature, food availability, and pseudofeces production according to the following:

$$FR = (I_{max} * f(T)_I / K_A) / PF_{min} \quad \text{for } [A] < K_A$$

$$FR = (I_{max} * f(T)_I / [A]) / PF_{min} \quad \text{for } [A] > K_A$$

where FR is filtration rate (mmol/mmol/d), I_{max} is maximum ingestion rate (mmol/mmol/d), $f(T)_I$ is filtration temperature function, K_A is optimum algal concentration (mmol/m^3), $[A]$ is algal concentration + particulate organic carbon (POC) concentration (mmol/m^3), and PF_{min} is minimum pseudofeces production (-).

The maximum ingestion rate is based on weight from length according to the following:

$$I_{max} = (a_I * W^{b_I})$$

$$W = (0.071/1000) * L^{2.8}$$

where I_{max} is maximum ingestion rate (mmol/mmol/d), a_I is maximum standard ingestion rate (mmol/mmol/d), W is weight (g), b_I is exponent for weight effect on ingestion, L in length (mm) (Schneider et al. 1992; Bierman et al. 2005).

The temperature dependence function (Thornton and Lessem 1978) was fit to zebra and quagga mussel data (Hetherington et al. Submitted) with optimal ingestion from 17°C to 20°C according to the following:

$$f(T)_I = 1 \quad \text{for } T_{min_I} \leq T \leq T_{max_I}$$

$$f(T)_I = ((2*(T-minT_I)/T_{min_I}) - (T-minT_I)^2/T_{min_I}^2) / ((2*(T_{max_I}-minT_I)/T_{max_I}) - (T_{max_I}-minT_I)^2/T_{max_I}^2)$$

for $minT_I < T < T_{max_I}$

$$f(T)_I = -(T^2 + 2*T_{max_I}*T - 2*T_{max_I}*maxT_I + maxT_I^2)/(T_{max_I}-maxT_I)^2 \quad \text{for } T_{max_I} < T < maxT_I$$

$$f(T)_I = 0 \quad \text{for } T \geq maxT_I \text{ or } T \leq minT_I$$

where T is temperature (°C), $minT_I$ is lower temperature for no ingestion (°C), T_{min_I} is lower temperature for optimum ingestion (°C), T_{max_I} is upper temperature for optimum ingestion, $maxT_I$ is upper temperature for no ingestion (°C).

Filtration rate is related to food concentration (Walz 1978, Sprung and Rose 1988, Schneider 1992; Bierman et al. 2005). The filtration rate is maintained at a maximum value for all food values less than saturation food concentration. The filtration rate decreases as food concentrations increase above this value.

Pseudofeces production is implicit as the difference between the mass filtered and consumed. According to Walz (1978), pseudofeces production (66%) was approximately double the ingestion rate (34%) at high food concentrations (Bierman et al. 2005).

Mussel density limits ingestion above some maximum density according to the following:

$$\begin{aligned} f(D) &= 1 && \text{for } D < D_{\max} \\ f(D) &= -(D^2 + 2*D_{\max}*D - 2*D_{\max}*maxD + maxD^2)/(D_{\max} - maxD)^2 && \text{for } D > D_{\max} \\ f(D) &= 0 && \text{for } D > maxD \end{aligned}$$

where D is density (mmol/m^2), D_{\max} is upper density for optimum ingestion (mmol/m^2), and $maxD$ is upper density for no ingestion (mmol/m^2).

An additional function to reduce ingestion is the suspended solids function which decreases ingestion with high inorganic loads according to the following:

$$\begin{aligned} f(SS) &= 1 && \text{for } SS < SS_{\max} \\ f(SS) &= -(SS^2 + 2*SS_{\max}*SS - 2*SS_{\max}*maxSS + maxSS^2)/(SS_{\max} - maxSS)^2 && \text{for } SS > SS_{\max} \\ f(SS) &= 0 && \text{for } SS > maxSS \end{aligned}$$

where SS is suspended solids (mg/L), SS_{\max} is upper suspended solids for optimum ingestion (mg/L), and $maxSS$ is upper suspended solids for no ingestion (mg/L) (Spillman et al. 2008).

Along with suspended solids, salinity limits ingestion according to the following:

$$\begin{aligned} f(S) &= 1 && \text{for } S_{\min} \leq S \leq S_{\max} \\ f(S) &= ((2*(S-minS)/S_{\min}) - (S-minS)^2/S_{\min}^2) / ((2*(S_{\min}-minS)/S_{\min}) - (S_{\min}-minS)^2/S_{\min}^2) && \text{for } minS < S < S_{\min} \\ f(S) &= -(S^2 + 2*S_{\max}*S - 2*S_{\max}*maxS + maxS^2)/(S_{\max}-maxS)^2 && \text{for } S_{\max} < S < maxS \\ f(S) &= 0 && \text{for } S \geq maxS \text{ or } S \leq minS \end{aligned}$$

where S is salinity (psu), $minS$ is lower salinity for no ingestion (psu), S_{\min} is lower salinity for optimum ingestion (psu), S_{\max} is upper salinity for optimum ingestion (psu), $maxS$ is upper salinity for no ingestion (psu) (Spillman et al. 2008).

4.3 Respiration

Respiration is modelled as a base or standard respiration rate based on weight and temperature (Spillman et al. 2008). Respiration rate coefficient at 20°C is based on weight from length according to the following:

$$\begin{aligned} R_{20} &= (a_R * W^{b_R}) \\ W &= (0.071/1000) * L^{2.8} \end{aligned}$$

where R_{20} is respiration rate coefficient at 20°C (mmol/mmol/d), a_R is standard respiration rate (mmol/mmol/d), W is weight (g), b_R is exponent for weight effect of respiration, and L is length (mm) (Schneider 1992).

The respiration rate coefficient is adjusted for temperature according to the following:

$$f(T)_{R\text{Spillman}} = \Theta_{R\text{Spillman}}^{T-20}$$

where $f(T)_{R\text{Spillman}}$ is respiration temperature function, $\Theta_{R\text{Spillman}}$ is temperature multiplier for bivalve respiration (-), and T is temperature ($^\circ\text{C}$) (Spillman et al. 2008).

Alternatively, respiration is modelled as a base or standard respiration rate based on weight and temperature in addition to the energetic cost of feeding. Respiration rate coefficient at 30°C is based on weight from length according to the following:

$$\begin{aligned} R_{30} &= (a_R * W^{b_R}) \\ W &= (0.071/1000) * L^{2.8} \end{aligned}$$

where R_{30} is respiration rate coefficient at 30°C (mmol/mmol/d), a_R is standard respiration rate (mmol/mmol/d), W is weight (g), b_R is exponent for weight effect of respiration, and L is length (mm) (Schneider 1992).

The temperature function follows Schneider's (1992) application of the model of Kitchell et al. (1977) to the data of Alexander and McMahon (2004) according to the following:

$$f(T)_{R\text{Schneider}} = V^X * e^{X * (1-V)}$$

$$V = ((T_{\max R} - T) / (T_{\max R} - maxT_R))$$

$$X = ((W * (1 + \text{SQRT}(1 + (40 / Y)))) / 20)^2$$

$$W = (\ln Q_R * (T_{\max R} - \text{maxT}_R)$$

$$Y = \ln Q_R * (T_{\max R} - \text{maxT}_R + 2)$$

where T is temperature ($^{\circ}\text{C}$), $T_{\max R}$ is upper temperature for optimum respiration ($^{\circ}\text{C}$), maxT_R is upper temperature for no respiration ($^{\circ}\text{C}$), and Q_R is respiration curve slope estimate (-). The maximum respiration occurs at 30°C with 43°C as the upper lethal temperature.

The energetic cost of feeding or specific dynamic action is applied only to the portion of ingestion that is not egested (Schneider 1992; Bierman et al. 2005; Gudimov et al. 2015).

4.4 Excretion

Excretion is modelled as a constant fraction of assimilated food (Schneider 1992; Bierman et al. 2005; Gudimov et al. 2015). Excretion data for zebra and quagga mussels are limited; therefore, the excretion formulation for *Mytilus edulis* derived by Bayne and Newell (1983) was used (Schneider 1992; Bierman et al. 2005; Gudimov et al. 2015).

4.5 Egestion

Egestion is modeled as a function of ingestion (Schneider 1992; Bierman et al. 2005; Gudimov et al. 2015). The model follows the assumption that ingestion is directly proportional to the food content of the water for all food concentrations less than the maximum which can be ingested. For all food concentrations above this saturation value, ingestion remains constant at a maximum value (I_{\max}) (Walz 1978).

4.6 Mortality

Mortality is a function of dissolved oxygen and predation (Equation 7). Mortality increases with low dissolved oxygen concentrations according to the following:

$$f(DO) = 1 + K_{BDO} * (K_{DO} / (K_{DO} + DO))$$

where DO is dissolved oxygen (mmol/m^3), K_{BDO} is basal respiration rate (mmol/m^3), and K_{DO} is half saturation constant for metabolic response to dissolved oxygen (mmol/m^3) (Spillman et al. 2008). A mortality rate coefficient (K_{MORT}) further influences the dissolved oxygen function. Additionally, mortality from predation is a constant rate added to the effect from dissolved oxygen.

4.7 Setup for Lake Erie

The model setup for mussels was implemented and run for Lake Erie over the period from April - October 2013. The mussel bed density was interpolated based on the data provided, indicated in Figure 6. Based on the mussel density, an assumed (constant) mass per mussel was adopted and used to initialise the biomass. Parameters were assigned as in Table 3.

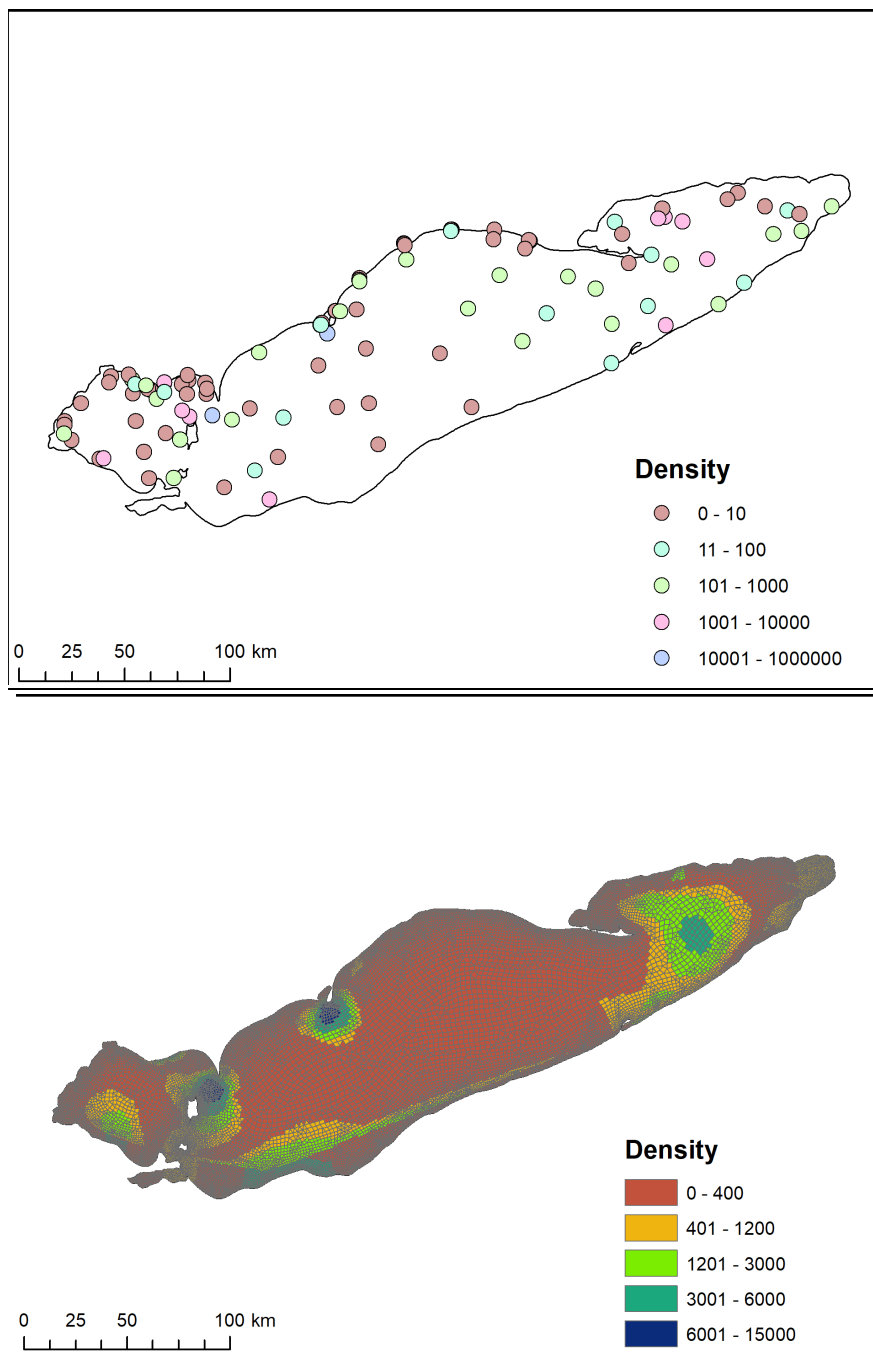


Figure 6: Mussel density data (top) and interpolated onto the model domain (b).

Table 5: Summary of mussel parameters, including values, units, and descriptions. Note :
DP = *Dreissena polymorpha* (zebra mussel); DRB = *Dreissena rostriformis bugensis* (quagga mussel).

Name	Code	DP Value	DRB Value	Units	Description
Initial					
Name	biv_name [string]	Zebra	Quagga	Text	Name of bivalve group
Length	biv_length [real]	15.0	15.0	mm	Length of bivalve (mm)
InitDens	biv_initial_density [real]	833.0	833.0	mmol/m ²	Initial density of bivalve (mmol/m ²)
MinDens	min_biv [real]	8.3	8.3	mmol/m ²	Minimum density of bivalve mass (mmol/m ²)
Ingestion					
N:C	INC_biv [real]	291.67	291.67	-	Ratio of internal nitrogen to carbon of bivalve (-)
P:C	IPC_biv [real]	64.58	64.58	-	Ratio of internal phosphorus to carbon of bivalve (-)
Ing	grzfunc_biv [integer]	0	0	-	Type of maximum ingestion for bivalve 0 = Enter (mmol/mmol/d) 1 = Calculate based on length (mm)
I _{max}	Rgrz_biv [real]	115.25	115.25	mmol/mmol/d	Maximum ingestion rate of bivalve (mmol/mmol/day) Calculated from Schneider (1992) based on 15 mm mussel
a _I	a_Rgrz_biv[real]	53.4	53.4	mmol/mmol/d	Maximum standard ingestion rate of bivalve (mmol/mmol/day) (Schneider 1992)
b _I	b_Rgrz_biv [real]	-0.39	-0.39	-	Exponent for weight effect on ingestion of bivalve (-) (Schneider 1992)
minT _I	minT_grz_biv [real]	4.0	4.0	°C	Lower temperature for no ingestion of bivalve (°C)
T _{minI}	Tmin_grz_biv [real]	17.0	17.0	°C	Lower temperature for optimum ingestion of bivalve (°C)
T _{maxI}	Tmax_grz_biv [real]	20.0	20.0	°C	Upper temperature for optimum ingestion of bivalve (°C)
maxT _I	maxT_grz_biv [real]	32.0	32.0	°C	Upper temperature for no ingestion of bivalve (°C)
K _A	Kgrz_biv [real]	187.5	187.5	mmolAlg/m ³	Optimum algae + POC concentration for ingestion of bivalve (mmol/m ³)
PF _{min}	fassim_biv [real]	0.34	0.34	-	Minimum proportion of food lost as pseudofeces for bivalve (-) (Bierman et al. 2005)
Dmax	Dmax_grz_biv [real]	8333.3	8333.3	mmol/m ²	Upper density for optimum ingestion of bivalve (mmol/m ²)
maxD	maxD_grz_biv [real]	83333.3	83333.3	mmol/m ²	Upper density for no ingestion of bivalve (mmol/m ²)
SSmax	SSmax_grz_biv [real]	20.0	20.0	mg/L	Upper suspended solids for optimum ingestion of bivalve (mg/L)
maxSS	maxSS_grz_biv [real]	100.0	100.0	mg/L	Upper suspended solids for no ingestion of bivalve (mg/L)
S	saltfunc_biv [integer]	0	0	-	Type of salinity function 0 = None 1 = Spillman et al. (2008)
minS	minS_grz_biv [real]	N/A	N/A	psu	Lower salinity for no ingestion of bivalve (psu)
Smin	Smin_grz_biv [real]	N/A	N/A	psu	Lower salinity for optimum ingestion of bivalve (psu)
Smax	Smax_grz_biv [real]	N/A	N/A	psu	Upper salinity for optimum ingestion of bivalve (psu)
maxS	maxS_grz_biv [real]	N/A	N/A	psu	Upper salinity for no ingestion of bivalve (psu)
Respiration					
R	respfunc_biv [integer]	0	0	-	Type of respiration function for bivalve (Schneider 1992 or Spillman et al. 2008) 0 = Schneider (1992) 1 = Spillman et al. (2008)
R _{maxtype}	Rmaxtypefunc_biv [integer]	0	0	-	Type of maximum respiration for bivalve (-) 0 = Enter (mmol/mmol/d) 1 = Calculate based on length (mm)
R ₂₀	Rresp_biv [real]	.02	.02	mmol/mmol/d	Respiration rate coefficient at 20°C of bivalve (mmol/mmol/day) Calculated from Schneider (1992) based on 15 mm mussel
Θ _{RSpillman}	theta_resp_biv [real]	1.08	1.08	-	Temperature multiplier for respiration of bivalve (-)
R ₃₀	Rmax_resp_biv [real]	.02	.02	mmol/mmol/d	Respiration rate coefficient at 30°C of bivalve (mmol/mmol/day) Calculated from Schneider (1992) based on 15 mm mussel
a _R	a_Rresp_biv [real]	16.759	16.759	mmol/mmol/d	Standard respiration rate of bivalve (mmol/mmol/day) (Schneider 1992)
b _R	b_Rresp_biv [real]	-0.25	-0.25	-	Exponent for weight effect on respiration of bivalve (-) (Schneider 1992)

Name	Code	DP Value	DRB Value	Units	Description
TmaxR	Tmax_resp_biv [real]	30.0	30.0	°C	Upper temperature for optimum respiration of bivalve (°C)
maxTR	maxT_resp_biv [real]	43.0	43.0	°C	Upper temperature for no respiration of bivalve (°C)
QR	Q_resp_biv[real]	2.3	2.3	-	Respiration curve slope estimate for bivalve (-)
SDA	SDA_biv [real]	0.285	0.285	-	Specific dynamic action of bivalve (-) (Schneider 1992)
Excretion					
KEXCR	fexcr_biv [real]	0.064	0.064	-	Excretion fraction of ingestion for bivalve (-) (Schneider 1992)
Egestion					
αEG	ffecal_biv [real]	0.315	0.315	-	Minimum proportion egested as feces for bivalve (-) (Schneider 1992)
γEG	EgCoeff_biv [real]	0.88	0.88	-	Coefficient for food availability dependence for bivalve (-) (Schneider 1992)
Mortality					
KMORT	Kmort_biv [real]	0.0	0.0	mmol/mmol/d	Mortality rate coefficient for bivalve (mmol/mmol/day)
KBDO	Kbdo_biv [real]	160.0	160.0	mmol/m ³	Basal respiration rate of bivalve (mmol/m ³) (Spillman et al. 2008)
KDO	Kdo_biv [real]	8.0	8.0	mmol/m ³	Half saturation constant for metabolic response to DO for bivalve (mmol/m ³) (Spillman et al. 2008)
PR	PR_mort_biv [real]	.01	.01	mmol/mmol/d	Mortality rate from predation of bivalve (mmol/mmol/day)

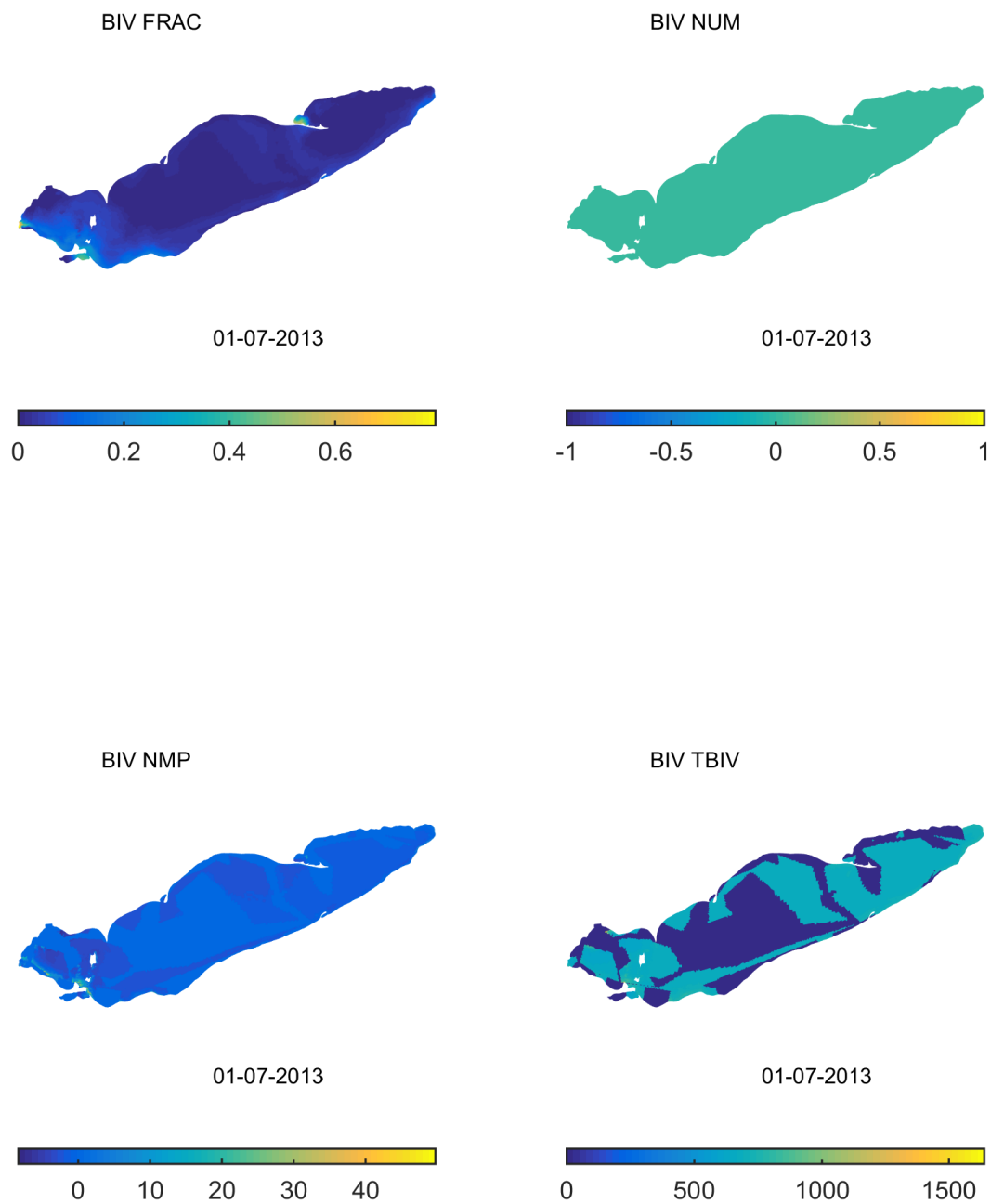


Figure 7. Example outputs from the mussel model, showing the fraction of water across the bottom that has been filtered by the mussels (BIV FRAC), the net mussel productivity (BIV NMP), and the total mussel biomass and number (right).

5 Cladophora Model implementation

The Cladophora model implemented in AED2 is based on the Higgins et al (2006) CGM model applications, customised to fit within the aed2_macroalgae model framework. The model allows for growth, based on light and temperature, respiration, and sloughing. Tissue phosphorus storage is also included and can limit the growth rate if it becomes reduced.

$$\frac{d \text{MAG}_{cgm}}{dt} = +f_{\text{uptake}}^{\text{MAG}_{cgm}} - f_{\text{resp}}^{\text{MAG}_{cgm}} - f_{\text{slough}}^{\text{MAG}_{cgm}}$$

The model is customised to grow in benthic environments with appropriate substrates. Substrate classes are configured within the model for each cell, and for this application we have assigned classes based on the latest benthic map available for the lake (Figure 8). For this setup, Cladophora was configured to grow on rock substrate. Results are shown in Section 8.

5.1 Photosynthesis and nutrient uptake

The rate of growth depends on the empirical growth response surface accounting for the effects of light and temperature, the tissue P concentration, and the effects of self-shading:

$$f_{\text{uptake}}^{\text{MAG}_{cgm}} = \underbrace{R_{\text{growth}}^{\text{MAG}_{cgm}}}_{\text{base growth rate}} \underbrace{\Phi_{\text{pplt}}^{\text{MAG}_{cgm}}(T, I)}_{\text{growth function}} \underbrace{\Phi_P^{\text{MAG}_{cgm}}(PO_4, \text{MAG}_{cgm-p})}_{\text{P limitation}} \underbrace{\Phi_{\text{shade}}^{\text{MAG}_{cgm}}(\text{MAG}_{cgm})}_{\text{self-shading}} [\text{MAG}_{cgm}]$$

where $\Phi_{\text{pplt}}^{\text{MAG}_{cgm}}(T, I)$ is the polynomial as taken from Higgins et al, and limitation due to self-shading effect is captured as:

$$\Phi_{\text{shade}}^{\text{MAG}_{cgm}}(\text{MAG}_{cgm}) = 1 - \left[\frac{\text{MAG}_{cgm}}{\text{MAG}_{max}} \right]$$

where

$$\text{MAG}_{max} = 20.83 (1.18 \bar{I} - 58.7)$$

$$\Phi_P^{\text{MAG}_{cgm}}(PO_4, \text{MAG}_{cgm-p}) = 1 - \left[\frac{\chi_P^{\text{cgm}}}{\text{MAG}_{cgm-p}} \right]$$

where

$$\chi_P^{\text{cgm}} = \frac{\text{MAG}_{cgm-p}}{\text{MAG}_{cgm}}$$

we can compute the changing tissue concentration of P from the uptake rate

$$\frac{d \text{MAG}_{cgm-p}}{dt} = +f_{\text{uptake}}^{\text{MAG}_{cgm}}$$

whereby

$$f_{\text{uptake}}^{\text{MAG}_{cgm-p}} = R_{\text{growth}}^{\text{MAG}_{cgm-p}} \Phi_T^{\text{MAG}_{cgm-p}}(T) \left[\frac{PO_4}{K_P^{\text{cgm}} + PO_4} \right] \left[\frac{K_q^{\text{cgm}}}{K_P^{\text{cgm}} + (\chi_P^{\text{cgm}} - \chi_{PMIN}^{\text{cgm}})} \right] \text{MAG}_{cgm-p}$$

and

$$\Phi_T^{\text{MAG}_{cgm-p}} = \begin{cases} \exp[(\bar{T} - 18)/39], & \bar{T} < 18 \\ \exp[(18 - \bar{T})/18.75], & \bar{T} \geq 18 \end{cases}$$

5.2 Respiration

The rate of mussel respiration is based on the dark rate presented in Higgins et al (2006), using the daily moving average of temperature:

$$f_{\text{resp}}^{\text{MAG}_{cgm}} = R_{\text{resp}}^{\text{MAG}_{cgm}} * (0.025 \bar{T} + 0.1)$$

5.3 Sloughing

The Canale and Auer model used in the Higgins implementation, also includes the loss of attached biomass due to detachment and sloughing. The approach to account for sloughing can consider surface wind conditions, shear stress, an

(empirically determined) maximum sloughing rate, and is proportional to the biomass. To work out the sloughing, a trigger value for sloughing, ω_{cgm} , must be met:

$$f_{slough}^{MAG_{cgm}} = \begin{cases} 0, & \omega_{cgm} > -0.4 \\ MAG_{cgm}, & \omega_{cgm} \leq -0.4 \end{cases}$$

where

$$\omega_{cgm} = R_{slough}^{MAG_{cgm}} (\bar{\tau} - \tau_{cgm}) \left(\frac{MAG_{cgm}}{MAG_{max}} \right)$$

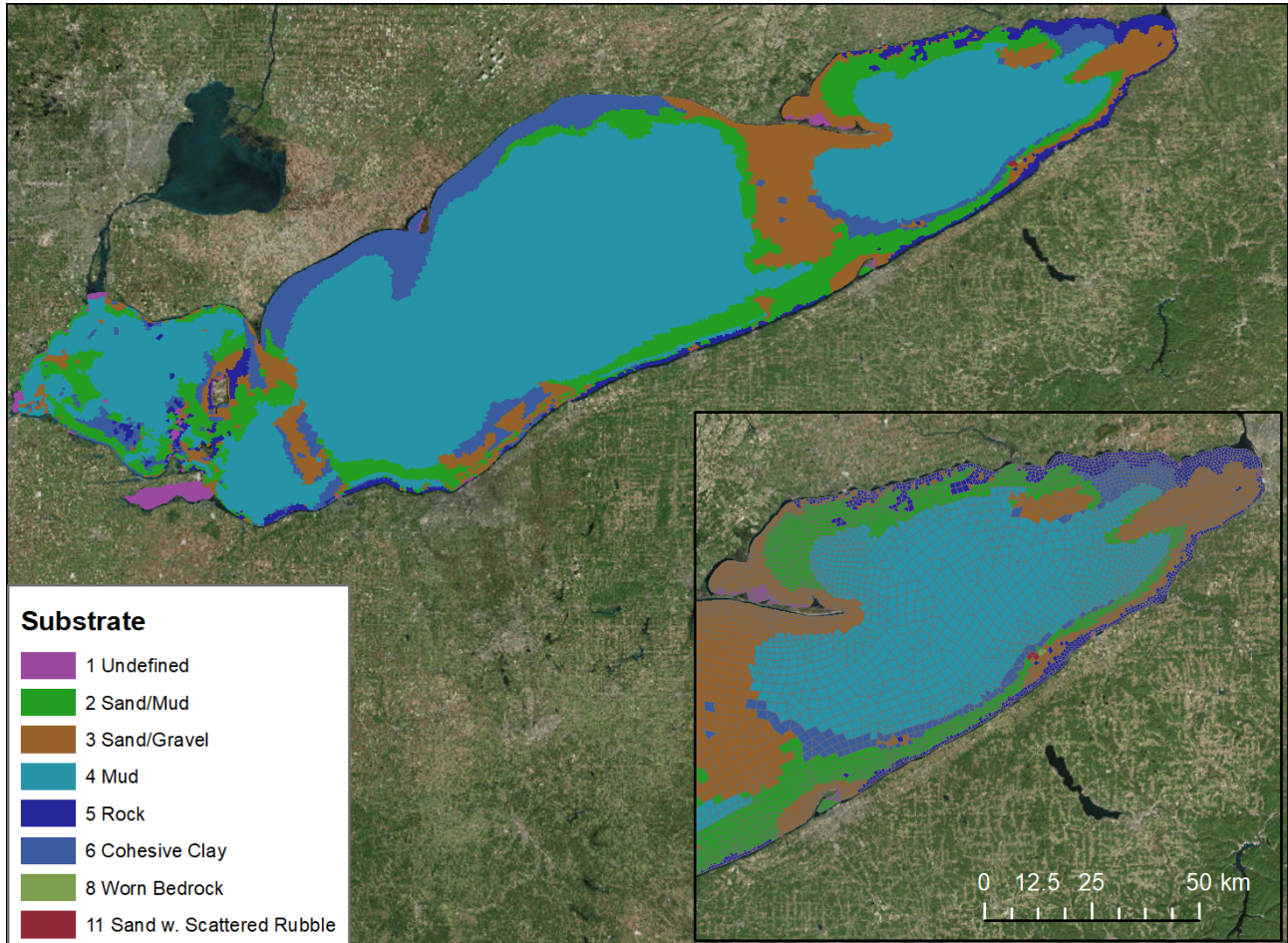


Figure 8. Assumed sediment "zones", used for assigning Cladophora habitat, and other sediment properties such as the sediment oxygen demand.

Table 6: Summary of Cladophora growth model parameters, including values, units, and descriptions.

Name	Code	Value	Units	Description
$R_{resp}^{MAG_{cgm}}$	R_resp [real]	0.151	/d	Respiration rate
$R_{growth}^{MAG_{cgm}}$	R_growth [real]		/d	Growth rate
$R_{growth-p}^{MAG_{cgm-p}}$	R_puptake [real]		/d	Uptake rate of phosphorus
K_q^{cgm}	- [real]	0.0028 * (12e3/31e3)	mmol P/mmol C	Half-saturation coefficient mediating uptake of P based on tissue concentration 0.07% = 0.0028gP/gC & 12/31 is mol weight conversion
X_{PMIN}^{cgm}	X_pmin [real]		mmol P/mmol C	Minimum tissue phosphorus
K_P^{cgm}	K_P [real]		mmol/m ³	Half-saturation coefficient for PO4 limitation
$R_{slough}^{MAG_{cgm}}$	- [real]	0.001	/d	Rate the sloughing trigger changes over time
τ_{cgm}	slough_stress [real]		N/m ²	Critical stress over which currents contribute to filament weakening and eventual sloughing

6 Sediment biogeochemistry

The sediment diagenesis model calculates reaction and transport of chemical species over many layers with depth (Figure 9). This type of model was originally developed by Berner (1980) and then applied by authors such as Boudreau (1996), Soetaert et al. (1996) and Van Cappellen and Wang (1996). Applications of this approach have been made to Lake Erie, for example, Gudimov et al. (2016). Following a review of the diagenesis model applications since 1996 (Paraska et al. 2014), the CANDI-AED model was developed at UWA to capture the best elements of those models used to date. The basic structure of this model is an adaptation of the C.CANDI code (Luff et al. 2000), which added extensions related to the geochemical aspects. Further additions to the C.CANDI code have been made to the organic matter and geochemical reactions.

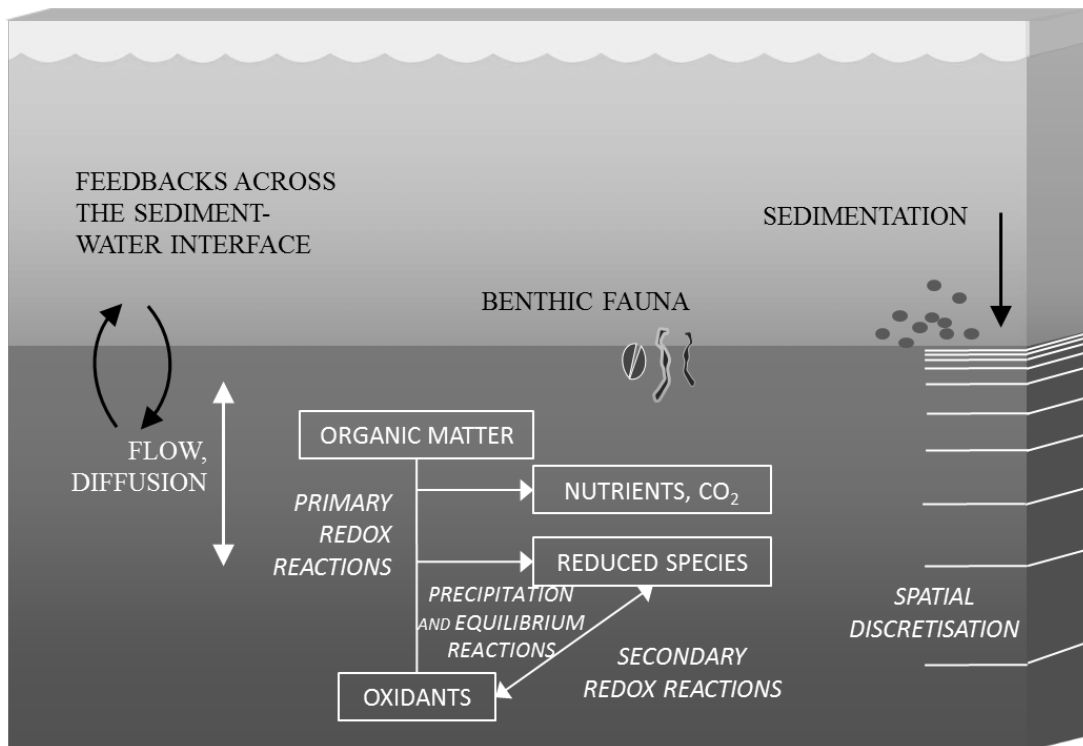


Figure 9. Conceptual basis of the AED2 early diagenesis model used to simulate sediment biogeochemistry in the lake.

The diagenesis model solves reaction and transport in one spatial dimension. It is generally assumed that the vertical variation in chemical concentration is more important than any lateral variation. It is also assumed that the variation is greatest at the sediment-water interface. Therefore, the model has millimetre scale resolution in the first few centimetres of depth, and then increasing layer sizes deeper down.

Transport is a result of the dispersion of solutes, from areas of high concentration to areas of low concentration. There is also the physical deposition of particles at the sediment-water interface, which shifts the spatial frame of reference at a rate of millimetres or centimetres per year.

The chemical reactions in the sediment model are primarily driven by organic matter deposition. As organic matter is consumed by bacteria via redox reactions, bacterial communities also consume different oxidants, including oxygen, and they produce by-products, such as reduced metal ions and hydrogen sulphide. The sediment model then solves the reactions of the secondary by-products through inorganic redox reactions, acid-base and precipitation-dissolution reactions, as the system shifts towards its equilibrium.

The chemical reactions included in this model are expanded upon below and summarised in Figure . The zones match those in Figure 8; these can be further broken down should further spatial refinement of sediment properties be desired. The advantage of this method is to achieve dynamic sediment properties, without excessive computational burden.

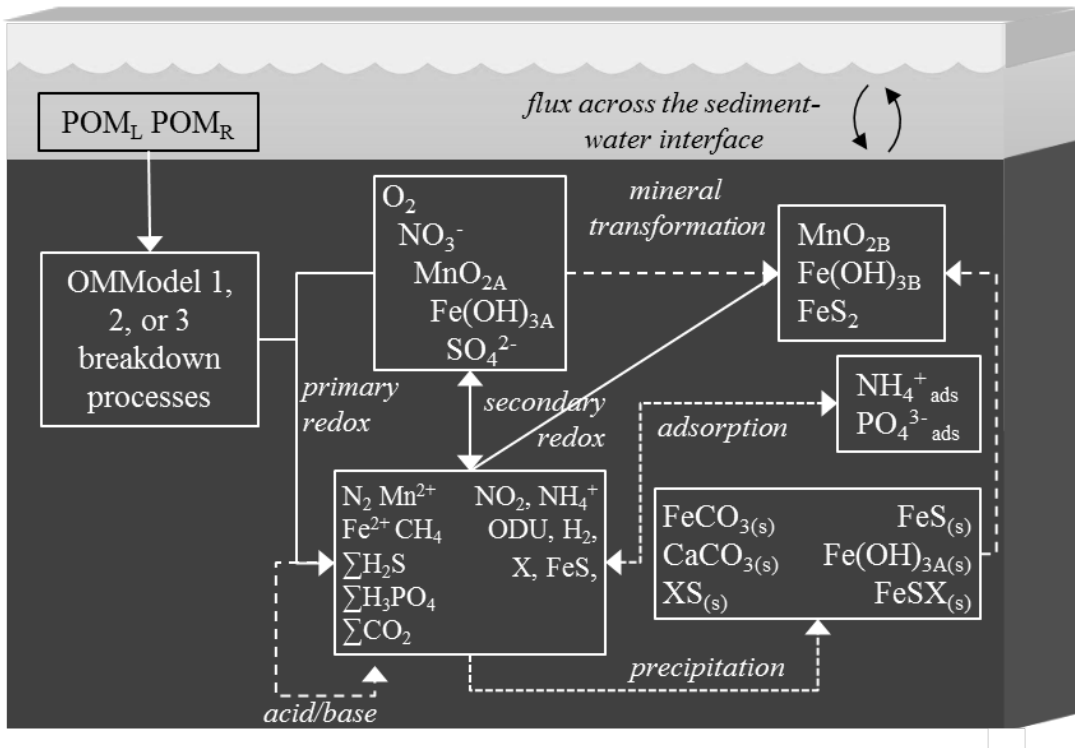


Figure 10. CANDI-AED includes chemical processes of organic matter transformation and oxidation, and reduction/oxidation, crystallisation, adsorption and precipitation reactions of inorganic by-products. Most of the processes are triggered by the input of POM at the sediment-water interface.

6.1 Primary redox reactions

The key chemical process that causes ongoing change in the sediment is the breakdown of organic matter. The user can decide how complex or simple the organic matter breakdown pathway should be, with three options of varying complexity for parameterising the pathways included. The terminal redox reaction pathways are the six pathways that are available in most diagenesis models, and are driven by different organic matter pools, depending on the OMModel configuration chosen from the above options. The rate equation for the oxidation of the oxidants with any of the pools above has a constant oxidation rate of OM, partitioned using R_{Ox_i} which is the reaction of a specific oxidant i (Arndt et al. 2013) (Table 7). The kinetic rate constant k_{OM} gives the maximum oxidation rate, which is different for each reactive type of OM, but the same for each oxidation pathway.

Table 7: Primary redox reactions simulated in the sediment biogeochemistry model. x,y and z indicate the reaction stoichiometry.

Description	Reaction
Aerobic respiration	OM + xO ₂ + (-y + 2z)HCO ₃ ⁻ → (x - y + 2z)CO ₂ + yNH ₄ ⁺ + zHPO ₄ ²⁻ + (x + 2y + 2z)H ₂ O
Denitrification	OM + 0.8xNO ₃ ⁻ → (0.2x - y + 2z)CO ₂ + 0.4xN ₂ + (0.8x + y - 2z)HCO ₃ ⁻ + yNH ₄ ⁺ + zHPO ₄ ²⁻ + (0.6x - y + 2z)H ₂ O + H ₃ PO ₄ + 177.2H ₂ O
Mn oxide reduction	OM + 2xMnO ₂ + (3x + y - 2z)CO ₂ + (x + y - 2z)H ₂ O → 2xMn ²⁺ + (4x + y - 2z)HCO ₃ ⁻ + yNH ₄ ⁺ + zHPO ₄ ²⁻
Fe oxide reduction	OM + 4xFe(OH) ₃ + (7x + y - 2z)CO ₂ + (x - 2z)H ₂ O → 4xFe ²⁺ + (8x + y - 2z)HCO ₃ ⁻ + yNH ₄ ⁺ + zHPO ₄ ²⁻ + (3x + y - 2z)H ₂ O
Sulfate reduction	OM + 0.5xSO ₄ ²⁻ + (y - 2z)CO ₂ + (y - 2z)H ₂ O → 0.5xH ₂ S + (x + y - 2z)HCO ₃ ⁻ + yNH ₄ ⁺ + zHPO ₄ ²⁻
Methanogenesis	OM + (y - 2z)H ₂ O → 0.5xCH ₄ + (0.5x - y + 2z)CO ₂ + (y - 2z)HCO ₃ ⁻ + yNH ₄ ⁺ + zHPO ₄ ²⁻

6.2 Secondary redox reactions

In the meta-analysis, we identified the many secondary redox reactions that have been included across the diversity of diagenesis model applications. In CANDI-AED, they are all included as options, and may be turned on or off as desired (Table 8).

Table 8: Secondary redox reactions simulated in the sediment biogeochemistry model.

Description	Reaction	Rate equation
NH ₄ ⁺ oxidation by O ₂	NH ₄ ⁺ + 2O ₂ + 2HCO ₃ ⁻ → NO ₃ ⁻ + 2CO ₂ + 3H ₂ O	$R_{NH_4Ox} = k_{NH_4Ox}[NH_4^+][O_2]$
Mn ²⁺ oxidation by O ₂	Mn ²⁺ + kX + 0.5O ₂ + 2HCO ₃ ⁻ → MnO _{2A-Xk} + 2CO ₂ + H ₂ O	$R_{MnOx} = k_{MnOx}[Mn^{2+}][O_2]$
Fe ²⁺ oxidation by O ₂	4Fe ²⁺ + O ₂ + 4CO ₂ + 2H ₂ O → 4Fe ³⁺ + 4HCO ₃ ⁻	$R_{FeOx} = k_{FeOx}[Fe^{2+}][O_2]$
H ₂ S oxidation by O ₂	H ₂ S + 2O ₂ + 2HCO ₃ ⁻ → SO ₄ ²⁻ + 2CO ₂ + 2H ₂ O	$R_{TSOx} = k_{TSOx}[H_2S][O_2]$
CH ₄ oxidation by O ₂	CH ₄ + O ₂ → CO ₂ + H ₂ O	$R_{CH_4Ox} = k_{CH_4Ox}[CH_4][O_2]$
FeS oxidation by O ₂	FeS-X _m + 2O ₂ → SO ₄ ²⁻ + Fe ²⁺ + mX	$R_{FeSOx} = k_{FeSOx}[FeS][O_2]$
FeS ₂ oxidation by O ₂	FeS ₂ -X _m + 3.5O ₂ + 2HCO ₃ ⁻ → Fe ²⁺ + mX + 2SO ₄ ²⁻ + 2CO ₂ + H ₂ O	$R_{FeS_2Ox} = k_{FeS_2Ox}[FeS_2][O_2]$
NH ₄ ⁺ oxidation by NO ₃ ⁻	NH ₄ ⁺ + NO ₃ ⁻ → N ₂ + 2H ₂ O	$R_{NH_4NO_3} = k_{NH_4NO_3}[NH_4^+][NO_3^-]$
Mn ²⁺ oxidation by NO ₃ ⁻	5Mn ²⁺ + 2NO ₃ ⁻ + 8HCO ₃ ⁻ + kX → 5MnO _{2A-Xk} + 8CO ₂ + 4H ₂ O + N ₂	$R_{MnNO_3} = k_{MnNO_3}[Mn^{2+}][NO_3^-]$
Fe ²⁺ oxidation by NO ₃ ⁻	5Fe ²⁺ + NO ₃ ⁻ + 6CO ₂ + 3H ₂ O → 0.5N ₂ + 5Fe ³⁺ + 6HCO ₃ ⁻	$R_{FeNO_3} = k_{FeNO_3}[Fe^{2+}][NO_3^-]$
ΣH ₂ S oxidation by NO ₃ ⁻	2.5H ₂ S + 4NO ₃ ⁻ + HCO ₃ ⁻ → 2.5SO ₄ ²⁻ + 2N ₂ + CO ₂ + 3H ₂ O	$R_{TSNO_3} = k_{TSNO_3}[H_2S][NO_3^-]$
Fe ²⁺ oxidation by MnO _{2A,B}	2Fe ²⁺ + 2IX + (MnO _{2A-Xk} + MnO _{2B-Xk}) + 2HCO ₃ ⁻ + 2H ₂ O → 2Fe(OH) _{3A-XI} + Mn ²⁺ + kX + 2CO ₂	$R_{FeMn_{A,B}} = k_{FeMn}[Fe^{2+}][MnO_{2A,B}]$
ΣH ₂ S oxidation by MnO _{2A,B}	H ₂ S + 4(MnO _{2A-Xk} + MnO _{2B-Xk}) + 6CO ₂ + 2H ₂ O → SO ₄ ²⁻ + 4Mn ²⁺ + 4kX + 6HCO ₃ ⁻	$R_{TSMnO_2} = k_{SMn}[H_2S][MnO_{2A,B}]$
FeS oxidation by MnO _{2A,B}	FeS-X _m + 4(MnO _{2A-Xk} + MnO _{2B-Xk}) + 8CO ₂ + 4H ₂ O → SO ₄ ²⁻ + 4Mn ²⁺ + Fe ²⁺ + (m + 4k)X + 8HCO ₃ ⁻	$R_{FeSMn} = k_{FeSMn}[FeS][MnO_{2A,B}]$
ΣH ₂ S oxidation by Fe(OH) _{3A,B}	H ₂ S + 8(Fe(OH) _{3A-XI} + Fe(OH) _{3B-XI}) + 14CO ₂ → SO ₄ ²⁻ + 8Fe ²⁺ + 8IX + 14HCO ₃ ⁻ + 6H ₂ O	$R_{TSFe_{A,B}} = k_{TSFe}[H_2S][Fe(OH)_{3A,B}]$
FeS oxidation by Fe(OH) _{3A,B}	FeS-X _m + 8(Fe(OH) _{3A-XI} + Fe(OH) _{3B-XI}) + 16CO ₂ → SO ₄ ²⁻ + 9Fe ²⁺ + (m + 8I)X + 16HCO ₃ ⁻ + 4H ₂ O	$R_{FeSFe_{A,B}} = k_{FeSFe}[FeS][Fe(OH)_{3A,B}]$
CH ₄ oxidation by SO ₄ ²⁻	CH ₄ + SO ₄ ²⁻ + CO ₂ → H ₂ S + 2HCO ₃ ⁻	$R_{CH_4SO_4} = k_{CH_4SO_4}[CH_4][SO_4^{2-}]$
H ₂ oxidation by SO ₄ ²⁻	5H ₂ + SO ₄ ²⁻ → H ₂ S + 4H ₂ O	$R_{HSO} = k_{HSO}[H_2][SO_4^{2-}]$
S ⁰ oxidation by H ₂ O	4S + 4H ₂ O → SO ₄ ²⁻ + 3HS ⁻ + 5H ⁺	$R_{SHO} = k_{SHO}[S]$

6.3 Equilibrium geochemistry

The pH is calculated as the sum of all charged species, where any unbalanced positive charge indicates H⁺. The charge balance is at each time step is solved as a state variable, which is subject to advection, diffusion and bioturbation reactions.

The precipitation of minerals is solved as an equilibrium reaction, dependent on the concentrations of the dissolved and solid substances, their K_{sp} and ion activity product (IAP). The equations are applied in a similar manner to those in Van Cappellen and Wang (1996) and numerous other studies, but with the exact forms of the equations based on those from Tufano et al. (2009). A positive rate indicates precipitation and a negative rate indicates dissolution. This model applies the function to all mineral simulated, including Fe(OH)₃, FeS, FeS₂, FeCO₃, CaCO₃ and MnCO₃.

This model has a process of mineral ageing, whereby iron and manganese oxides become crystalline and no longer react with organic matter, but can still undergo secondary redox reactions.

6.4 Setup

The model is configured using the aed2_seddiagenesis module. For the example simulations presented here the configured setup includes variables as indicated in Table 9. The boundaries at the sediment-water interface were taken from the time-varying outputs of the water column modules for the variables ammonium, nitrate, phosphate, oxygen, organic matter and sulfate. Other variables were set to a fixed concentration for solutes, or a fixed flux for solids. Although sulfate was not simulated in the water column, it was assumed that its concentration would be low, and correlated with total salinity. Organic matter depositional flux was calculated as the product of the organic matter concentration and the settling rate of particulate organic matter that was used in the water column simulation (0.06 m day⁻¹).

For this setup, porosity (ϕ) decreased with depth from 0.9 to 0.6. For bioturbation the model uses a diffusion coefficient that varies with depth ($D_{B(x)}$) as a two-layer function or a Gaussian decrease (Boudreau 1996). For the porewater components, diffusion coefficients are used that are based on free-solution molecular diffusion constants corrected for sediment tortuosity, Θ . The rate of deposition of total solids was 1 cm y⁻¹. (Table 11)

Note that, the model does not run the sediment diagenesis model in each grid cell but in each sediment "zone". In this case the model averages the overlying water column conditions before interfacing with the sediment model calculations, by engaging the feature do_zone_averaging.

Table 10: Summary of simulated species in the sediment biogeochemistry model, all resolved over depth.

Symbol	Units	Description	
Substrates			
POM_{Lab}	mmol L ⁻¹	Labile POM	flux estimated from water column simulation, as mmol m ⁻² y ⁻¹
POM_{Ref}	mmol L ⁻¹	Refractory POM	set as 0 mmol m ⁻² y ⁻¹
Terminal electron acceptors			
O_2	mmol L ⁻¹	Dissolved oxygen	from water column simulation
NO_3^-	mmol L ⁻¹	Nitrate	from water column simulation
MnO_{2A}	mmol L ⁻¹	Amorphous manganese (IV) oxide	set as 500 mmol m ⁻² y ⁻¹
$Fe(OH)_{3A}$	mmol L ⁻¹	Amorphous iron (III) hydroxide	set as 500 mmol m ⁻² y ⁻¹
SO_4^{2-}	mmol L ⁻¹	Sulfate	from water column simulation, based on salinity
Secondary by-products and other inorganic substances			
$\sum CO_2$	mmol L ⁻¹	All carbonate species	set as 1800 mmol L ⁻¹
$NH_4^+, NH_4^{+(ads)}$	mmol L ⁻¹	Dissolved and adsorbed ammonium	from water column simulation
$\sum PO_4^{3-}, PO_4^{3-(ads)}$	mmol L ⁻¹	Dissolved and adsorbed phosphate	from water column simulation
MnO_{2B}	mmol L ⁻¹	Crystalline manganese (IV) oxide	set as 0 mmol m ⁻² y ⁻¹
Mn^{2+}	mmol L ⁻¹	Manganese (II)	
$Fe(OH)_{3B}$	mmol L ⁻¹	Crystalline iron (III) hydroxide	set as 0 mmol m ⁻² y ⁻¹
Fe^{2+}	mmol L ⁻¹	Iron (II)	set as 0 mmol L ⁻¹
FeS	mmol L ⁻¹	Iron sulphide	set as 0 mmol m ⁻² y ⁻¹
FeS_2	mmol L ⁻¹	Pyrite	set as 0 mmol m ⁻² y ⁻¹
$\sum H_2S$	mmol L ⁻¹	Sulphide species	set as 0 mmol L ⁻¹
CH_4	mmol L ⁻¹	Methane	set as 0 mmol L ⁻¹
X	mmol L ⁻¹	Adsorbed metals arsenic, copper, cadmium, lead, nickel or zinc	set as 0 mmol L ⁻¹
$ChgBal$	mmol L ⁻¹	Charge balance	
$Chl-a$	mmol L ⁻¹	Chlorophyll	set as 0 mmol m ⁻² y ⁻¹
Zoo	mmol L ⁻¹	Zooplankton debris	set as 0 mmol m ⁻² y ⁻¹
Ca^{2+}	mmol L ⁻¹	Calcium	set as 0 mmol L ⁻¹
$CaCO_3$	mmol L ⁻¹	Calcite	set as 2.2 mmol m ⁻² y ⁻¹
$MnCO_3$	mmol L ⁻¹	Rhodochrosite	set as 0 mmol m ⁻² y ⁻¹
$FeCO_3$	mmol L ⁻¹	Siderite	set as 0 mmol m ⁻² y ⁻¹

Table 11: Parameters describing the physical setup and transport conditions within the sediment biogeochemistry model.

Parameter name	Unit	Example value	Description
db0	$\text{cm}^2 \text{y}^{-1}$	10	Biodiffusion coefficient at sediment-water interface
imix	0/1	0	Bioturbation function: 0-Gaussian; 1 – two-layer model
xs	cm	3	Half depth for Gaussian mixing (imix - 0)
x1	cm	1	Depth at which db starts to decrease (imix -1)
x2	cm	5	Depth at which db is zero (imix -1)
irrig	0/1	1	Bioirrigation switch
alpha0	y^{-1}	15	Irrigation coefficient
xirrig	cm	4	Maximum irrigation depth
ventflow	cm y^{-1}	0	Advective flux (positive value indicates from below)
w00	cm y^{-1}	0.75	Sediment accumulation velocity at maximum depth
p0	-	0.90	Porosity at sediment-water interface (ϕ_0)
p00	-	0.80	Porosity at maximum depth (ϕ_{x1})
bp	-	2.5	Porosity attenuation coefficient
torteq	1/2/3	3	Tortuosity calculation method switch: 1-Archie; 2-Burger; 3-Weissberg
an	-	2.14	Porosity exponent for tortuosity (if Archie)
aa	-	3.79	Porosity exponent for tortuosity (if Burger)
ab	-	2.02	Porosity exponent for tortuosity (if Weissberg)
xl	cm	100	Maximum simulation depth
maxnpts	-	40	Number of vertical layers

6.5 Results

Results for the 2013 simulation period undertaken for a single sediment zone are shown in Figure 11, with a focus on the evolution of sediment oxygen and phosphate over depth. The results highlight the dynamic nature of the sediment-water interface, and how surface changes in OM deposition and oxygen conditions propagate into the surficial sediment.

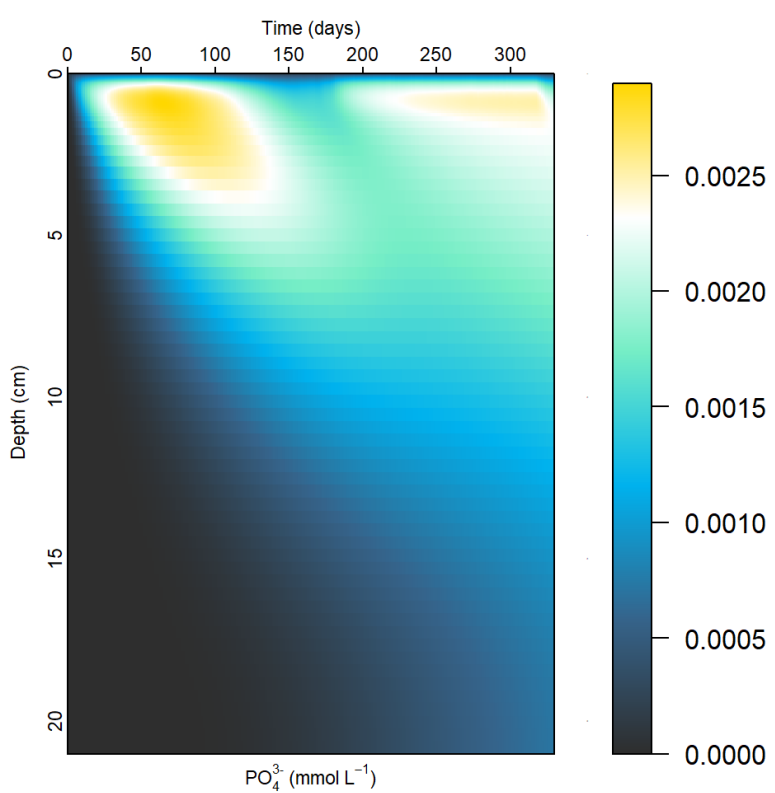
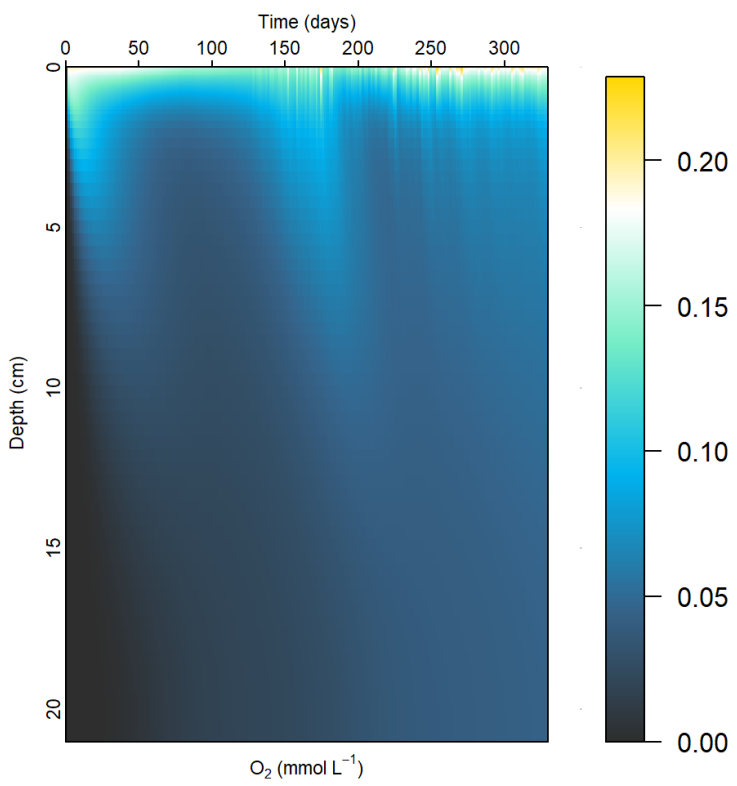


Figure 11. Time evolution of oxygen (top) and phosphate (bottom) in the selected sediment zone

7 Integrated simulations

The focus of the project to date has been on developing model capability and as such the model has not had a detailed calibration effort to compare the outputs with data. Nonetheless, in this section we present the model outputs of the latest code version demonstrating the indicative outputs of the model simulation and the successful operation of the model with mussels and ice included (Figures 12-16). The time-series plotting scripts presented, and available online (see Section 8) are able to aggregate and plot validation data once organised in the appropriate format (Appendix B).

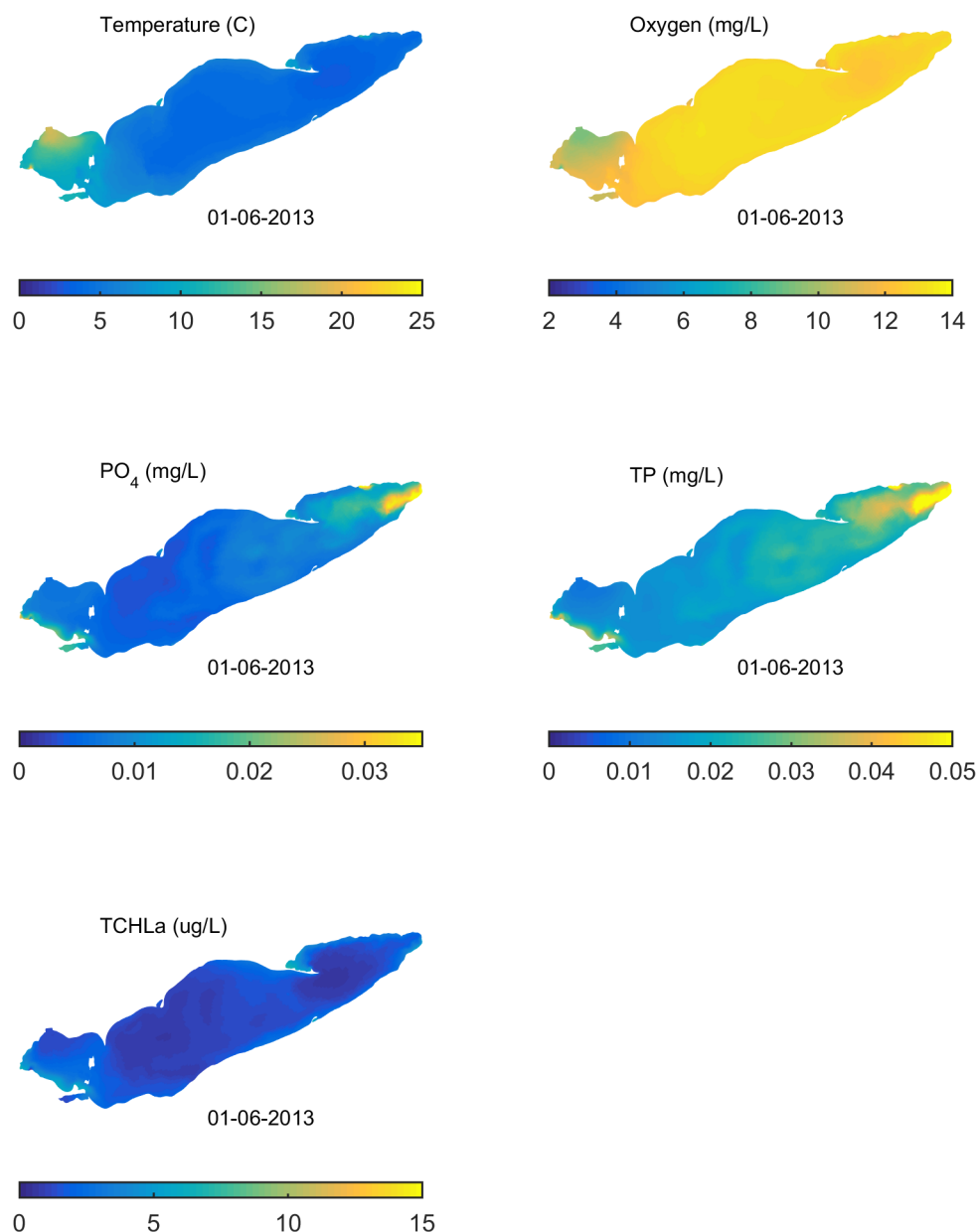


Figure 12: Results from June showing the spatial heterogeneity in key simulated variables.

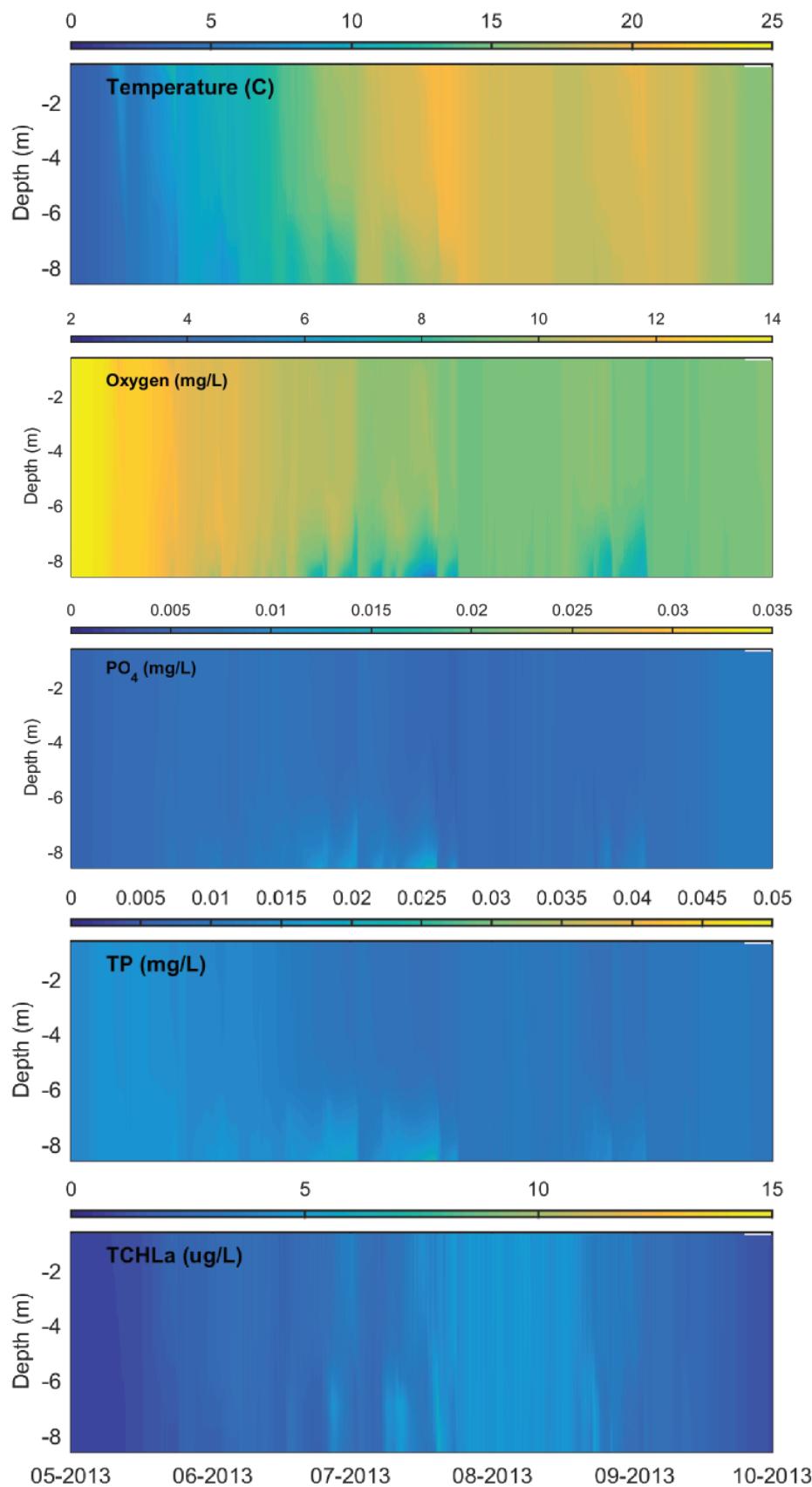


Figure 13a: Results from west basin.

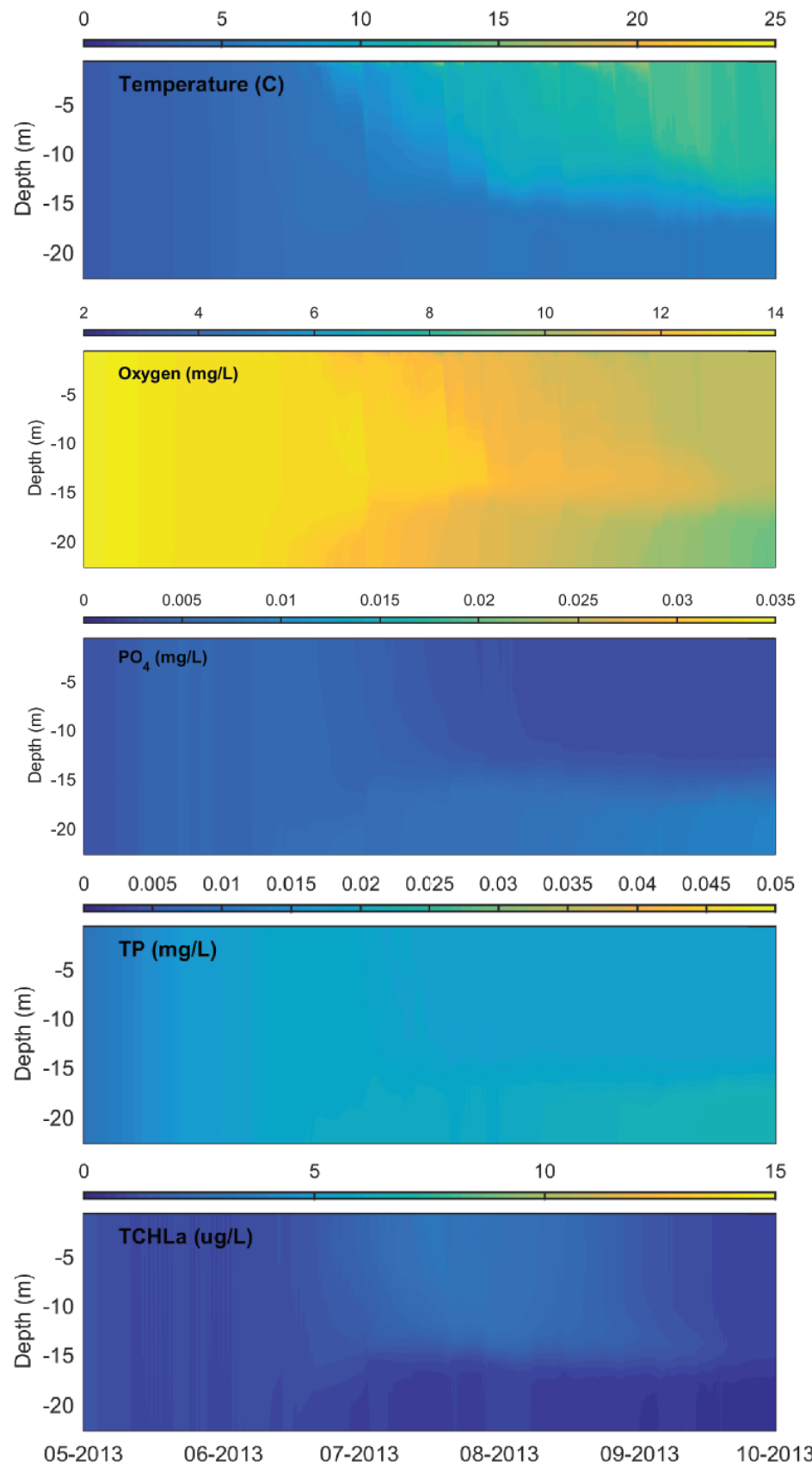


Figure 13b: Results from central basin.

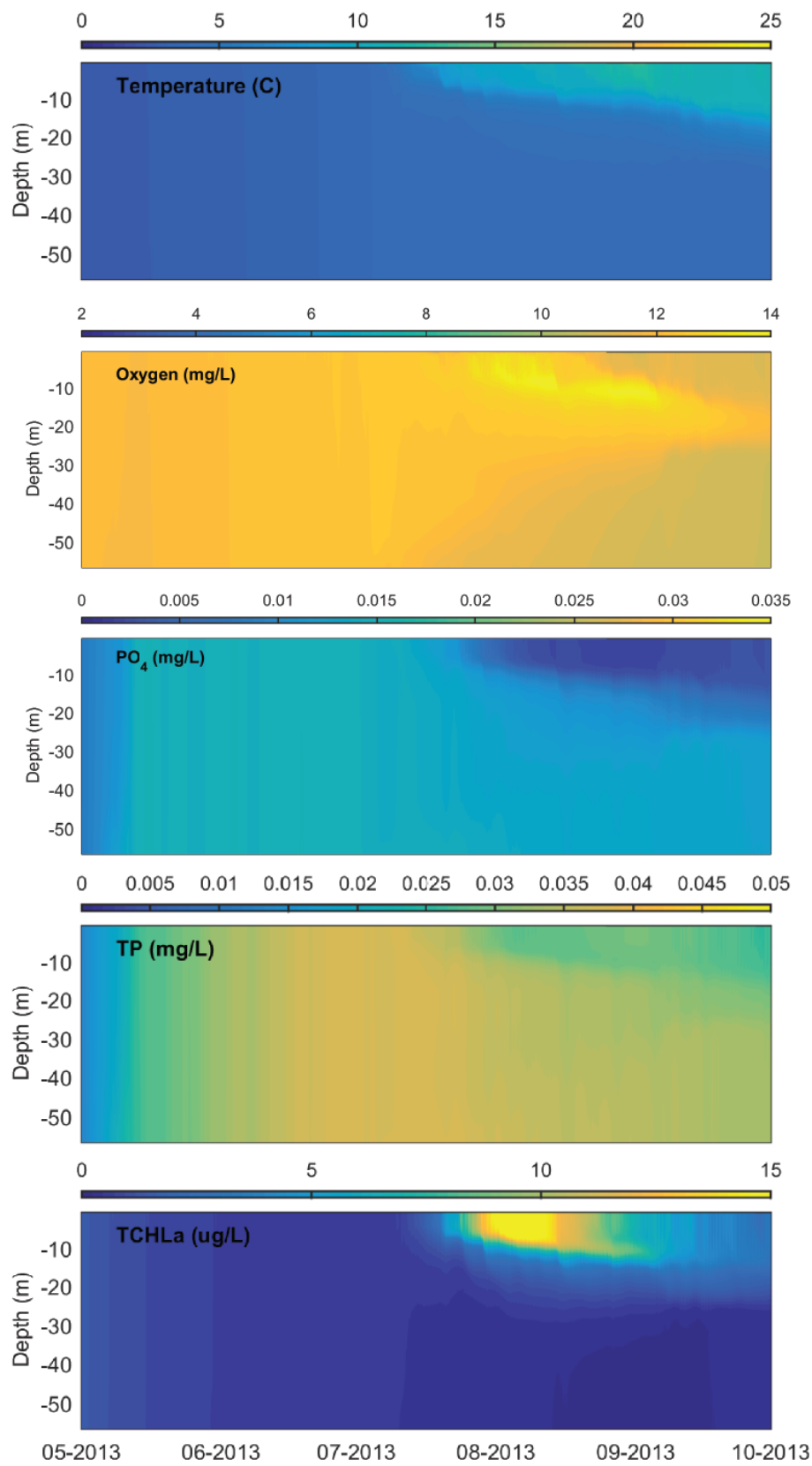


Figure 13c: Results from east basin.

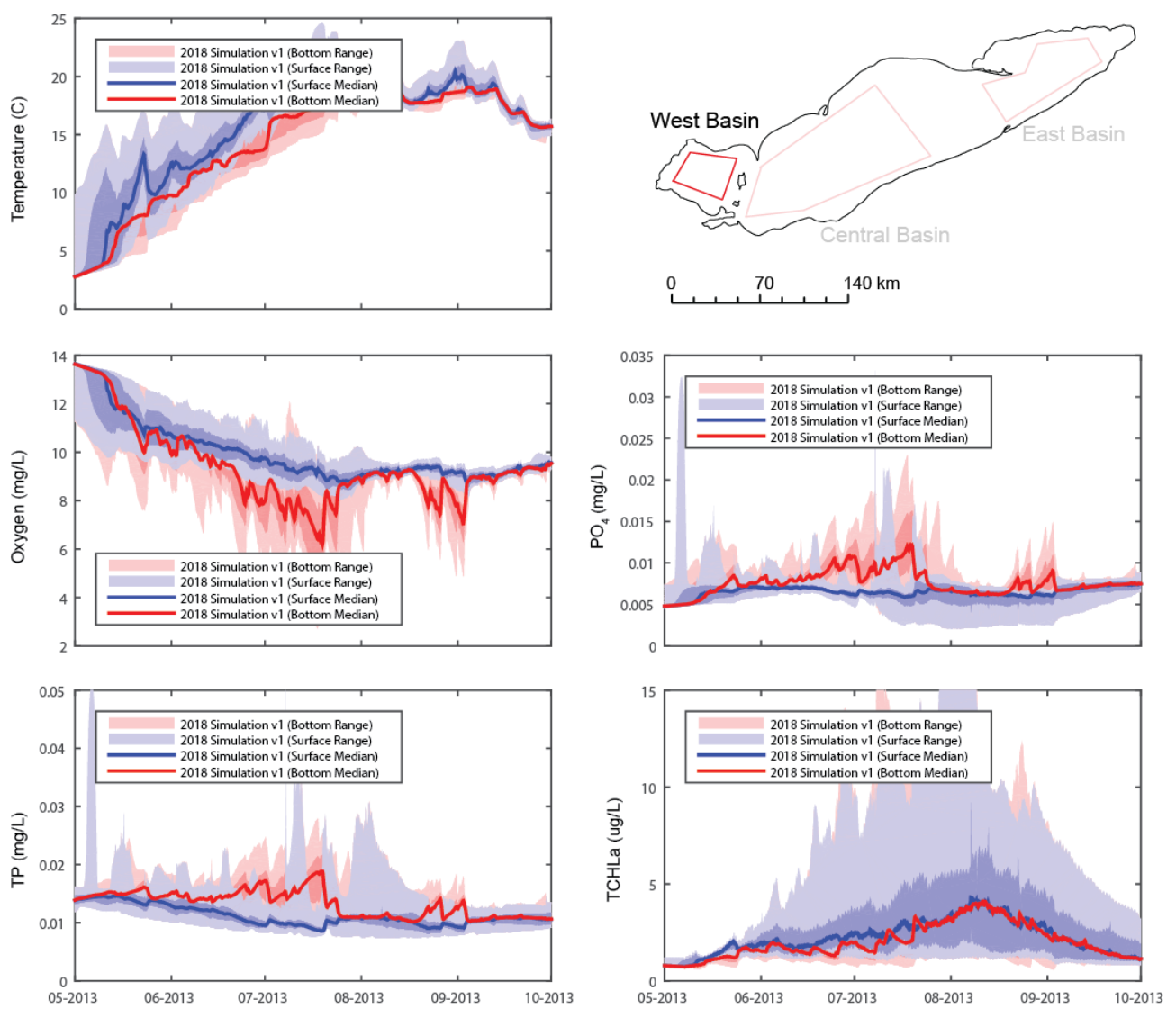


Figure 14a: Variation in key variables from West Basin over the summer, showing the range of predictions at the surface and bottom.

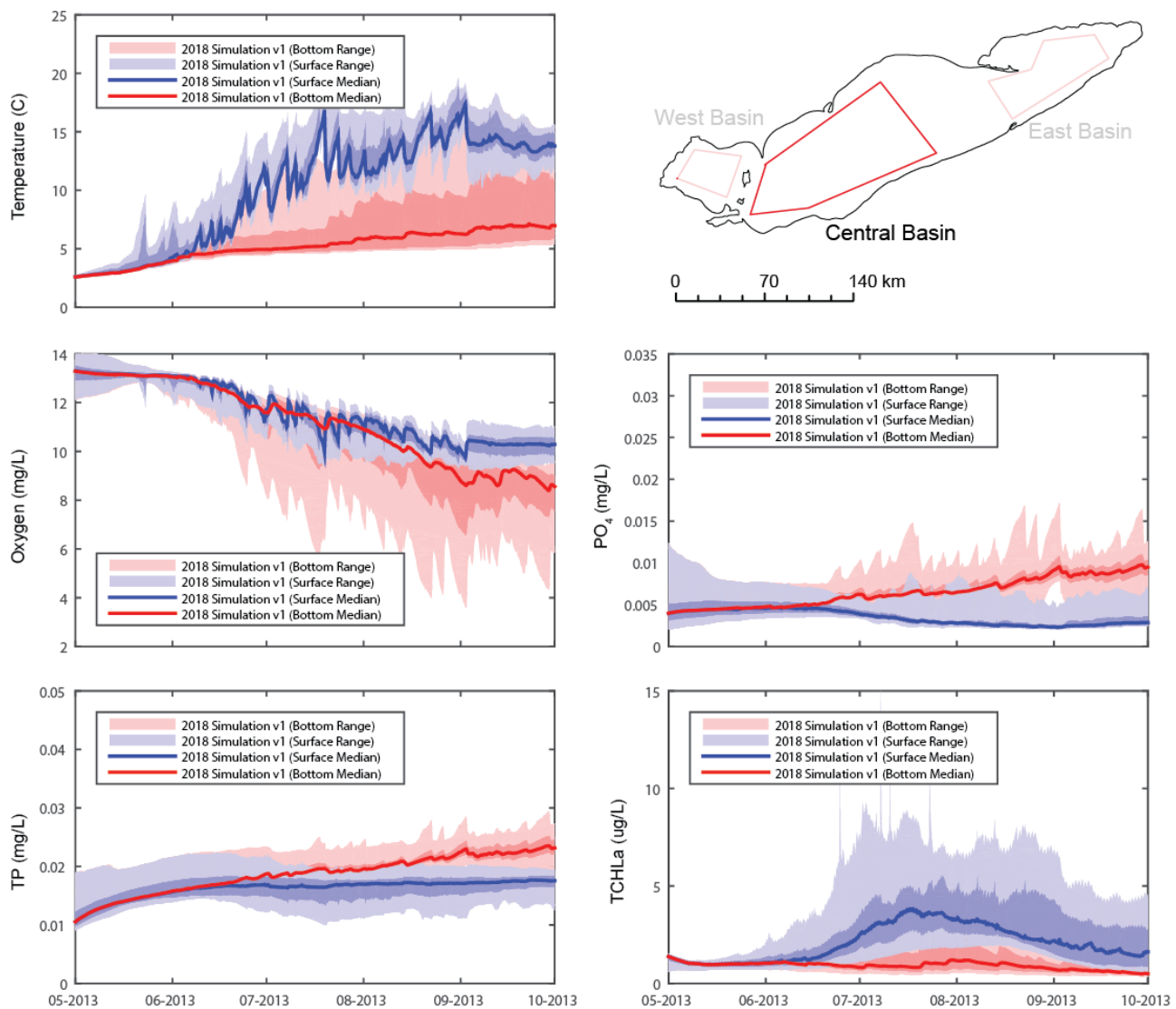


Figure 14b: Variation in key variables from Central Basin over the summer, showing the range of predictions at the surface and bottom.

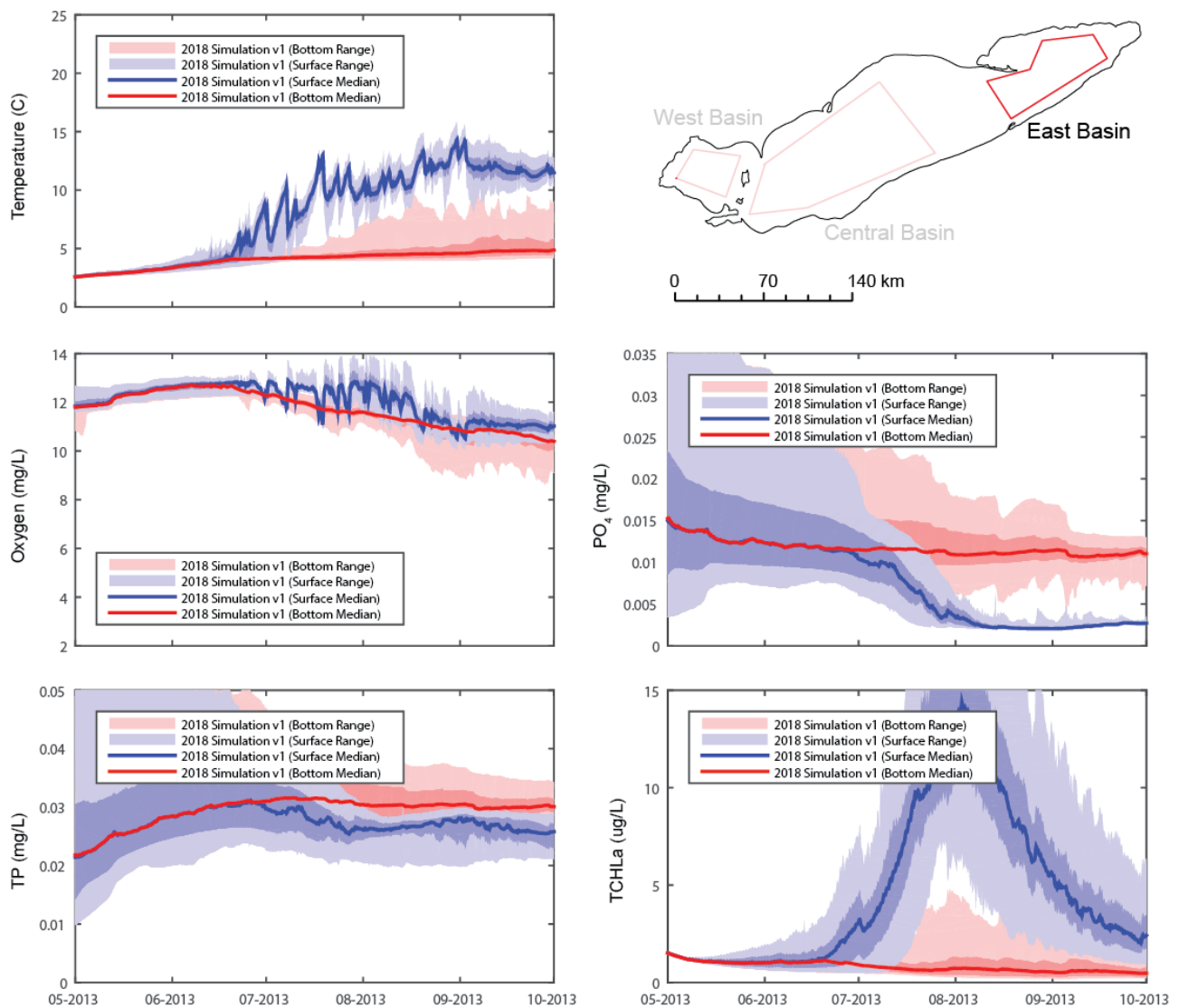


Figure 14c: Variation in key variables from East Basin over the summer, showing the range of predictions at the surface and bottom.

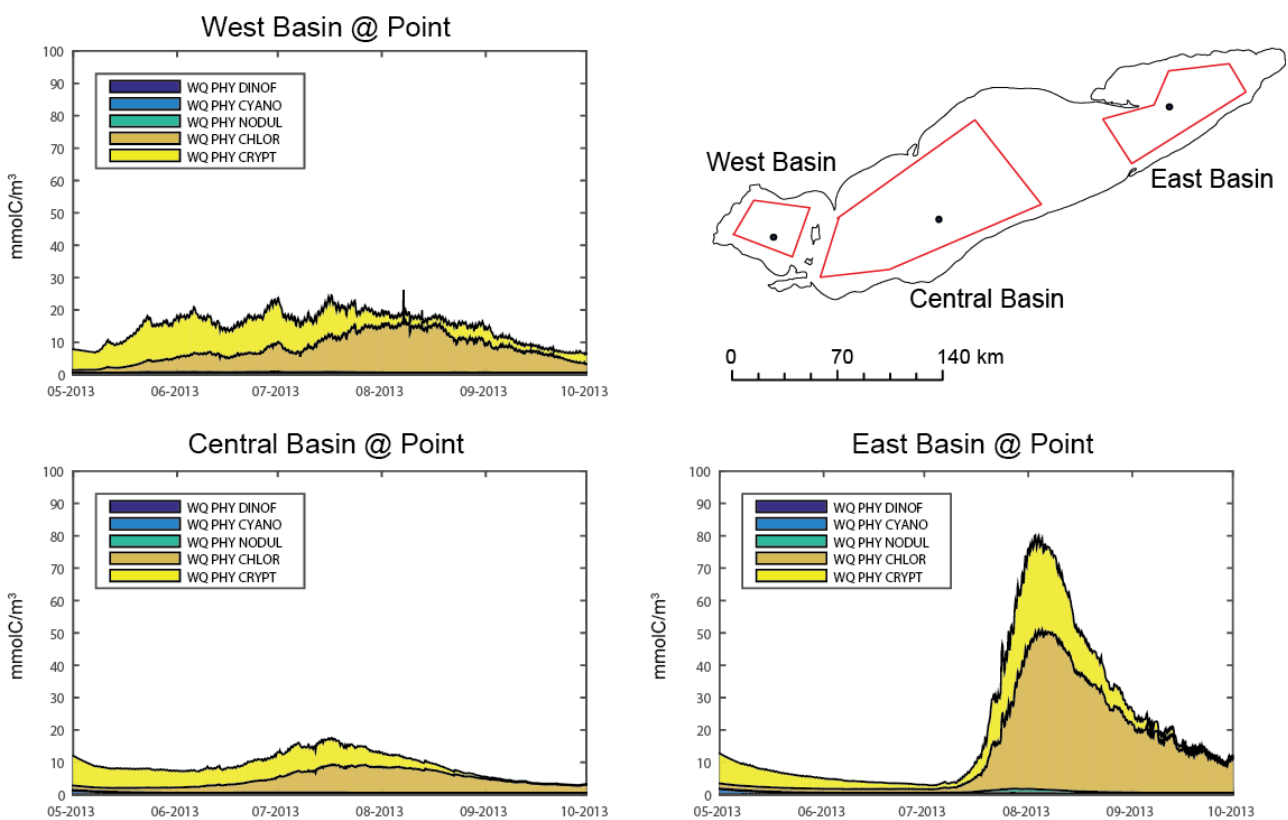


Figure 15. Composition of the simulated algal groups over time, in the three polygon regions.

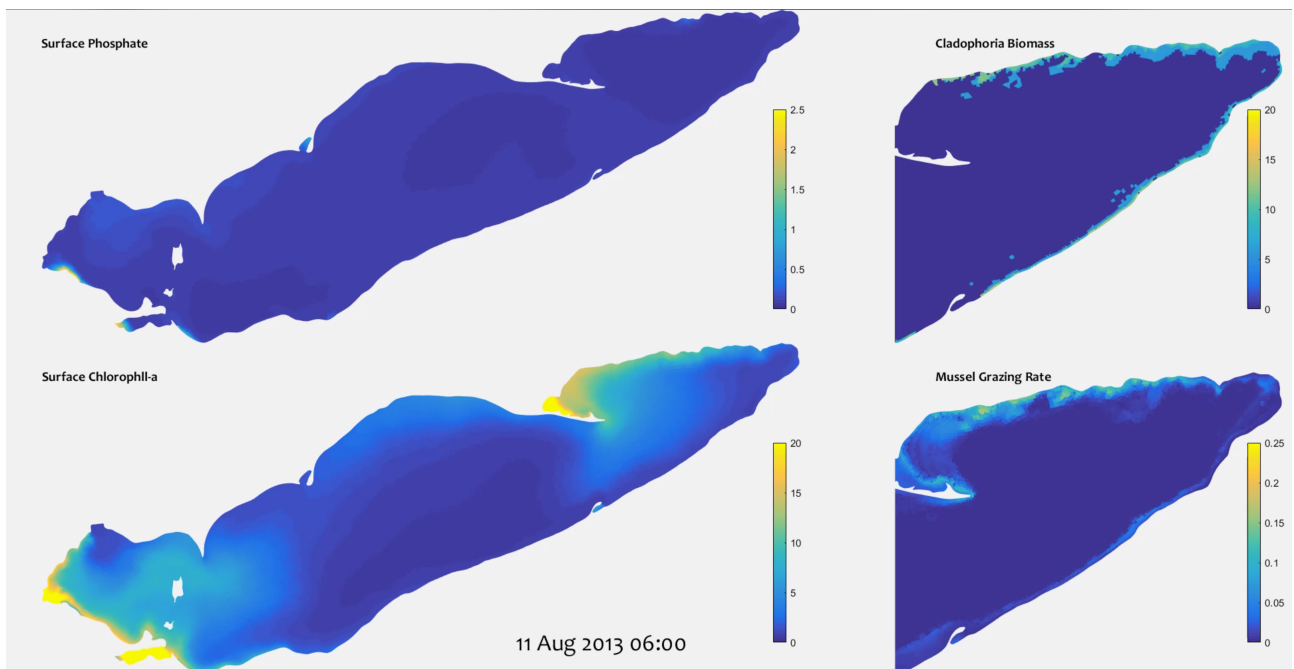


Figure 16. Snapshot of spatial variation in lake PO₄ and Chl-a (left), and response of mussels to Chl-a provision and Cladophora biomass to PO₄ in the East Basin, over the summer.

8 Model access and version control

The current generation of Lake Erie simulation is labelled as V3. The input files and processing scripts are under version controlled on the AquaticEcoDynamics GitHub repository:

<https://github.com/AquaticEcoDynamics/Lake-Erie>

The folder contains:

- Input files for the V3 of the Lake Erie setup.
- MATLAB scripts for the preparation of plots, including images in this report.

Note, for file compatibility, the model versions used to run Lake Erie are:

- TUFLOW-FV 2019: available at <https://www.tuflow.com/FV%20All%20Download.aspx>
- AED2 1.3.0 (Hipsey et al., 2019a): available at <https://zenodo.org/record/2538495#.XJzufy1L1R4>
- AED2+ 1.3.0 (available on request and required for bivalves, macroalgae and seddiagenesis modules).

Precompiled binaries for AED2 and version information are available from :
<http://aed.see.uwa.edu.au/research/models/AED/download.html>

Specific code developments undertaken as part of this project relate to changes to AED2+ (`aed2_bivalves`, `aed2_macroalgae`, `aed2_seddiagenesis`), accessible on GitHub via:

<https://github.com/AquaticEcoDynamics/libaed2-plus>

9 Concluding Remarks

The present report summarises the development of the TUFLOW-FV finite volume hydrodynamic model and AED2 biogeochemistry model to extend their capability for the simulation of Lake Erie. Whilst it is acknowledged that the model application needs further refinement and validation for Lake Erie going forward, the present analysis has prepared the model for a more detailed calibration in light of the available data and required detail for the system to be simulated.

Main advances and functionality now include:

- an ice cover model within TUFLOW FV, so simulations in Lake Erie can be undertaken all year round.
- fully functional routines for data input and output, including ability to use restart files.
- ice model integration with the ecological model AED2, allowing for full-year coupled simulations.

The model application to Lake Erie provided encouraging results in terms of timing and patterns of ice formation and disintegration.

Main advances and improved functionality for the AED2 model include:

- an advanced mussels model was implemented, allowing for spatial variation in biomass, and size classes.
- the CGM macroalgal model, which can be activated in the fringing regions of the lake with suitable substrate, and includes an attached component, plus ability to slough and drift.
- a dynamic and vertically resolved sediment biogeochemistry model for capturing behaviour of different sediments over time

The present model code base is a major advance in capability that can be used to further support lake understanding and hypothesis testing, nutrient budgeting, and scenario assessment. Further application and testing of the model requires:

- Assessment of model temperature predictions, including stratification in the 3 main basins.
- Validation of oxygen and nutrient variables
- Validation and refinement of the phytoplankton groups, and conformation of their timing,
- Validation of the AED2 CGM (Cladophora Growth Model) module, that was incorporated, within the nearshore zone.
- Focus on attributes of the different sediment biogeochemical zones to allow for spatially variable response of the sediment to organic matter deposition and overlying water properties.

The modules and functionality developed herein will be more easily calibrated and tested also using the GLM (1D) simulation that has capability to resolve the sediment and benthic properties as described herein.

10 References

- Alexander, J.E., Jr. and McMahon, R.F. 2004. Respiratory response to temperature and hypoxia in the zebra mussel *Dreissena polymorpha*. Comparative Biochemistry and Physiology Part A. 137: 425–434.
- Arndt, S., B. B. Jørgensen, D. E. Larowe, J. J. Middelburg, R. D. Pancost, and P. Regnier. 2013. Quantifying the degradation of organic matter in marine sediments: A review and synthesis. Earth-Science Reviews 123: 53-86.
- Ashton, G.D. (1986). River and lake ice engineering. Water Resources Publishing.
- Bayne, B.L. and Newell, R.C. 1983. Physiological energetics of marine molluscs, p. 407-515. In *The Mollusca*. Vol. 4. Academic Press, New York, NY.
- Berner, R. 1980. Early diagenesis: A theoretical approach. Princeton University Press
- Bierman, V.J., Kaur, J., DePinto, J.V., Feist, T.J., Dilks, D.W. 2005. Modeling the role of zebra mussels in the proliferation of blue-green algae in Saginaw Bay, Lake Huron. Journal of Great Lakes Research. 31: 32-55.
- Bocaniov, S. A., R. E. H. Smith, C. M. Spillman, M. R. Hipsey, and L. F. Leon. 2013. The nearshore shunt and the decline of the phytoplankton spring bloom in the Laurentian Great Lakes: insights from a three-dimensional lake model. Hydrobiologia DOI 10.1007/s10750-013-1642-2.
- Boudreau, B. P. 1996. A method-of-lines code for carbon and nutrient diagenesis in aquatic sediments. Computers & Geosciences 22: 479-496.
- Bruce, L.C., Cook, P.L.M. and Hipsey, M.R., 2011. Using a 3D hydrodynamic-biogeochemical model to compare estuarine nitrogen assimilation efficiency under anoxic and oxic conditions. In: Chan, F., Marinova, D. and Anderssen, R.S. (eds) MODSIM2011, 19th International Congress on Modelling and Simulation. Modelling and Simulation Society of Australia and New Zealand, December 2011, pp. 3691-3697. ISBN: 978-0-9872143-1-7
- Chao, X., Jia, Y., Shields, F.D., Wang, S.S.Y. and Cooper, C.M. (2010) Three-dimensional numerical simulation of water quality and sediment-associated processes with application to a Mississippi Delta lake. *Journal of Environmental Management*, 91, 1456–1466.
- Crowe, S. A., Canfield, D. E., Mucci, A., Sundby, B. and Maranger, R. (2012) Anammox, denitrification and fixed-nitrogen removal in sediments from the Lower St. Lawrence Estuary. *Biogeosciences* 9, 4309–4321.
- Gal, G., Hipsey, M.R., Paparov, A., Makler, V. and Zohary, T., 2009. Implementation of ecological modeling as an effective management and investigation tool: Lake Kinneret as a case study. *Ecological Modelling*, 220: 1697-1718.
- Gudimov, A., Kim, D-K, Young, J.D., Palmer, M.E., Dittrich, M, Winter, J.G., Stainsby, E., Arhonditsis, G.B. 2015. Examination of the role of dreissenids and macrophytes in the phosphorus dynamics of Lake Simcoe, Ontario, Canada. *Ecological Informatics*. 26: 36-53.
- Gudimov, A. McCulloch, J., Chen, J., Doan, P., Arhonditsis, G., Dittrich, M. 2016. Modeling the interplay between deep water oxygen dynamics and sediment diagenesis in a hard-water mesotrophic lake, *Ecological Informatics* 31 (2016) 59–69.
- Hamilton D.P., Schladow, S.G. (1997) Prediction of water quality in lakes and reservoirs. Part 1 – Model description. *Ecological Modelling* 96, 91–110.
- Hetherington, A.L. 2016. Chapter 1 - Comparison of clearance rates of zebra and quagga mussels (*Dreissena polymorpha* and *Dreissena rostriformis bugensis*) across annual lake temperatures. PhD Thesis, Cornell University, USA.
- Higgins, S.N., Hecky, R.E. and Guildford, S.J., 2006. Environmental controls of Cladophora growth dynamics in eastern Lake Erie: application of the Cladophora growth model (CGM). *Journal of Great Lakes Research*, 32(3), pp.629-644.
- Hipsey, M.R., Bruce, L.C., Boon, C., Busch, B., Carey, C.C., Hamilton, D.P., Hanson, P.C., Read, J.S., de Sousa, E., Weber, M. and Winslow, L.A., 2019. A General Lake Model (GLM 3.0) for linking with high-frequency sensor data from the Global Lake Ecological Observatory Network (GLEON). *Geoscientific Model Development*, 12(1), pp.473-523.
- Hipsey, M.R., Boon, C., Paraska, D., Bruce, L.C., and Huang, P. 2019. AquaticEcoDynamics/libaed2: v1.3.0-rc2, Aquatic EcoDynamics (AED) Model Library & Science Manual, 1–34, doi:10.5281/zenodo.2538495.
- Kim, D.K., Zhang, W., Watson, S. and Arhonditsis, G.B., 2014. A commentary on the modelling of the causal linkages among nutrient loading, harmful algal blooms, and hypoxia patterns in Lake Erie. *Journal of Great Lakes Research*, 40, pp.117-129.
- Kitchell, J.F., Stewart, D.J., and Weininger, D. 1977. Applications of a bioenergetics model to yellow perch (*Perca flavescens*) and walleye (*Stizostedion vitreum vitreum*). *Journal of Fisheries of Research Board Canada*. 34: 1922-1935.
- Leon, L.F., Smith, R.E.H., Hipsey, M.R., Bocaniov, S.N., Higgins, S.N., Hecky, R.E., Antenucci, J.P., Guildford, S.J., 2011. Application of a 3D hydrodynamic-biological model for seasonal and spatial dynamics of water quality and phytoplankton in Lake Erie. *Journal of Great Lakes Research*. 37: 41-53
- Oveisy, A., Boegman, L., Imberger, J. (2012) Three-dimensional simulation of lake and ice dynamics during winter. *Limnology and Oceanography*, 57(1). doi:10.4319/lo.2011.57.1.0000
- Paraska, D., Hipsey, M.R., Salmon, S.U., 2014. Sediment diagenesis models: model approaches, challenges and opportunities. *Environmental Modelling & Software*, 61: 297-325

- Petrone, K.C., Richards, J.S., Grierson, P.F. (2009) Bioavailability and composition of dissolved organic carbon and nitrogen in a near coastal catchment of south-western Australia. *Biogeochemistry* 92, 27–40.
- Roberts, K. L., V. M. Eate, B. D. Eyre, D. P. Holland, and P. L. M. Cook. 2012. Hypoxic events stimulate nitrogen recycling in a shallow salt-wedge estuary: The Yarra River Estuary, Australia. *Limnology and Oceanography*, 57: 1427–1442.
- Rogers, C.K., Lawrence, G., Hamblin, P. F.. 1995. Observations and numerical simulation of a shallow ice-covered midlatitude lake. *Limnology and Oceanography* 40: 374–385, doi:10.4319/lo.1995.40.2.0374.
- Romero, J.R., Antenucci, J.P. and Imberger, J. (2004) One- and three-dimensional biogeochemical simulations of two differing reservoirs. *Ecological Modelling* 174, 143–160.
- Schneider, D.W. 1992. A bioenergetics model of zebra mussels, *Dreissena polymorpha*, Growth in the Great Lakes. Canadian Journal of Fisheries and Aquatic Sciences. 49: 1406-1416.
- Schwab, D.J., Beletsky, D., DePinto, J. and Dolan, D.M., 2009. A hydrodynamic approach to modeling phosphorus distribution in Lake Erie. *Journal of Great Lakes Research*, 35(1), pp.50-60.
- Soetaert, K., Herman, P.M. and Middelburg, J.J., 1996. A model of early diagenetic processes from the shelf to abyssal depths. *Geochimica et Cosmochimica Acta*, 60(6), pp.1019-1040.
- Spillman, C.M., Hamilton, D.P., Hipsey, M.R., and Imberger, J. 2008. A spatially resolved model of seasonal variation and phytoplankton and clam (*Tapes philippinarum*) biomass in Baramarco Lagoon, Italy. *Estuarine, Coastal, and Shelf Science*. 79: 187-203.
- Sprung, M. and Rose, U. 1988. Influence of food size and food quantity on the feeding of the mussel *Dreissena polymorpha*. *Oecologia*. 77:526-532.
- Thornton, K.W. and Lessem, A.S. 1978. A temperature algorithm for modifying biological rates. *Transactions of the American Fisheries Society*. 107: 284-287.
- Trolle, D., Hamilton, D.P., Hipsey, M.R., Bolding, K., Bruggeman, J., Mooij, W. M., Janse, J. H., Nielsen, A., Jeppesen, E., Elliott, J. E., Makler-Pick, V., Petzoldt, T., Rinke, K., Flindt, M. R., Arhonditsis, G.B., Gal, G., Bjerring, R., Tominaga, K., Hoen, J., Downing, A. S., Marques, D. M., Fragoso Jr, C. R., Søndergaard, M. and Hanson, P.C. 2012. A community-based framework for aquatic ecosystem models. *Hydrobiologia*, 683(1): 25-34.
- TVA (1972). Heat and Mass Transfer between a Water Surface and the Atmosphere. Water Resources Research Laboratory Report n. 14. Tennessee Valley Authority Report n. 0-6803.
- Umlauf, L. and Burchard, H., 2003. A generic length-scale equation for geophysical turbulence models. *Journal of Marine Research*, 61(2), pp.235-265.
- Van Cappellen, P. and Wang, Y., 1996. Cycling of iron and manganese in surface sediments; a general theory for the coupled transport and reaction of carbon, oxygen, nitrogen, sulfur, iron, and manganese. *American Journal of Science*, 296(3), pp.197-243.
- Valipour, R., Bouffard, D., Boegman, L. and Rao, Y.R., 2015. Near-inertial waves in Lake Erie. *Limnology and Oceanography*, 60(5), pp.1522-1535.
- Vavrus, S. J., Wynne, R. H., Foley, J. A. 1996. Measuring the sensitivity of southern Wisconsin lake ice to climate variations and lake depth using a numerical model. *Limnol. Oceanogr.* 41: 822–831, doi:10.4319/lo.1996.41.5.0822
- Walz, N. 1978. The energy balance of the freshwater mussel *Dreissena polymorpha* Pallas in laboratory experiments and in Lake Constance. I. Pattern of activity, feeding and assimilation efficiency. *Archiv für Hydrobiologie – Supplements*. 55(1): 83-105.

Appendix A: Model Parameters

The variables outlined in Table 2 were configured to be simulated within the AED2 control file (aed2.nml). In total, more than 20 state (transportable) variables were simulated (see Table 2) from the "aed2_noncohesive", "aed2_oxygen", "aed2_silica", "aed2_nitrogen", "aed2_phosphorus", "aed2_organic_matter", and "aed2_phytoplankton" modules, and numerous diagnostic variables were also output (of which only several are presented in the results). Indicative parameters for the simulations are summarised below for these modules; refer to the main sections for mussels, cladophora and sediment. Table A1 summarises the phytoplankton groups, Table A2 summarises the main biogeochemical parameter values, and Table A3 summarises the default sediment flux parameters used.

Table A1: Phytoplankton parameter overview relevant to the Lake Erie model configuration.

parameter	description	units	value				
			DINOF	CYANO	NODUL	CHLOR	CRYPT
R_{growth}^{PHY}	phytoplankton growth rate at 20C	d ⁻¹	1.3	1.2	1.8	1.55	0.55
I_K	light ½ saturation constant for algal limitation	μE m ⁻² s ⁻¹	200	100	200	380	180
K_e^{PHY}	specific attenuation coefficient	mmol C m ⁻³ m ⁻¹	0.0408	0.0051	0.048	0.048	0.048
ϑ_{growth}^{PHY}	Arrhenius temperature scaling for growth	-	1.06	1.08	1.06	1.07	1.10
T_{std}	standard temperature	C	20	20	18	15	20
T_{opt}	optimum temperature	C	28	28	25	20	25
T_{max}	maximum temperature	C	38	38	37	35	35
R_{resp}^{PHY}	phytoplankton respiration rate at 20C	d ⁻¹	0.07	0.08	0.12	0.14	0.05
k_{fres}^{PHY}	fraction of metabolic loss that is respiration	-	0.7	0.7	0.7	0.7	0.7
k_{fdom}^{PHY}	fraction of metabolic loss that is DOM	-	0.3	0.3	0.3	0.3	0.3
ϑ_{resp}^{PHY}	Arrhenius temperature scaling for respiration	-	1.05	1.08	1.08	1.08	1.08
X_{NCON}^{PHY}	average internal N concentration	mmol N mmol C ⁻¹	0.15	0.15	0.15	0.137	0.15
K_N	half-saturation concentration of nitrogen	mmol N m ⁻³	1.786	2.143	2.50	1.60	3.57
$R_{NUptake}^{PHY}$	maximum nitrogen uptake rate	mmol N m ⁻³ d ⁻¹	0.069	0.032	0.257	0.206	
X_{NMIN}^{PHY}	minimum internal nitrogen concentration	mmol N mmol C ⁻¹	-	0.054	-	-	-
X_{NMAX}^{PHY}	maximum internal nitrogen concentration	mmol N mmol C ⁻¹	-	0.107	-	-	-
X_{PCON}^{PHY}	average internal P concentration	mmol N mmol C ⁻¹	0.0094	0.0094	0.0039	0.0039	0.0094
K_P	half-saturation concentration of phosphorus	mmol P m ⁻³	0.3226	0.1935	0.3226	0.2400	0.161
$R_{PUptake}^{PHY}$	maximum phosphorus uptake rate	mmol P m ⁻³ d ⁻¹	0.0031	0.0019	0.0015	0.0023	
X_{PMIN}^{PHY}	minimum internal phosphorus concentration	mmol P mmol C ⁻¹	-	0.0039	-	-	-
X_{PMAX}^{PHY}	maximum internal phosphorus concentration	mmol P mmol C ⁻¹	-	0.0077	-	-	-
K_{Si}	half-saturation concentration of silica	mmol Si m ⁻³	8.0	8.0	15.71	3.9	0
$X_{C:Si}^{PHYa}$	internal silicate concentration	mmol Si mmol C ⁻¹	0.0171	0.0214	0.01	0.1096	0.01
ω_{PHY}	phytoplankton sedimentation rate	m d ⁻¹	-0.1	0	0.0	-0.30	+0.1

Parameters based on the following information:

Leon et al (2011), prior CAEDYM calibrations
Kim et al (2014) review of parameter choice

Table A2: Summary of water column biogeochemical parameter descriptions, units and values adopted (note these are not calibrated values).

Symbol	Description	Units	Value	Comment
<i>Atmospheric exchange</i>				
$k_{atm}^{O_2}$	oxygen transfer coefficient	m s^{-1}		calculated Wanninkhof (1992)
$[O_2]_{atm}$	atmospheric oxygen concentration	$\text{mmol O}_2 \text{ m}^{-3}$		calculated Riley and Skirrow (1975)
$k_{atm}^{CO_2}$	carbon dioxide transfer coefficient	m s^{-1}		calculated
$[CO_2]_{atm}$	atmospheric carbon dioxide concentration	mmol C m^{-3}		calculated
$k_{atm}^{CH_4}$	methane transfer coefficient	m/s		calculated
$[CH_4]_{atm}$	atmospheric methane concentration	mmol C m^{-3}		calculated
dz_{smin}	Minimum depth of a surface cell for flux computation	m	0.2	Chosen to prevent large concentrations
<i>Chemical oxidation</i>				
$\chi_{N:O_2}^{nitrif}$	stoichiometry of O_2 consumed during nitrification	g N g O_2^{-1}	0.44	1/32
R_{nitrif}	maximum rate of nitrification	d^{-1}	0.5	0.5 ^B
K_{nitrif}	half saturation constant for oxygen dependence of nitrification rate	$\text{mmol O}_2 \text{ m}^{-3}$	78.1	78.1 ^B
θ_{nitrif}	temperature multiplier for nitrification	-	1.08	1.08 ^B
$\chi_{CH_4:O_2}^{nitrif}$	stoichiometry of O_2 consumed during CH_4 oxidation	g C g O_2^{-1}	0.38	12/32
R_{ch4ox}	maximum rate of methane oxidation	d^{-1}	0.5	0.5 ^B
K_{ch4ox}	half saturation constant for oxygen dependence of methane oxidation rate	$\text{mmol O}_2 \text{ m}^{-3}$	78.1	78.1 ^B
θ_{ch4ox}	temperature multiplier for methane oxidation	-	1.08	1.08 ^B
<i>Dissolved organic matter transformations</i>				
$\chi_{C:O_2}^{miner}, \chi_{C:O_2}^{PHY}$	stoichiometry of O_2 consumed during aerobic mineralization and photosynthesis	g C g O_2^{-1}	0.38	12/32
$R_{miner}^{DOC}, R_{miner}^{DON}, R_{miner}^{DOP}$	maximum rate of aerobic mineralisation of labile dissolved organic matter @ 20C	d^{-1}	0.5	0.001 – 0.006 ^D 0.01 – 0.05 ^A 0.001 – 0.028 ^D
$K_{miner}^{DOC}, K_{miner}^{PON}, K_{miner}^{DOP}$	half saturation constant for oxygen dependence on aerobic mineralisation rate	$\text{mmol O}_2 \text{ m}^{-1}$	31.25	47 – 78 ^A
$\theta_{miner}^{DOC}, \theta_{miner}^{DON}, \theta_{miner}^{DOP}$	temperature multiplier for aerobic mineralisation	-	1.08	1.05 – 1.11
R_{denit}	maximum rate of denitrification	d^{-1}	0.5	0.5 ^B
K_{denit}	half saturation constant for oxygen dependence of denitrification	$\text{mmol O}_2 \text{ m}^{-3}$	21.8	21.8 ^B
θ_{denit}	temperature multiplier for temperature dependence of denitrification	-	1.08	1.08 ^B
R_{photo}^{DOMR}	maximum rate DOM-R photolysis per mol of light	$\text{mmol C m}^{-3} \text{ d}^{-1}$		calculated from Eq 12 using c = 7.52 and d = 0.0122, assuming 3 bandwidth fractions based on mean wavelengths of 298, 358 and 440 nm
f_{photo}	fraction of DOM-R photolysis that leads to mineralisation	-	0.1	assumed
<i>Particulate organic matter transformations</i>				
$R_{decom}^{POC}, R_{decom}^{PON}, R_{decom}^{POP}$	maximum rate of decomposition of particulate organic material @ 20C	d^{-1}	0.5	0.01 – 0.07 ^A ; 0.008 ^C
$K_{decom}^{DOC}, K_{decom}^{PON}, K_{decom}^{DOP}$	half saturation constant for oxygen dependence on particulate decomposition (hydrolysis) rate	$\text{mmol O}_2 \text{ m}^{-3}$	31.25	47 – 78 ^A
$\theta_{decom}^{POC}, \theta_{decom}^{PON}, \theta_{decom}^{POP}$	temperature multiplier for temperature dependence of mineralisation rate	-	1.08	1.08 ^B
$R_{breakdown}^{CPOM}$	Rate of breakdown of CPOM to POM	d^{-1}	0.0003	10% per year
$\chi_{C:N}^{CPOM}, \chi_{C:P}^{CPOM}$	C:N and C:P stoichiometry of CPOM	mol:mol	106:16:1	Redfield
$\omega_{POC}, \omega_{PON}, \omega_{POP}$	settling rate of particulate organic material	m d^{-1}	-0.05	-1.0 ^B
ω_{CPOM}	settling rate of coarse particulate organic material	m d^{-1}	-0.1	assumed
f_{ref}	Fraction of POM breakdown that returns to DOM-R	-	0.01	assumed
<i>Adsorption/desorption parameters</i>				
$\Phi_{ads}^{PH}(pH)$	Function characterizing pH effect on	-	calculated	$-0.0088(pH)^2 + 0.0347(pH) + 0.9768^E$
c_{ads}^r	ratio of adsorption and desorption rate coefficients	L mg^{-1}	0.7	0.7 ^F
c_{ads}^{max}	maximum adsorption capacity of SS	mmol P mg SS^{-1}	0.00016	0.00016 ^F
Parameters based on the following information:				
^A	Converted from data on oligotrophic lakes (Romero et al., 2004) to eutrophic lakes (Gal et al., 2009), and justifications therein.			
^B	Based on Bruce et al. (2011) FABM-AED application; estimated from data from Roberts et al. (2013).			
^C	Based on Hamilton and Schladow (1997) for Prospect Reservoir			
^D	Based on incubations by Petrone et al. (2009) for Swan Estuary (Western Australia)			
^E	Based on regression of data from Salmon et al. (2017) based on data review from 6 papers therein			
^F	Based on model of Chao et al. (2010).			

Table A3: Summary of sediment parameter descriptions, units and typical values.

Symbol	Description	Units	Assigned value	Comment
$F_{max}^{O_2}$	maximum flux of oxygen across the sediment water interface into the sediment	mmol O ₂ m ⁻² d ⁻¹	80.0	Lake: 22.4 ^G River: 9.4 – 20.3 ^B Estuary: 48 ^C ; 79 ^D ; ~50 ^E
$K^{O_2}_{sed}$	half saturation constant for oxygen dependence of sediment oxygen flux	mmol O ₂ m ⁻³	130	Estuary: 150 ^C ; ~50 ^F
$\theta^{O_2}_{sed}$	temperature multiplier for temperature dependence of sediment oxygen flux	-	= θ_{sed} = 1.08	1.04 – 1.10 ^A
F_{max}^{RSi}	maximum flux of silica across the sediment water interface	mmol Si m ⁻² d ⁻¹	4	Estuary: 4 – 40 ^E
K^{RSi}_{sed}	half saturation constant for oxygen dependence of sediment silica flux	mmol Si m ⁻³	150	estimated
θ^{RSi}_{sed}	temperature multiplier for temperature dependence of sediment silica flux	-	= θ_{sed} = 1.08	1.04 – 1.10 ^A
$F_{max}^{PO_4}$	maximum flux of phosphate across the sediment water interface	mmol P m ⁻² d ⁻¹	0.2	Lake: 0.01 – 0.07 ^G River: 0.01 – 0.10 ^B Estuary: 0.3 – 4 ^E
$K^{PO_4}_{sed}$	half saturation constant for oxygen dependence of sediment phosphate flux	mmol O ₂ m ⁻³	20	Estuary: >200 ^F
$\theta^{PO_4}_{sed}$	temperature multiplier for temperature dependence of sediment phosphate flux	-	= θ_{sed} = 1.08	1.04 – 1.10 ^A
F_{max}^{DOP}	maximum flux of dissolved organic phosphorus across the sediment water interface	mmol P m ⁻² d ⁻¹	0.05	River: 0.05 – 0.10 ^B
K^{DOP}_{sed}	half saturation constant for oxygen dependence of sediment dissolved organic phosphorus flux	mmol O ₂ m ⁻³	150	estimated
θ^{DOP}_{sed}	temperature multiplier for temperature dependence of sediment dissolved organic phosphorus flux	-	= θ_{sed} = 1.08	1.04 – 1.10 ^A
$F_{max}^{NH_4}$	maximum flux of ammonium across the sediment water interface	mmol N m ⁻² d ⁻¹	30.0	Lake: 1.3 ^G River: 4.3 – 12.8 ^B Estuary: 30 ^C ; 5 – 25 ^E
$K^{NH_4}_{sed}$	half saturation constant for oxygen dependence of sediment ammonium flux	mmol N m ⁻¹	31.25	Estuary: 31.25 ^C
$\theta^{NH_4}_{sed}$	temperature multiplier for temperature dependence of sediment ammonium flux	-	1.08	1.04 – 1.10 ^A
$F_{max}^{NO_3}$	maximum flux of nitrate across the sediment water interface	mmol N m ⁻² d ⁻¹	5.2	River: 4.3 – 12.8 ^B Estuary: 5.2 ^C ; -7.2 – 7.1 ^E ; 0.4 ^H
$K^{NO_3}_{sed}$	half saturation constant for oxygen dependence of sediment nitrate flux	mmol O ₂ m ⁻³	100.0	Estuary: 100 ^C
$\theta^{NO_3}_{sed}$	temperature multiplier for temperature dependence of sediment nitrate flux	-	= θ_{sed} = 1.08	1.04 – 1.10 ^A
F_{max}^{DON}	maximum flux of dissolved organic nitrogen across the sediment water interface	mmol N m ⁻² d ⁻¹	5.2	River: 1.28 – 2.20 ^B
K^{DON}_{sed}	half saturation constant for oxygen dependence of sediment dissolved organic nitrogen flux	mmol N m ⁻³	100.0	estimated
θ^{DON}_{sed}	temperature multiplier for temperature dependence of sediment dissolved organic nitrogen flux	-	= θ_{sed} = 1.08	1.04 – 1.10 ^A
Parameters based on the following information:				
A	Converted from data on oligotrophic lakes (Romero et al., 2004) to eutrophic lakes (Gal et al., 2009), and justifications therein.			
B	Based on Hipsey et al. (2010) ELCOM-CAEDYM model of the lower Murray River; estimated from data.			
C	Based on Bruce et al. (2011) GETM-FABM-AED application; estimated from data from Roberts et al. (2013).			
D	Net flux measured during eddy correlation experiment in the Upper Swan Estuary (Department of Water, unpublished data); varied in the range 20 – 150 mmol O ₂ /m ² /d with a background concentration of 260 mmol O ₂ /m ³ , therefore $F_{max}^{O_2} \sim 50/(260/(260+150)) = 79$ mmol O ₂ /m ² /d.			
E	Based on benthic chamber studies showing an average net flux of 50 mmol O ₂ /m ² /d the Upper Swan estuary (Smith et al., 2007).			
F	Based on Smith et al., (2007) assessment of data from the Upper Swan estuary, limitation at low oxygen concentrations is not observed			
G	Based on Fisher et al., (2005) benthic fluxes in Lake Okeechobee.			
H	Based on Crowe et al., (2012) Table 4 synthesis and measurements of N flux in St Lawrence Estuary.			

Appendix B: Observation Data Format for Validation Plotting

The *.mat file is a matlab structure of observational data (e.g., nutrients, temperature) that can be optionally loaded and plotted on the time-series plots to facilitate validation.

The file has the layout:

Project → Site → Variable → Data

where Data has the following variables:

Variable Name	Type	
X	Number	(Required)
Y	Number	(Required)
Data	[3412×1double]	(Required)
Date	[3412×1double]	(Required)
Depth	[3412×1double]	(Required)
Units	Cell	(Optional)
Title	Cell	(Optional)
Variable_Name	String	(Optional)

An example is provided. To plot Conductivity for Elizabeth_Bay in the example great.mat:

```
load great.mat  
plot(great.Elizabeth_Bay.Conductivity.Date,great.Elizabeth_Bay.Conductivity.Data);
```

The X,Y are the locations, and this information needs to be in the same projection as the model; the data must also be in the same units as the model. Some common model variables are below.

Variable	Units *	Common Name
Physical variables		
<i>T</i>	°C	Temperature
<i>S</i>	psu	Salinity
<i>EC</i>	uS cm ⁻¹	Electrical conductivity
<i>I_{PAR}</i>	mE m ⁻² s ⁻¹	Shortwave light intensity
<i>I_{UV}</i>	mE m ⁻² s ⁻¹	UV light intensity
<i>η_{PAR}</i>	m ⁻¹	PAR extinction coefficient
<i>η_{UV}</i>	m ⁻¹	UV extinction coefficient
Core biogeochemical variables		
<i>DO</i>	mmol O ₂ m ⁻³	Dissolved oxygen
<i>RSi</i>	mmol Si m ⁻³	Reactive Silica
<i>FRP</i>	mmol P m ⁻³	Filterable reactive phosphorus
<i>FRP-ADS</i>	mmol P m ⁻³	Particulate inorganic phosphorus
<i>NH₄⁺</i>	mmol N m ⁻³	Ammonium
<i>NO₃⁻</i>	mmol N m ⁻³	Nitrate
<i>DOC</i>	mmol C m ⁻³	Dissolved organic carbon
<i>DON</i>	mmol N m ⁻³	Dissolved organic nitrogen
<i>DOP</i>	mmol P m ⁻³	Dissolved organic phosphorus
<i>POC</i>	mmol C m ⁻³	Particulate organic carbon
<i>PON</i>	mmol N m ⁻³	Particulate organic nitrogen
<i>POP</i>	mmol P m ⁻³	Particulate organic phosphorus
<i>TP</i>	mmol P m ⁻³	Total Phosphorus
<i>TN</i>	mmol N m ⁻³	Total Nitrogen
<i>TKN</i>	mmol N m ⁻³	Total Kjedahl Nitrogen
Plankton groups		
<i>GRN</i>	mmol C m ⁻³	Chlorophytes
<i>TCHLA</i>	ug Chla L ⁻¹	Total Chlorophyll-a
Benthic groups		
<i>MAG</i>	mmol C m ⁻²	Cladophora biomass
Suspended sediment and related properties		
<i>SS_s</i>	g SS m ⁻³	Suspended solids groups
<i>Turbidity</i>	NTU	Turbidity